

Copyright

by

Catherine Grace Hovell

2007

**Evaluation of Redundancy in Trapezoidal Box-Girder Bridges
Using Finite Element Analysis**

by

Catherine Grace Hovell, B.S.C.E.

Thesis

Presented to the Faculty of the Graduate School of

The University of Texas at Austin

in Partial Fulfillment

of the Requirements

for the Degree of

Master of Science in Engineering

The University of Texas at Austin

August 2007

**Evaluation of Redundancy in Trapezoidal Box-Girder Bridges
Using Finite Element Analysis**

**APPROVED BY
SUPERVISING COMMITTEE:**

Eric B. Williamson

Karl H. Frank

To my family and friends,
for their love and support

Acknowledgements

I would like to thank my advisor, Dr. Eric B. Williamson, for the guidance he has provided over the past two years and for showing a personal interest in my endeavors within and beyond laboratory research. You challenged and encouraged me to a standard of work of which I am proud. I am thankful for the help of Dr. Karl H. Frank, my second reader and co-PI of this project, in particular for his patience and understanding of the mishaps that occur in research and his wisdom in how to move forward from them.

I would like to acknowledge my research partners, Timothy Barnard, Joshua Mouras, and Jim Sutton, for their dedication to this project. For his help with the concrete modeling, I thank Matthieu Caullet. For their financial support which made this project possible, I thank the Texas Department of Transportation and the Federal Highway Administration.

I am grateful for my fellow analysis students, in particular Daniel Williams and Jason Stith, who made my hours in the computer lab more enjoyable. For their friendship (and willingness to proofread), I am thankful for Kim Talley and Ryan Chancey.

To the professors at the University of Virginia, thank you for sharing your excitement in civil engineering and helping me find my path in this field. Particular thanks go to Dr. Roseanna Neupauer for her unofficial advising role and Dr. Jose Gomez for his enthusiastic support. I would like to give a special thanks to Dr. Rodney Davis for his guidance through my undergraduate thesis and for introducing me to the University of Texas program. Credit must also be given to Chip Dumais and Art Ruggieri, who would not let me do anything but my best.

The staff of Ferguson Structural Engineering Laboratory, including our lab technicians and administrative personnel, deserve thanks for their helpful attitudes and unfaltering work ethic.

To Mom, Dad, and John: thank you for your love, patience, and support. You give me strength.

August, 2007

Abstract

Evaluation of Redundancy in Trapezoidal Box-Girder Bridges Using Finite Element Analysis

Catherine Grace Hovell, M.S.E.

The University of Texas at Austin, 2007

SUPERVISOR: Eric B. Williamson

The AASHTO Bridge Design specifications define a fracture-critical member as a component in tension whose failure is expected to result in the collapse of a bridge. The tension flanges of twin box-girder bridges are thus labeled as fracture-critical. In order to avoid the catastrophic collapse suggested by the AASHTO specifications, fracture-critical bridges, constituting 11% of all steel bridges in the country, are subjected to frequent and stringent evaluation and inspection.

The Texas Department of Transportation, interested in reducing the cost of an otherwise attractive bridge design, is now questioning the validity of the original statement by AASHTO. In particular, it is not clear whether or not a single localized fracture can lead to the collapse of a bridge. Contrary to this belief, there have been multiple instances of fracture-critical bridges with two tension flanges that have experienced fracture without collapse. This project was designed to determine the level of redundancy that can be found in twin box-girder bridges.

To achieve this goal, a full-scale test specimen of a box-girder bridge was built at the Ferguson Structural Engineering Laboratory in Austin, Texas. In unison, a finite element model of the bridge was built using ABAQUS/Standard. A fracture was initiated

in one bottom flange of the test specimen. The data gathered during the test were compared to the calculated response from the model to verify the predictive capabilities of the model. If able to predict response accurately, a computer model could be used during design to indicate the presence of redundancy and the decreased need for frequent inspection of a bridge.

The computer model was used to simulate a full-depth web fracture event in the exterior girder of a twin-girder bridge with a very large horizontal radius of curvature. The model was then modified to consider the influence of several parameters, including radius of curvature, structural redundancy through continuous spans, and external bracing. Results obtained from the finite element model indicate that adequate redundancy exists in the bridge design to maintain stability after the fracture of one girder. The most significant design change is to add continuity through spans, as adding structural redundancy greatly reduced the expected deflections and stresses that would be induced in the system.

Further study using the modeling techniques presented in this thesis should begin by verifying or improving upon the assumptions that were made. Specifically, the concrete material model and the shear stud modeling method should be examined in more detail and should be used to predict the response of smaller-scale laboratory tests. With further refinement, this model could be utilized during the design phase to verify the presence of redundant load paths and thus reduce the necessity for frequent inspections.

Table of Contents

List of Tables.....	xiii
List of Figures.....	xiv
CHAPTER 1 Introduction and Scope of Research	1
1.1 Introduction.....	1
1.2 Project Motivation	2
1.3 Scope of Project	3
1.4 Overview of Report.....	4
CHAPTER 2 Literature Review	5
2.1 Introduction.....	5
2.2 Fracture-Critical Bridges	7
2.3 Fatigue Cracking.....	8
2.4 Development of Specifications	9
2.5 Specification Shortcomings	11
2.6 Previous Fracture Events	13
2.7 Controlled Fracture Test	14
2.8 Research Using Finite Element Analysis.....	16
2.9 Alternative Redundancies	18
2.9.1 Structural Redundancy.....	19
2.9.2 Internal Redundancy	19
2.10 Summary and Conclusions	21
CHAPTER 3 Details of Test Specimen.....	22
3.1 Introduction.....	22
3.2 Full-Scale Test Specimen	23

3.2.1 Girder Geometry	23
3.2.2 Plate Thicknesses	24
3.2.3 Longitudinal Design.....	24
3.2.4 Deck Design.....	28
3.2.5 Rail Design.....	29
3.2.6 Shear Studs.....	30
3.3 Live Load Application	31
3.4 Fracture Event.....	32
3.4.1 Expected Response	33
3.4.2 Actual Response.....	34
3.5 Instrumentation	35
3.5.1 Girder Gauges	35
3.5.2 Deck Gauges	37
3.6 Summary and Conclusions	38
CHAPTER 4 Using ABAQUS for Structural Analysis.....	39
4.1 Finite Element Computer Programs.....	39
4.2 Selection of ABAQUS for Use in this Study.....	39
4.3 ABAQUS Programs.....	40
4.3.1 CAE	40
4.3.2 Command Prompt	41
4.3.3 Viewer.....	41
4.4 General Rules for Using ABAQUS	42
4.4.1 Unit Consistency	42
4.4.2 Project Folder.....	42
4.4.3 Input Files	43
4.5 Overview of the Major Steps Involved in Using ABAQUS.....	43
4.5.1 Create Nodes	44
4.5.2 Create Elements	46

4.5.3 Define Section Properties	50
4.5.4 Define Material Models	50
4.5.5 Define Boundary Conditions	51
4.5.6 Enforce Physical Constraints	51
4.5.7 Write Load Steps.....	53
4.5.8 Submit the Job.....	55
4.5.9 Monitor Progress of the Job.....	55
4.6 Summary and Conclusions	56
CHAPTER 5 Details of the Finite Element Model	57
5.1 Introduction.....	57
5.2 Specifics of the ABAQUS Model.....	57
5.2.1 Define Nodes	58
5.2.2 Restrain Movement.....	61
5.2.3 Assign Section Properties	61
5.2.4 Define Material Models	63
5.2.5 Define Elements.....	71
5.2.6 Compile Load Sets.....	78
5.2.7 Define Load Steps.....	78
5.3 Areas of Special Focus.....	80
5.3.1 Modeling of the Rails.....	81
5.3.2 Modeling of the Shear Studs.....	85
5.3.3 Modeling the Fracture.....	88
5.4 Correlation with Test Specimen.....	93
5.4.1 Girder Instrumentation.....	95
5.4.2 Deck Instrumentation.....	97
5.4.3 Stud Instrumentation	98
5.5 Summary and Conclusions	100

CHAPTER 6	Results and Comparisons	101
6.1	Introduction	101
6.2	Preliminary Verifications	102
6.2.1	Mesh Density	102
6.2.2	Deck Element Type	103
6.2.3	Concrete Load Application	105
6.3	Comparisons to Measured Data	107
6.3.1	Deflections	107
6.3.2	Live Load Testing	110
6.3.3	Fracture Event	111
6.4	Prediction of Full Fracture Response	116
6.5	Effect of Dynamic Loading	122
6.6	Alternative Geometries	125
6.6.1	Variable Radius	125
6.6.2	Influence of External Bracing	136
6.6.3	Benefits of Structural Redundancy	138
6.7	Summary and Conclusions	148
CHAPTER 7	Conclusions and Recommendations	150
7.1	Summary of Research	150
7.2	Conclusions	151
7.2.1	Full Fracture Response	152
7.2.2	Consideration of Dynamic Load Factors	152
7.2.3	Effect of Radius	153
7.2.4	Effect of External Bracing	153
7.2.5	Effect of Structural Redundancy	153
7.3	Recommendations for Future Work	154
7.3.1	Fracture	155
7.3.2	Shear Studs	156

7.3.3	Concrete Material Model	157
7.4	Summary	159
APPENDIX A	Introduction to Finite Element Analysis.....	160
A.1	Introduction.....	161
A.2	Overview of Methodology	161
A.2.1	Stiffness Method	163
A.2.2	Flexibility Method	167
A.2.3	Improving the Model	171
A.2.4	Mapping Elements	173
A.2.5	Choosing a Method	174
A.3	Summary and Conclusions	175
APPENDIX B	Full Input File.....	176
APPENDIX C	Table of Longitudinal Node Locations.....	207
APPENDIX D	List of Commonly Used Keywords.....	209
APPENDIX E	Example *mpc File.....	211
	References.....	213
	Vita.....	219

List of Tables

Table 3-1: Measured and designed plate thicknesses (Barnard 2006).....	24
Table 5-1: Section properties definitions.....	62
Table 5-2: Material model definitions	64
Table 5-3: Element numbers corresponding to foil gauges and rosettes on the test specimen	96
Table 5-4: Element numbers corresponding to deck rebar gauges on the test specimen .	98
Table 5-5: Element numbers corresponding to shear stud gauges on the test specimen ..	99
Table 6-1: Comparison of reaction forces under dead load using solid and shell deck elements	105
Table 6-2: Variation in reaction forces at each of four supports for three bridges of different radii	133
Table 6-3: Maximum change in deflection at midspan of the fractured girder with and without external cross-bracing.....	136

List of Figures

Figure 1-1: A typical twin box-girder overpass in Austin, TX.....	1
Figure 2-1: Comparison of internal redundancy in (a) a box-girder design, (b) a four plate-girder design, and (c) a twin plate-girder design	6
Figure 2-2: Flaw growth through repeated loading (modified from Frank 2007)	9
Figure 2-3: The Point Pleasant Bridge, (a) pre- and (b) post-collapse (unknown, Connor et al. 2005)	10
Figure 2-4: Mianus River Bridge, post-collapse (Fisher 2005)	11
Figure 2-5: Full-depth fracture in I-79 bridge in Pittsburg, PA (unknown)	14
Figure 2-6: Cross-section of the I-40 bridge tested by Idriss et al. (1995)	15
Figure 2-7: Transverse bracing profile for the three-span bridge tested by Idriss et al. (1995).....	15
Figure 2-8: Fracture steps in New Mexico test; hashing indicates fractured area	16
Figure 2-9: Finite element analysis in SAP2000 of the I-435 bridge (Crampton et al. 2006)	18
Figure 2-10: Structural redundancy in (a) a continuous span, and (b) a double-cantilevered response	19
Figure 2-11: The Hoan Bridge in Wisconsin, post fracture of two of the three plate girders (Connor et al. 2005).....	20
Figure 3-1: Cross-section of the trapezoidal box girders, deck, and rails.....	22
Figure 3-3: Box girder cross-sectional geometry.....	24
Figure 3-4: Bending distortion in unrestrained webs (Gilchrist 1997).....	25
Figure 3-5: Internal brace structural design	26
Figure 3-6: Designed and built bracing locations	27
Figure 3-7: Rotation differential during construction (Barnard 2006)	28
Figure 3-8: External brace structural design.....	28
Figure 3-9: Rebar profile in cast-in-place concrete deck.....	29
Figure 3-10: Dimensions of T501 cast-in-place rail (TxDOT).....	30

Figure 3-11: Standard AASHTO HS-20 truck (AASHTO 2004).....	32
Figure 3-12: Concrete used to represent the AASHTO truck on the test specimen	32
Figure 3-13: Cut edge of the trial plate.....	33
Figure 3-14: Test specimen, with containment shield in place, 21 October 2006.....	34
Figure 3-15: Bottom flange, post-fracture	35
Figure 3-16: Foil and rosette gauge locations, presented in plan view (Barnard 2006) ...	36
Figure 3-17: Foil gauge (F) and rosette gauge (R) locations within cross-section (Barnard 2006)	36
Figure 3-18: Rebar strain gauge locations (Barnard 2006).....	37
Figure 3-19: Shear stud bolt gauge locations (Barnard 2006)	38
Figure 4-1: ABAQUS menu under Programs in Windows XP (Microsoft 2001).....	40
Figure 4-2: Global (1 – 2) and local (1' – 2') axes along an element	45
Figure 4-3: Element type nomenclature (HKS, Inc. 2006).....	47
Figure 4-4 Correct and incorrect numbering schemes for a 4-noded element.....	48
Figure 4-5: Outward normal directions for (a) beam and (b) shell elements (HKS, Inc. 2006)	48
Figure 4-6: Multi-point constraints (type linear) (HKS, Inc. 2006)	52
Figure 4-7: ABAQUS Command Prompt window (DOS interface)	55
Figure 5-1: Node numbering scheme transverse to the girder profile (girder boundaries marked with a bold blue line)	59
Figure 5-2: Node numbering scheme vertically through the girders, deck, and rails.....	60
Figure 5-3: Concrete material model stress-strain curve for plastic response	66
Figure 5-4: Steel material model stress-strain curve for plastic response	68
Figure 5-5: Stretching of the deck elements upon reactivation without using fakedeck elements (scale factor = 10).....	69
Figure 5-6: Element numbering around internal girder; the interior edge is to the left....	72
Figure 5-7: Stresses in the rail during fracture, magnified to show hourglassing in the reduced integration rail elements	76
Figure 5-8: ABAQUS view of the end of the modeled bridge, showing block railing	83

Figure 5-9: Use of the bilinear multi-point constraint (HKS, Inc. 2006)	85
Figure 5-10: Load-deflection curve for test specimen shear stud geometry (Sutton 2007)	87
Figure 5-11: (a) Square tip of fracture path using *model change, (b) stress concentration that results	90
Figure 5-12: Edge loading directions and nomenclature for four-noded shell elements (HKS, Inc. 2006).....	92
Figure 5-13: Variation in strain using different strain equations.....	95
Figure 6-1: Comparison of dead load deflections with 60 and 120 elements down the length (curves overlap)	103
Figure 6-2: Comparison of dead load deflections using solid and shell deck elements (curves overlap)	104
Figure 6-3: Comparison of dead load deflections while applying deck load as a surface load on the top flange (applied) or as a gravity load.....	106
Figure 6-4: Deflection profile for a midspan node on the external girder from girder erection through external cross-brace removal.....	107
Figure 6-5: Deck load deflection comparison using ABAQUS, UTrAp, and measured data.....	108
Figure 6-6: Deck and girder dead load deflection comparison using reduced- and full- integration girder elements (<i>s4r</i> and <i>s4</i>)	109
Figure 6-7: Measured and calculated strain changes in the girders during loading. Measured values are on the exterior of the girders in blue; calculated values are on the interior in red italics.	110
Figure 6-8: Measured and calculated strain changes in the girders during unloading. Measured values are on the exterior of the girders in blue; calculated values are on the interior in red italics.	111
Figure 6-9: Comparison of the change in deflections calculated in ABAQUS and measured on the test-specimen using a laser-level	112

Figure 6-10: Measured and calculated strain changes in the girders during fracture event. Measured values are on the exterior of the girders in blue; calculated values are on the interior in red italics. Blank spots indicate broken gauges.	113
Figure 6-11: Ellipse of near-zero stress surrounding the flange fracture (blue is low, red is high)	115
Figure 6-12: Change in deflections of the interior and exterior flange during a simulated full-depth flange and web fracture	118
Figure 6-13: Schematic of the rebar stress figures shown in Figures 6-14 and 6-15.....	121
Figure 6-14: Predicted total stresses from live load in (a) interior and (b) exterior deck and rail rebar at midspan.....	121
Figure 6-15: Predicted total stresses after a full-depth flange and web fracture in (a) interior and (b) exterior deck and rail rebar at midspan.....	121
Figure 6-16: Example of the difference in peak values from static (blue dashed line) and dynamic (red solid line) load application.....	123
Figure 6-17: Measured peak and calculated base and amplified strain values during fracture event at locations indicated on inset (6 ft south of centerline)	124
Figure 6-18: Change in displacement of the exterior girder during a full-web fracture with variable radii: blue solid line is 400 ft radius, red dashed is 800 ft, and green dotted is 1365 ft	127
Figure 6-19: Deflection of the bottom flange of the exterior girder after flange fracture	128
Figure 6-20: Total deflection of the bottom flange of the exterior girder down the length of the bridge, post-web fracture	129
Figure 6-21: von Mises stresses calculated in the bottom flange of the interior girder after each stage of fracture for three different geometries ($R = 400, 800, \text{ and } 1365 \text{ ft}$)	130
Figure 6-22: Support locations and lettering scheme	131
Figure 6-23: Total reaction forces after a full web and flange fracture event for three different geometries ($R = 400, 800, \text{ and } 1365 \text{ ft}$).....	132

Figure 6-24: Change in support reactions during a full web and flange fracture event for three different geometries ($R = 400, 800, \text{ and } 1365 \text{ ft}$).....	134
Figure 6-25: Moment about the centerline of each bearing pad for three bridges of different radii. The bearings are located beneath the internal and external (Int and Ext) girders at the north and south ends of the bridge (N and S).....	135
Figure 6-26: Total stresses calculated in the (a) south and (b) north external brace elements after flange and web removal (actual braces connect at girder web; drawn for clarity in data presentation).....	137
Figure 6-27: Difference in average midspan stresses across the seven elements of the interior girder bottom flange with and without external braces after a full-depth fracture. Negative values indicate the stresses with the braces in place were higher.	138
Figure 6-28: Total vertical deflections of the exterior girders before and after a full-depth web fracture at the centerline of the middle span	142
Figure 6-29: Total vertical deflections of the exterior girders before and after a full-depth web fracture at the centerline of the first span.....	143
Figure 6-30: Change in displacement of the exterior girder during a full-web fracture for a single span design as compared to continuous bridges with end- and center-span fractures.....	144
Figure 6-31: Reaction forces at an end support and a middle support (typical) before and after a full-depth web fracture at the centerline of the middle span	146
Figure 6-32: Change in support reactions during a full-depth web fracture event in an end span	147
Figure A-1: Axial element with applied load $p(x)$	157
Figure A-2: Axial degrees of freedom numbering and sign convention	159
Figure A-3: Beam degrees of freedom numbering and sign convention	162
Figure A-4: (a) Forces on an axially rigid beam element; (b) dependent forces written in terms of independent forces	163
Figure A-5: (a) A tapered element, (b) represented by two constant-area members	167

Figure A-6: Example mode shape not caught using reduced integration. Full integration points shown with X's, reduced integration point shown with single O.	168
Figure A-7: Global degrees of freedom for a pin-roller simply supported beam	169
Figure E-1: Bilinear mpc explanation (HKS, Inc. 2006)	171

CHAPTER 1

Introduction and Scope of Research

1.1 INTRODUCTION

In recent years, an increasing interest has developed in designing bridges to be aesthetically pleasing, in addition to functional and cost-efficient. One of the most popular designs that has come out of this movement are steel trapezoidal box-girder bridges. In terms of capacity, a single steel box girder effectively replaces two plate girders. To maintain a clean and smooth external appearance, the girders feature a hidden interior space where structural bracing can be located, out of sight of passing motorists. Especially in the design of elevated flyovers at highway interchanges, steel box girders present a streamlined look from below while still achieving tight radii of curvature. A typical box-girder design, in use in Austin, TX, is shown in Figure 1-1.



Figure 1-1: A typical twin box-girder overpass in Austin, TX

Highway flyovers usually include one or two lanes of traffic; the necessary deck width can be handled by four plate girders or two trapezoidal box girders. The main difference between the two exists in what the American Association of State Highway and Transportation Officials (AASHTO) considers to be the most critical location: the tension flange. Four plate girders have four tension flanges while two box girders only have two.

The AASHTO Load and Resistance Factor Design (LRFD) Bridge Design specifications define a fracture-critical member (FCM) as a “component in tension whose failure is expected to result in the collapse of the bridge or the inability of the bridge to perform its function” (AASHTO 2004). In the case of a two-girder bridge, both bottom flanges (as well as the webs and the weld between the two) are labeled fracture-critical. Because of this classification, a twin box-girder bridge is a fracture-critical bridge (FCB); a four plate-girder bridge is not.

In order to avoid the catastrophic collapse suggested by the AASHTO specifications, fracture-critical bridges, constituting 11% of all steel bridges in the country, are subjected to frequent and stringent evaluation and inspection (Connor et al. 2005). The goals of the inspections include finding cracks in the tension members and evaluating the remaining life in a bridge with fracture-critical members. These inspections, however useful in finding defects, are extremely expensive for the bridge owner, adding an estimated increase in cost between 200% and 500% (Connor et al. 2005).

1.2 PROJECT MOTIVATION

Owners of fracture-critical bridges (e.g., state departments of transportation), interested in reducing the cost of an otherwise attractive bridge design are now questioning the validity of the original statement by AASHTO. In particular, it is not clear whether or not a single localized fracture can lead to the collapse of a fracture-critical bridge. Contrary to this belief, there have been multiple instances of fracture-critical bridges with two tension flanges that have experienced fracture without collapse.

In the United States, only two catastrophic failures have been attributed to a lack of redundancy. In both cases (the Point Pleasant Bridge in West Virginia and the Mianus River Bridge in Connecticut), the bridges were found to have additional problems with poor material properties and corrosion, respectively, which helped lead to their collapse (Connor et al. 2005).

In response to the uncertainty associated with the role of fracture-critical members on overall bridge behavior, the Texas Department of Transportation (TxDOT) and the Federal Highway Administration (FHWA) have funded the current project to evaluate methods of assessing the redundancy of steel bridges. The project includes the construction of a full-scale twin steel trapezoidal box-girder experimental test specimen and the development of analytical models to determine the redundancy within these structures. Both the experimental test setup and the analytical models feature a fracture event similar to what might occur during a fatigue failure. Data from the experimental test specimen were used to validate the accuracy of the finite element model.

A major objective of the research project is to determine whether an AASHTO-defined fracture-critical bridge can withstand a full-depth fracture under load without collapse. The analyses presented in this report provide methods of predicting performance of a bridge in a fractured state. Results showing redundancy in trapezoidal box girders could allow TxDOT and other owners to reduce the frequency or stringency of their fracture-critical inspections, saving money every year.

1.3 SCOPE OF PROJECT

This project, TxDOT 0-5498, began in the fall of 2005 with a proposed three-year test plan. At the conclusion of the second year, great progress has been made towards completing the objectives set forth at the beginning. Specifically, to this point, the project has included:

- building a full-scale test specimen, including TxDOT-approved deck and rails;
- instrumentation of the bridge in locations of interest in a fracture situation;

- application and detonation of an explosive to simulate the fracture of the bottom flange, which potentially could create a fracture that would propagate through the webs of the exterior girder, under load;
- experimental investigation of the pullout strength of shear studs (detailed by Sutton (2007));
- development of a finite element model of the test specimen;
- comparison of data between the model and the structure under live loads and during the fracture situation; and
- performing parameter studies using the model to consider the effects of various typical bridge details.

The upcoming year will include further modifications to the analytical model and possibly a second fracture event of the test specimen. More details of and suggestions for future research can be found in later chapters.

1.4 OVERVIEW OF REPORT

The remainder of this report includes details of the programming and use of a finite element model of the constructed full-scale steel trapezoidal box-girder test specimen. Chapter 2 provides background information on fracture-critical bridges, including examples of previous incidents. The specifics of the test specimen, including geometry and instrumentation locations, are given in Chapter 3. Chapter 4 introduces the finite element analysis program ABAQUS, while Chapter 5 details the specifics of the model written in ABAQUS for this project, including material models and load step definitions. Chapter 6 presents comparisons of the calculated and measured deflections and strains during various loading situations and at multiple locations on the girders. Chapter 7 summarizes the research and conclusions within the scope of this project and suggests further research to be completed.

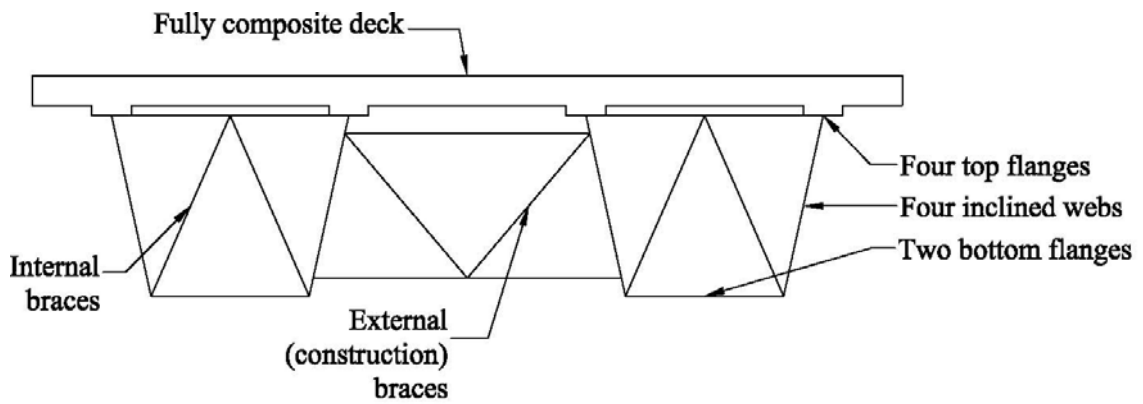
CHAPTER 2

History of Fracture-Critical Bridges

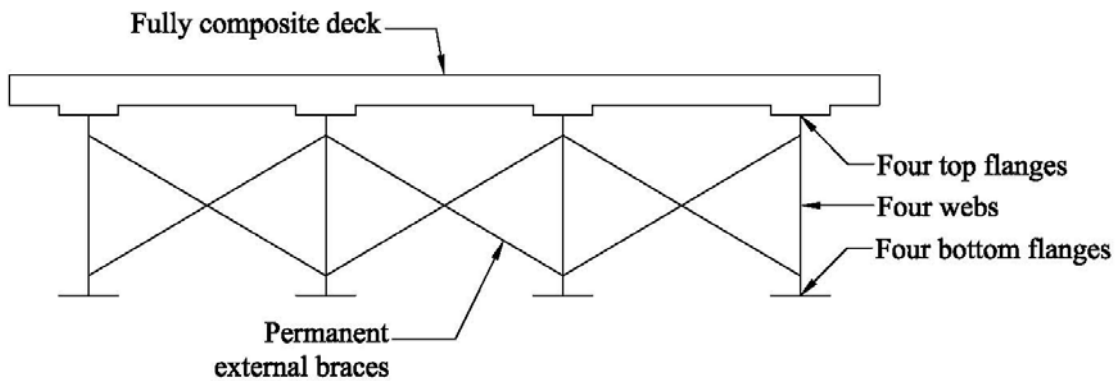
2.1 INTRODUCTION

The failures of the Point Pleasant Bridge in 1967 and the Mianus River Bridge in 1983 led to the development of federal regulations for bridge maintenance and inspection of publicly-owned bridges (Lovejoy 2003). Of particular concern were nonredundant bridges, or those bridges without multiple load paths, which were given the classification of “fracture-critical.” Since the development of the regulations, fracture-critical bridges (FCBs) have been subjected to special “fracture-critical” inspections, which are more intensive and thus more expensive than the inspection required for redundant structures.

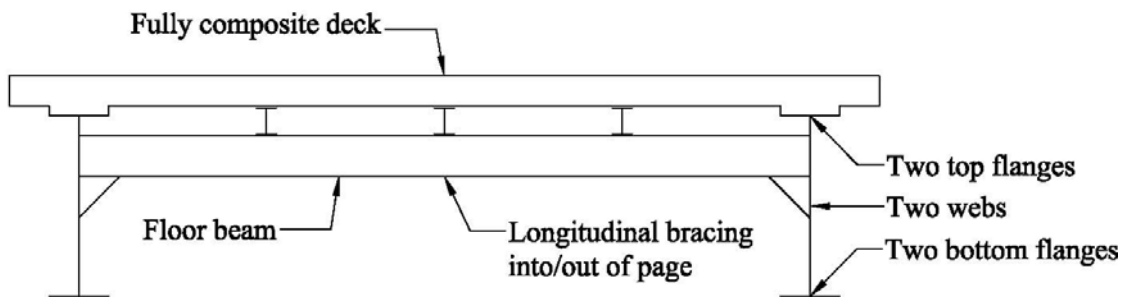
In an effort to reduce inspection costs, bridge owners have begun questioning the appropriateness of the fracture-critical classification. Specifically, twin trapezoidal box-girder bridges are classified as fracture-critical, as there are only two tension flanges; however, considering load-carrying details of the design (Figure 2-1), the response of the structure after a fracture event may be more similar to that of a four plate-girder bridge than a two plate-girder bridge. Previous events and research, detailed further in this chapter, and the research done for this project aim to determine the proper classification of twin box-girder bridges.



(a)



(b)



(c)

Figure 2-1: Comparison of internal redundancy in (a) a box-girder design, (b) a four plate-girder design, and (c) a twin plate-girder design

In the past twenty years, the National Cooperative Highway Research Program (NCHRP) has released three reports focusing on redundancy in steel bridges. The first,

NCHRP Report 319 (Daniels et al. 1989), suggests guidelines for redundant design and a rating system for two-girder steel bridges. The second, NCHRP Report 406 (Ghosn and Moses 1998), discusses redundancy in bridge superstructures. The third, NCHRP Report 458 (Liu et al. 2001), applies the same thoughts and theories from Report 406 to bridge substructures.

Following these three reports, NCHRP released Synthesis 354 (Connor et al. 2005), which summarizes the history of the fracture-critical designation and the resulting specifications. Additionally, Synthesis 354 suggests changes to current practices as well as ideas for future research, some of which overlap the intended goals of this project, TxDOT 0-5498.

This chapter provides an overview of what was presented in these four NCHRP publications and gives an introduction to other completed research relating to the inspection, maintenance, and failure of fracture-critical bridges, including studies of FCBs using finite element analysis. The history of the development of current specifications is also discussed, explaining the state of current inspection requirements.

2.2 FRACTURE-CRITICAL BRIDGES

Steel bridge design in the United States is governed by the Load and Resistance Factor Design (LRFD) specifications, developed by the American Association of State Highway and Transportation Officials (AASHTO). Within the LRFD specifications, bridges with less than three tension flanges are referred to as fracture-critical. These bridges are believed to be without redundancy, where redundancy is defined as “the capability of a bridge to continue to carry loads after the damage or failure of one of its main structural elements” (AASHTO 2006). FCBs constitute approximately 11% of all steel bridges in the United States (Connor et al. 2005).

Damage to, or failure of, a structural element can be caused by either sudden (often man-made) attack or by long-term degradation. The former includes instances of damage to a bridge girder or pier by such things as a vehicle collision, a seismic event, or

an explosive charge. The latter includes damage due to causes such as corrosion, scour, or fatigue.

To ensure against failure due to natural degradation of a bridge and its constituent materials, fracture-critical bridges are inspected frequently and in great depth (detailed further in Section 2.4). Despite the high cost, FCBs are being constructed in increasing numbers: Texas alone has built close to two hundred in the past twenty years (Connor et al. 2005). Bridge owners, such as the Texas DOT, are now interested in determining if the fracture-critical classification is appropriate for all types of two-girder bridges.

2.3 FATIGUE CRACKING

The fabrication of steel bridge girders results in many minor imperfections, particularly in welded areas. Under repetitive loading (e.g., truck traffic across a bridge), fatigue cracks can form from these imperfections. With each repeated load cycle, the imperfection grows slightly. After enough cycles, the damage reaches a threshold size and the crack grows uncontrollably (Frank 2007).

The detectable initial flaw size is dictated by the technology available for inspection both prior to installation and over time. The critical flaw size, which is defined as the threshold at which a crack will grow unabated, is a function of the material properties, specifically, the toughness. The relationship between fatigue cycle and flaw size is shown graphically in Figure 2-2. The expected remaining fatigue life dictates inspection frequency, as to allow multiple inspections between when the crack is detected and when it nears the critical length.

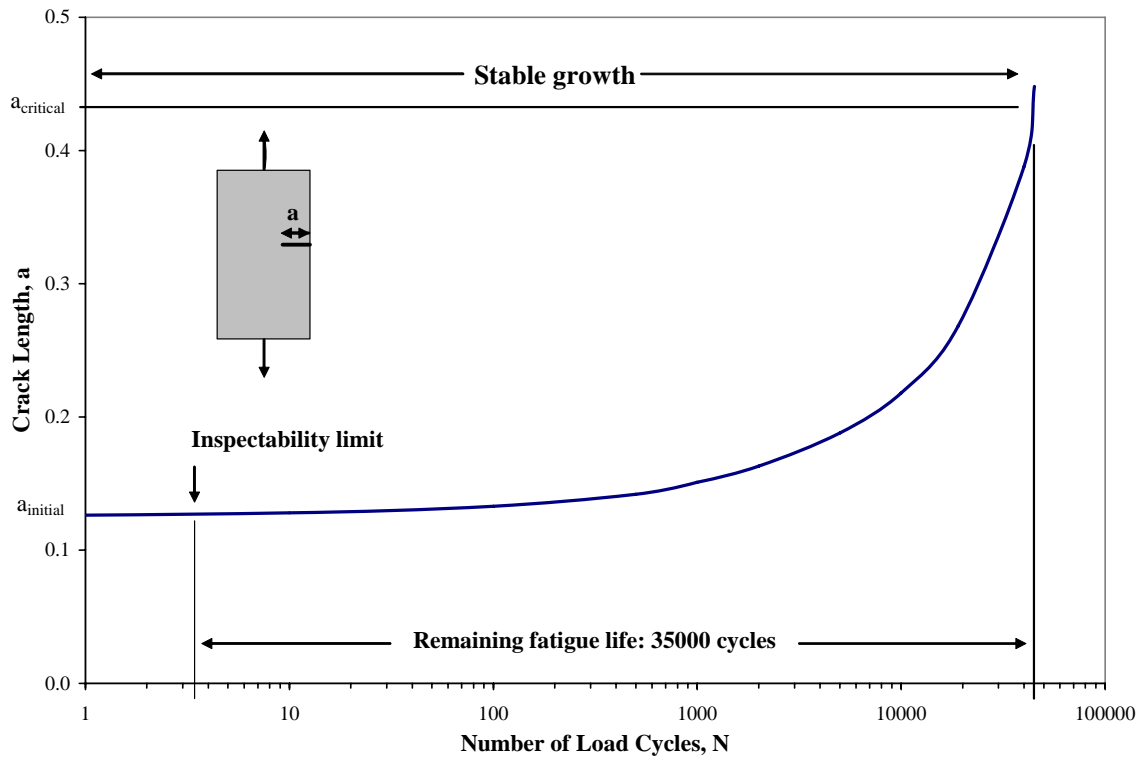


Figure 2-2: Flaw growth through repeated loading (modified from Frank 2007)

2.4 DEVELOPMENT OF SPECIFICATIONS

On a cold day in 1967, the Point Pleasant Bridge over the Ohio River collapsed (Figure 2-3). The bridge, constructed of eyebar chains, failed when one of the eyebars fractured and there was no alternative load path. A post-collapse investigation determined that the steel used – 1928 vintage, heat-treated AISI 1060 steel – was of very low toughness, especially at low temperatures (Scheffey 1971). The collapse of the Point Pleasant Bridge, which caused forty-six deaths, initiated the first developments of material and inspection requirements against fracture in steel bridges.



Figure 2-3: The Point Pleasant Bridge, (a) pre- and (b) post-collapse (unknown, Connor et al. 2005)

In the following years, the Federal Highway Administration began establishing a fracture control plan to improve safety in nonredundant structures. Two main features of this original plan were to limit defects in steel structures and ensure certain levels of material toughness (Dexter 2004). These requirements were satisfied through proper fabrication and inspection practices, and use of the Charpy V-notch toughness test, respectively.

In 1968, the National Bridge Inspection Standards (NBIS) were established. The current NBIS (1988) dictates two-year inspection cycles for highway bridges. The inspection conditions depend on the bridge type and can be as simple as a visual assessment from the ground (Dexter 2004) or may require a thorough “hands-on” inspection (described below).

In 1983, one span of the Mianus River Bridge in Connecticut collapsed (Figure 2-4). As with the Point Pleasant Bridge, where poor material properties contributed to the failure, the Mianus River Bridge did not fail solely because of fatigue loading or cracking. The failure was determined to have been caused by corrosion in a nonredundant, improperly designed pin and hanger assembly (Failla 1985).



Figure 2-4: Mianus River Bridge, post-collapse (Fisher 2005)

In response to this second catastrophic failure, in which three deaths occurred, the NBIS was modified in 1988. The modifications included increasing the stringency of fracture-critical member inspections. Specifically, the inspections were required to be “hands-on”. For box girders, this requirement means the inspector must get inside the box (likely a small, dark, and uncomfortable space) and use non-destructive testing (NDT) methods to determine if observable flaws exist. Due to the resources needed for a fracture-critical inspection – traffic control, equipment for bridge access, man-hours, NDT equipment – owners of FCBs estimated in an NCHRP survey a 200% to 500% increase in inspection costs over non-fracture-critical bridges (Connor et al. 2005).

In summary, the current requirements to ensure the safety of fracture-critical bridges include four major features. The first places a requirement for toughness on the steel, which increases with the critical flaw size. The second reduces the allowable fatigue stress ranges, which slows crack growth. The third implements stricter quality control of weld details, which decreases the number and size of flaws. Lastly, in-field, hands-on inspections of critical tension sections are mandatory every two years, which is sufficiently frequent to allow for deflection of flaws.

2.5 SPECIFICATION SHORTCOMINGS

One of the existing limitations in current design and inspection codes is a lack of specificity. For instance, in considering bridge geometry, there is no distinction between

two-girder bridges made of plate girders versus box girders, even though it has been shown that boxes have much higher torsional rigidity and multiple load paths through internal bracing and connections with the composite deck (Dowling 1975, Ghosn 1998). Rather, a bridge is considered as a whole and requires frequent inspection if the tension (i.e., critical) sections are not great enough in number to be thought redundant. Looking solely at individual members or components ignores system effects such as structural redundancy, as would occur in a multi-span continuous girder bridge, and internal redundancy, which would consider the internal bracing in a box girder. These two design alternatives are discussed more fully in Section 2.8.

As is pointed out in NCHRP Synthesis 354 (Connor et al. 2005), the lack of a clear definition of requirements extends to the loads expected to be resisted. Considering what is currently required, the authors highlight that “these definitions are not clear about what load type, magnitude, distribution on the bridge, dynamic amplification, and load factors are supposed to be resisted by the damaged structure.” A change in applied load in a damaged state could be the difference between resisting collapse and failing to do so.

The redundancy provisions given by AASHTO also fail to give credit to material improvements that have occurred since the codes were first developed. Unlike the steel of the Point Pleasant Bridge, most ordinary steels manufactured currently outperform the required notch toughness criteria, especially in warmer climates (Dexter 2004). High-performance steels respond even better than ordinary steels, thus further decreasing the chance of a fatigue crack that would not be noticed prior to collapse.

The lack of clarity in current specifications, combined with events that show redundancy in structures classified as non-redundant (as described in the next section), have led to research projects such as the current one and pressure by owners for inspection requirements to be loosened. A better understanding of what loads must be resisted by a structure and whether redundant load paths exist are needed to ensure the safety of steel bridges before inspection cycles are lengthened.

2.6 PREVIOUS FRACTURE EVENTS

The NCHRP report on redundancy in highway bridge substructures (Liu et al. 2001) defines collapse as “a major change in the geometry of a bridge rendering it unfit for use.” With the exception of the two failure events mentioned above (the Point Pleasant and Mianus bridges), both caused by a combination of factors including, but not limited to, fatigue, there have not been any collapses of major steel bridges with fractured superstructures (Connor et al. 2005). There have, however, been multiple bridges, some with only two girders, which have been able to withstand partial- or full-depth cracks without collapse. These instances include:

- *US-52 Bridge over the Mississippi River, 1976*

This incident involved a two-girder bridge that experienced a full-depth fracture through the web and tension flange of one girder. Deflections of 2.5 in. were noticed relative to an adjacent span 48 days before the fracture was found. During those 48 days, the fractured span deflected an additional 4-6.5 in. (Fisher 1977).

- *I-79 bridge in Pittsburg, Pennsylvania, 1977 (Figure 2-5)*

This incident involved a two-girder bridge that experienced a full-depth fracture through the web and tension flange of one girder. The deflections were so slight that the fracture was not noticed until a passing ship captain noticed light through the girder (Schwendeman 1978).

- *US-422 Bridge near Pottstown, Pennsylvania*

This incident involved a two-girder bridge that experienced a partial-depth fracture of one web and tension flange. The fracture was approximately 9 in. deep.



Figure 2-5: Full-depth fracture in I-79 bridge in Pittsburg, PA (unknown)

2.7 CONTROLLED FRACTURE TEST

In addition to fractures that occur during the service life of a bridge, testing has been done on twin-girder fracture-critical bridges. In 1993, researchers from New Mexico State University tested a twin plate-girder bridge on I-40 in New Mexico. The bridge was a straight, continuous, three-span unit with two parallel plate girders, shown in Figure 2-6. Transverse floor beams were spaced at 20.4 ft to 21.7 ft longitudinally, and angles were used for cross-bracing, shown in Figure 2-7 (Idriss et al. 1995). The change in brace spacing corresponds with the locations of the intermediate supports.

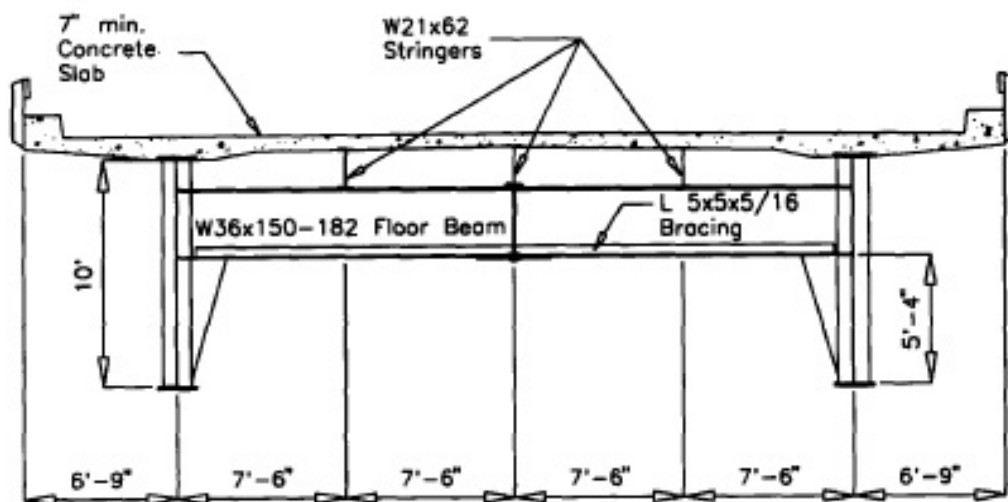


Figure 2-6: Cross-section of the I-40 bridge tested by Idriss et al. (1995)

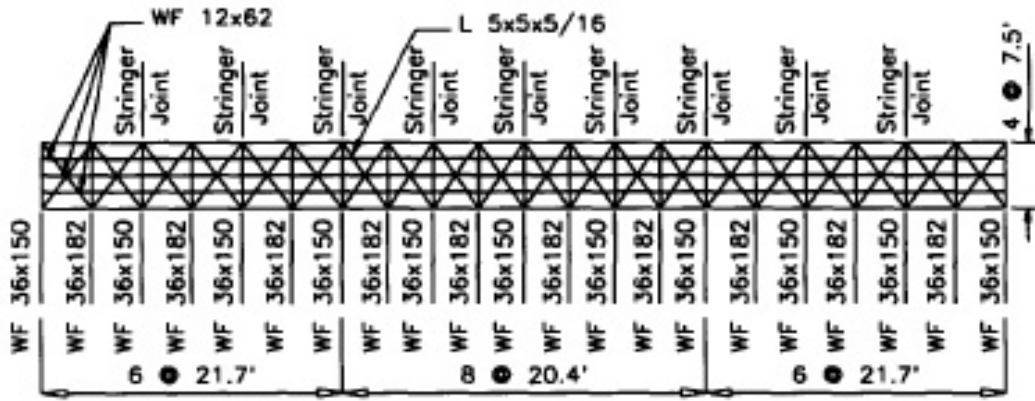


Figure 2-7: Transverse bracing profile for the three-span bridge tested by Idriss et al. (1995)

The test, run statically, involved cutting the bottom flange and web of one girder of the central span. Before one girder was cut, temporary supports were erected to help keep both girders in position. After the cuts were made, the supports were slowly released, allowing the researchers to measure the deflections and stresses during the “fracture event”.

The fracture event occurred in four stages, illustrated in Figure 2-8. The first step removed a two-foot section in the middle of the web. The second continued the fracture of the web down to the flange. The third step involved cutting a quarter of the bottom flange from each exterior edge, resulting in the bottom flange being half the design width. Finally, the remainder of the bottom flange was removed. The measured strains at various points on the girders showed little change until the final step. It was only after both the flange and the web were severed that the load had to redistribute fully. The measured deflection at the fracture location was 1.2 in.

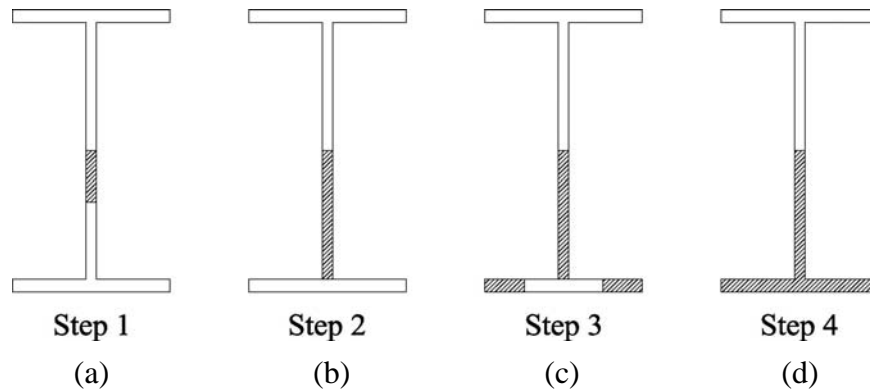


Figure 2-8: Fracture steps in New Mexico test; hashing indicates fractured area

One limitation with this test set-up is that it does not mimic the staging of an actual fracture event. While a fracture could initiate near the center of the web (in this case, where the floor beams framed in), a possible worse-case could be if the crack began at the weld between the web and bottom flange. In that case, the fracture could continue up the web and out the bottom flange at the same time. Additionally, a static test does not capture dynamic effects of a fracture event. Idriss et al. (1995) mention that fracturing the web and half of the flange did not cause crack propagation through the remainder of the flange; however, dynamically applied loads could have caused such damage.

According to basic dynamics principles, dynamically applied loads can induce stresses comparable to those experienced from twice the statically applied load (Chopra 2000). Research, specifically in progressive collapse of buildings, has shown that damping, inelastic material response, and loading rate effects reduce the increase from dynamic load redistribution to closer to 1.5 times the static load (Ruth et al. 2006). Considering either dynamic amplification factor, the stresses in the bottom flange of the New Mexico test could have been high enough to propagate the fracture through the flanges.

2.8 RESEARCH USING FINITE ELEMENT ANALYSIS

Finite element analysis (FEA) has been used since its inception to analyze the response of bridges and many other types of structures under loads. This section highlights a few studies of twin-girder bridges run in SAP2000 (Computers and Structures, Inc. 2006), a commercially-available structural analysis program. Additionally, a brief overview of the trapezoidal box-girder analysis program UTrAp (Popp et al. 2004) is given.

Crampton et al. (2006) used SAP2000 to evaluate the structural redundancy of the I-70 Poplar Street Complex. The two-girder bridge experienced brittle fractures in three girder webs over five years. The analysis was geared towards determining loads that would need to be resisted in a retrofit shear plate designed to recover the strength lost with the fractures. A non-linear analysis allowed for a reduction in the number of fasteners and a decreased plate depth compared to the original elastic design.

Elastic models were also run to determine the redundancy in two-girder structures post-fracture. The pre-fracture shear and moment demands were calculated and compared to the post-fracture capacity. The research also considered the two-girder I-435 bridge spanning the Missouri River after fatigue cracks were discovered there. A SAP2000 analysis was written and run (Figure 2-9) considering elastic and inelastic behavior. The results showed the bridge to be unable to withstand a full-depth fracture (Crampton et al. 2006).

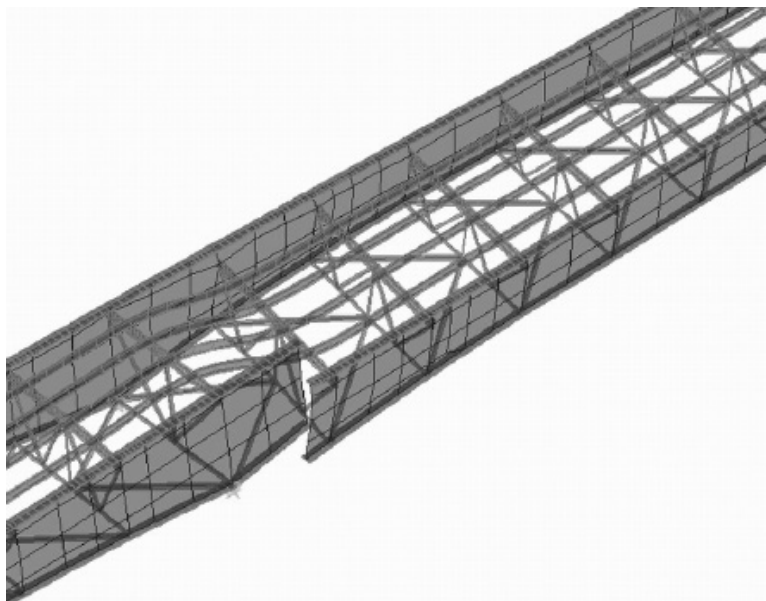


Figure 2-9: Finite element analysis in SAP2000 of the I-435 bridge (Crampton et al. 2006)

In 2002, a research team at the University of Texas at Austin released the trapezoidal box-girder analysis program UTrAp (Popp et al. 2004). UTrAp was designed to calculate the elastic and buckling responses of box-girder bridges during construction loading. The program uses shell elements for both the girder sections and the deck elements, truss elements for internal and external bracing, and linear spring elements for the shear studs (Topkaya and Williamson 2003). Calculated values from UTrAp are used later in this research project to make comparisons between computational methods and between analytical and experimental data. In its present state, a post-construction fracture module could be added.

2.9 ALTERNATIVE REDUNDANCIES

The wording of the definition for redundancy in the AASHTO specifications does not give engineers a clear method for determining redundant load paths in the structures they design. Especially for two-girder bridges, there are two main load-carrying members: each of the two girders into which the deck and bracing are framed. However, the NCHRP reports have pointed towards alternative sources of redundancy that might

not be initially evident upon considering a structure. Specifically, transverse bracing systems and structurally indeterminate designs can create alternative load-transfer capabilities (Daniels et al. 1989). While most design methods ignore the contribution of bracing members, the researchers showed through finite element analysis that redundancies do exist in these additional structural systems.

The following sections highlight two of the redundancies that can exist in a bridge design that are not accounted for in the AASHTO specifications. The first is structural or longitudinal redundancy, as exists in a continuous structure. The second is internal or transverse redundancy, which considers the bracing systems and composite deck connecting the two girders.

2.9.1 Structural Redundancy

All the fractured bridges mentioned in Section 2.6 had continuous spans, unlike the test specimen studied in TxDOT 0-5498. To illustrate the effects of redundancy, consider a continuous beam with three spans and a centralized fracture (Figure 2-10). For this scenario, the end spans become similar to two overhung cantilevers. Although the transverse profile may not seem redundant, the longitudinal system with a centralized fracture is statically determinate and could be stable. The change in structural geometry is shown in Figure 2-10, with an exaggerated approximation of the deflected shape shown as a dashed line.

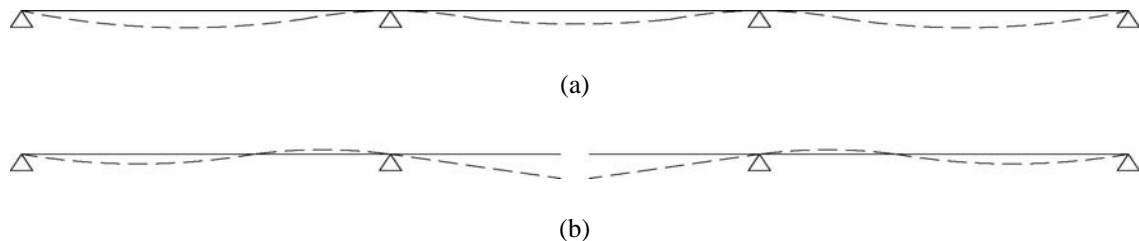


Figure 2-10: Structural redundancy in (a) a continuous span, and (b) a double-cantilevered response

A simply-supported structure does not necessarily have structural redundancy. For a single-girder bridge, all forces would have to be resisted by the deck and rails,

which is unlikely to be possible. A second girder could create transverse redundancy, adding an alternative load path through the deck to the second, unfractured girder.

2.9.2 Internal Redundancy

It is important to note that the previous fracture events occurred on plate girders, rather than box girders. While a twin box-girder bridge does have only two tension flanges, the two girders include four webs and four top flanges, as was shown in Figure 2-1. Within each girder, the internal bracing, designed to resist deformation during construction loading (prior to composite behavior being established), connects the two webs together. This bracing makes one tub girder with a fractured flange comparable to two fractured plate girders connected with stability bracing.

AASHTO does not consider bridges with more than two girders, or two independent load paths, to be fracture-critical. There have been several cases of multi-girder bridges with partial- or full-depth fractures that have not resulted in collapse. One such bridge is the Hoan Bridge in Wisconsin (Connor et al. 2005). In the winter of 2000, fractures were found in the Hoan Bridge, a continuous three-span structure with three girders. Two of the three girders were fully fractured; the third was partially fractured. Even so, the structure remained stable, although deformed (Figure 2-11).

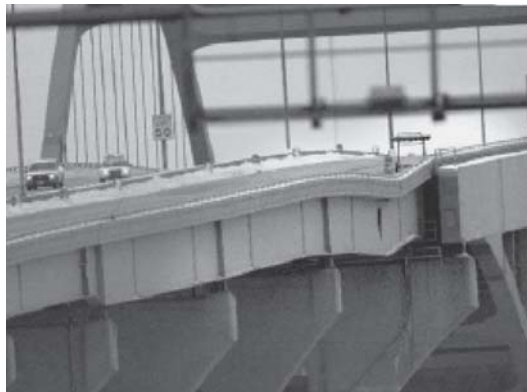


Figure 2-11: The Hoan Bridge in Wisconsin, post fracture of two of the three plate girders (Connor et al. 2005)

Another less severe example is the Brandywine River Bridge on I-95 in Delaware (Quiel 2003). The three-span continuous bridge has six haunched 8-ft deep plate girders. An unnoticed weld flaw grew through fatigue into a seven foot fracture of the fascia (outermost) girder of the center span. Like the I-79 bridge in Pittsburg, the fracture was not noticed by the state DOT nor drivers, but by a citizen walking below the bridge.

Internal redundancy can also refer to the connection details of a built up member, depending on whether a crack can propagate between two adjoining pieces of steel (Liu et al. 2001). A plate or box girder with bolted connections would have this type of internal redundancy. Welded connections, as are used on the bridge studied in this project, do not. Bolted continuity plates have been used to create redundancy or repair a bridge after a fracture event, such as by the Illinois DOT at the Poplar Street Complex (Crampton et al.).

2.10 SUMMARY AND CONCLUSIONS

The classification of some steel bridges as fracture-critical, while necessary in some cases, may have been applied too broadly to all twin-girder bridges. Unlike twin plate-girder bridges, twin box-girders have webs and internal bracing that is similar to a four plate-girder structure. Considering the high cost that is spent on bi-annual inspections of fracture-critical bridges and the necessity for safe bridges, there is a need to more fully understand the redundancies that exist in twin box-girder bridges.

In this project, a full-scale test specimen was constructed and tested. The results were compared and combined with those from a finite element analysis model of the bridge that was designed considering previous research using FEA. The next chapter presents details of the test specimen.

CHAPTER 3

Test Specimen Details

3.1 INTRODUCTION

This project was originally proposed as one based on analytical modeling and small-scale laboratory tests. The scope was expanded when a full-scale twin steel box-girder bridge became available to the research team. The girders were in use in a high-occupancy vehicle (HOV) bus lane in Houston that was dismantled in the fall of 2005. During demolition of the previously existing deck in Houston, the girders suffered some damage and were repaired at Trinity Industries, Inc. in Houston, TX. In January, 2006, the girders were shipped to the University of Texas at Austin.

Between June and August, 2007, the bridge was reconstructed following current TxDOT design and construction practices, with an outside contractor building the deck and rails. TxDOT engineers developed the plans, and a TxDOT inspector oversaw the contractor's work. The result was a full-scale test specimen similar in design and construction to one that could exist in the field. A sketch of the bridge cross-section is given in Figure 3-1.

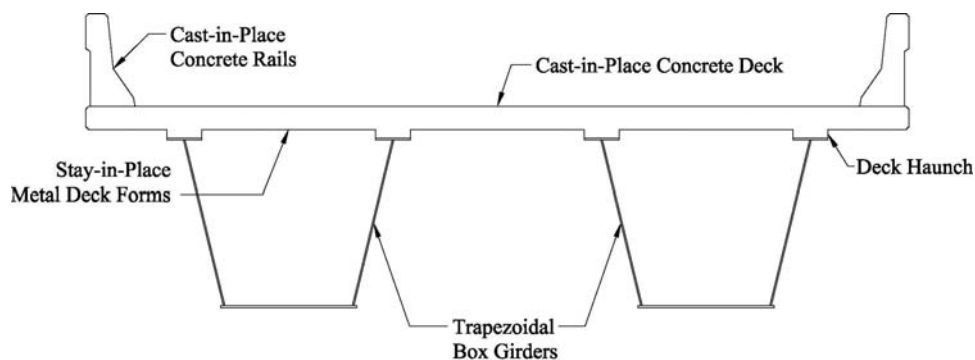


Figure 3-1: Cross-section of the trapezoidal box girders, deck, and rails

In parallel with the specimen construction, a finite element model matching the real bridge was created in ABAQUS (HKS, Inc. 2006). The following sections detail the physical structure, and Chapter 5 provides a detailed description of the ABAQUS model that was developed. Each chapter focuses on specific areas of interest that arose during the investigation.

3.2 FULL-SCALE TEST SPECIMEN

Before the girders arrived in Austin, the research team constructed concrete piers to act as supports for the structure. During this time, the girders were at Trinity Industries, Inc., being repaired from the damage done during demolition. The repairs included heating and straightening parts of the top flanges, webs, and internal bracing. Additionally, many deformed shear studs were replaced. In January, 2006, the girders arrived in Austin and were erected. A local contractor began forming the deck in late June. By late September, instrumentation had been placed along and within the girder and deck, the deck and rails were cast, and the concrete had cured sufficiently to be ready for testing.

The following sections present further details to the construction and instrumentation. A more complete description of the test specimen can be found in Barnard (2006).

3.2.1 Girder Geometry

The test specimen consists of two trapezoidal girders with a slight horizontal curvature. The centerline length is 120 ft and the width from flange tip to flange tip is 19 ft (Figure 3-2). The girder depth is 4 ft-9 in., constructed with inclined webs. The bottom flange is 3 ft-11 in., and the top flanges are 6 ft apart at their centers. The cross-sectional dimensions of the girders can be found Figure 3-2.

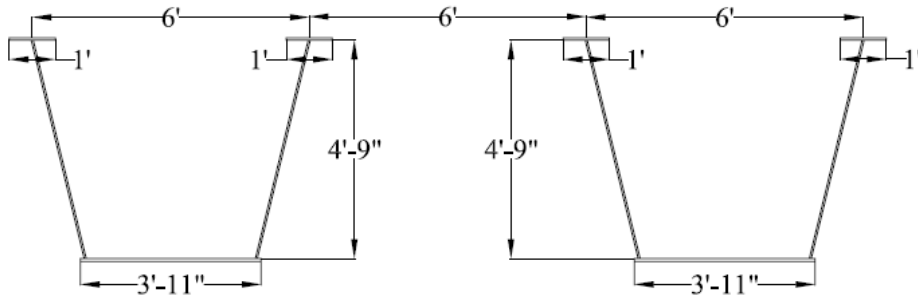


Figure 3-2: Box girder cross-sectional geometry

3.2.2 Plate Thicknesses

The girder webs and flanges are made up of constant-thickness plates. The design calls for a bottom flange thickness of 0.75 in., web thicknesses of 0.5 in., and top flange thicknesses of 0.625 in. These values were confirmed with spot testing along the girders; a comparison of the designed and measured averages can be found in Table 3-1.

Table 3-1: Measured and designed plate thicknesses (Barnard 2006)

	Average Measured Thickness, in.	Plan Thickness, in.	% Difference
Top Flange	0.646	0.625	3.3%
Web	0.503	0.500	0.5%
Bottom Flange	0.757	0.750	0.9%

3.2.3 Longitudinal Design

The bridge has a radius of curvature of 1365.4 ft, meaning the interior girder has a centerline length of 119.5 ft and the exterior girder has a centerline length of 120.5 ft. Each girder has a solid 0.5-in. plate internal diaphragm at the support points, located 1 ft-1.5 in. from the end of the girder. Another diaphragm connects the two girders to one another. The original design used pot bearings bolted to the bent caps for support; the pot bearings were removed and destroyed during the deconstruction of the bridge in Houston. As an alternative, elastomeric bearing pads were used when the bridge was reconstructed

outside the Ferguson Structural Engineering Laboratory (FSEL) at the University of Texas at Austin. The pads are made of approximately 3-in thick neoprene pads with nine 1/16th-in. embedded steel plates (Barnard 2006).

Along the length, the girders feature four different types of bracing: vertical stiffeners, internal stiffening trusses, top lateral braces, and external construction braces. The function and structural design of each of these braces are detailed below.

3.2.3.1 Vertical Stiffeners

Vertical stiffeners are welded perpendicular to the webs and provide bracing against local buckling of the webs under construction and service loads. On the test specimen, the vertical stiffeners measure 0.625-in. thick by 7-in. wide and are located every twelve feet down the length of the girder.

3.2.3.2 Internal Braces

During construction, unrestrained webs can bend outwards, distorting the cross-section (Figure 3-3) (Gilchrist 1997). In an effort to prevent or limit this mode of deformation, internal K-frame braces are used down the length of each girder with one placed every twelve feet. On the test specimen, the K-frames consist of three steel angles forming a downwards-facing K, as shown in Figure 3-4. The top member is a L5×5×3/8, and the two angled members are L3×3×1/4s. The orientation of the vertical stiffeners is also shown.



Figure 3-3: Bending distortion in unrestrained webs (Gilchrist 1997)

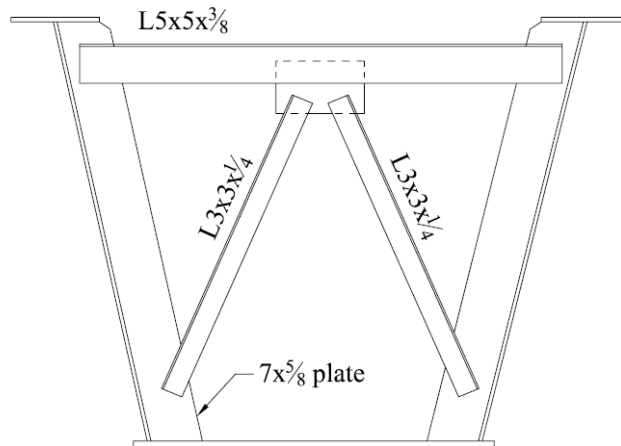


Figure 3-4: Internal brace structural design

3.2.3.3 Top Lateral Braces

One of the strengths of trapezoidal box girders is that, once fully constructed with a composite deck, the section is closed. Closed geometries are extremely stiff against torsion and are thus excellent in curved bridge structures (Salmon and Johnson 1980). However, before the composite deck hardens, an unbraced tub girder is an open section and has very low torsional stiffness. Top lateral braces, which span across the open top of the box, create a semi-closed section and add significant resistance against torsion and warping during deck placement.

The largest stresses the braces should experience occur during construction, as, once the deck is cast, the concrete deck closes the section. A lack of bracing has been cited as the cause of multiple failures during construction (Sennah and Kennedy 2001). The top lateral braces in the bridge tested in this project consist of an alternating pattern of steel L-sections that connect the flanges every twelve feet. A plan view of the bridge and top bracing can be seen in Figure 3-5.

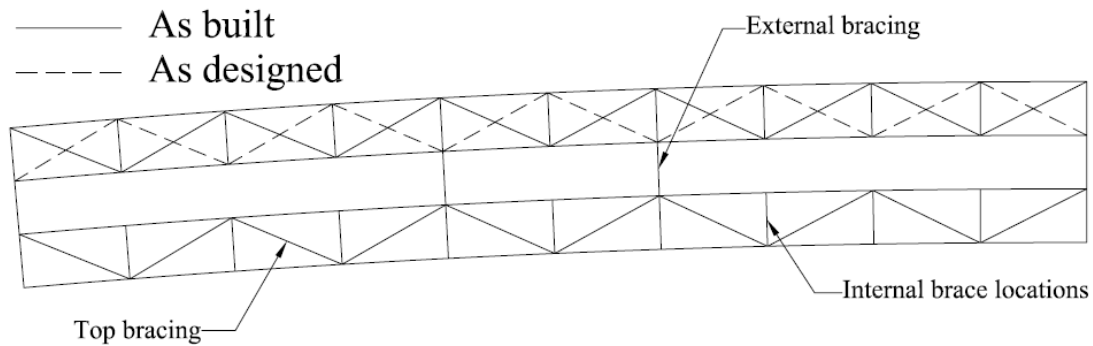


Figure 3-5: Designed and built bracing locations

The top lateral bracing on the bridge highlights the importance of confirming the as-built status of the bridge to the plans: the original plans showed the top bracing alternating direction between the inside and outside girder. When the girders arrived, however, it was noted that the constructed design did not match the original design as seen in Figure 3-5.

3.2.3.4 External Braces

With two girders, each can rotate independently from the other, creating a differential between the exterior top flange on the interior girder and the interior top flange on the exterior girder (Figure 3-6). Unchecked, the differential displacement will result in a non-uniform deck. The analysis program UTrAp (Popp et al. 2004) was used to compute the rotations at midspan for a single girder under load (i.e., half of the bridge used in this study). The rotation across the girder was then used to project an expected differential between the interior and exterior girders for the two-girder bridge. The differential was between 0.25 in. and 0.5 in, or enough to warrant the use of external braces.

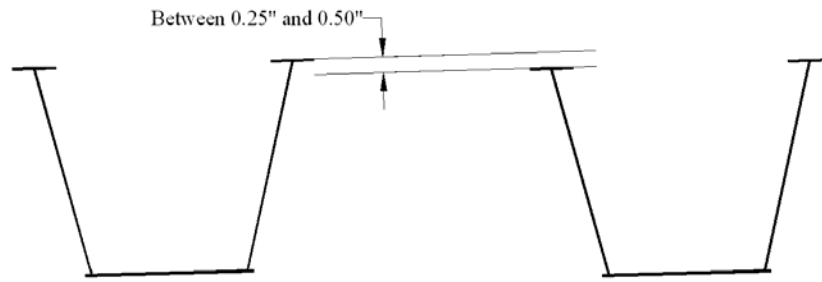


Figure 3-6: Rotation differential during construction (Barnard 2006)

The original bridge was built in Houston with four external brace locations, one every 24 ft down the length. The results from UTrAp showed this bracing layout to be more conservative than what was needed; two would be adequate. The braces were installed 12 ft north and south of the centerline where bolt holes already existed in the web. The two brace points lined up with the internal stiffeners, which minimized web distortion while restricting independent rotation of the girders. The external brace location can be seen in Figure 3-5, and the structural details can be seen in Figure 3-7.

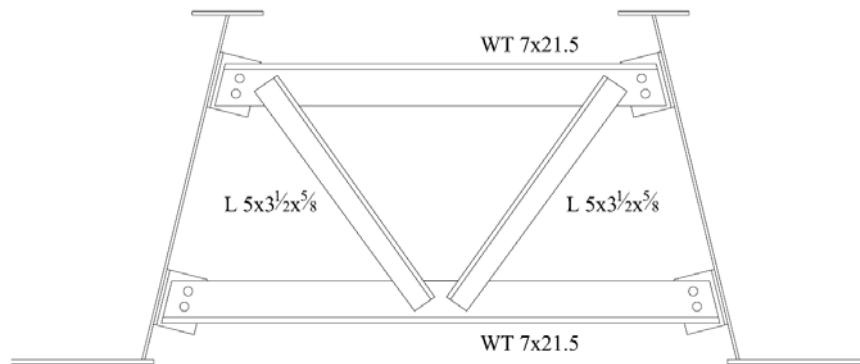


Figure 3-7: External brace structural design

3.2.4 Deck Design

To ensure that the test specimen would closely parallel in situ conditions, the constructed deck and rails matched the original design, were built by an outside

contractor, and were inspected as is standard in the field. The result is a bridge deck and rail system typical of what exists on constructed trapezoidal box girder bridges across the state.

The overall deck dimensions are 23 ft-8 in. in width and 120 ft in length. The design depth is 8 in. with a 3 in. haunch over each flange. This haunch is a typical detail to account for differences in the flange thickness and superelevation of the bridge along its length.

The deck concrete is reinforced with two layers of rebar placed transversely and longitudinally. The rebar profile can be seen in Figure 3-8. The haunch can also be seen above the flange.

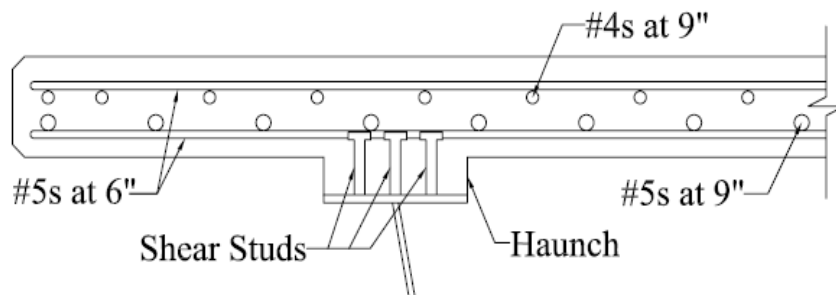


Figure 3-8: Rebar profile in cast-in-place concrete deck

3.2.5 Rail Design

The constructed rails are TxDOT T501 safety rails (TxDOT 2003), measuring 2 ft-8 in. high on the backside and 1 ft-5 in. in total width. As was the TxDOT requirement until recently, expansion joints were included along the length, placed every 30 ft. Meeting this requirement meant placing an expansion joint in the rails at the centerline of the bridge, above the fracture initiation point. The rail profile can be seen in Figure 3-9.

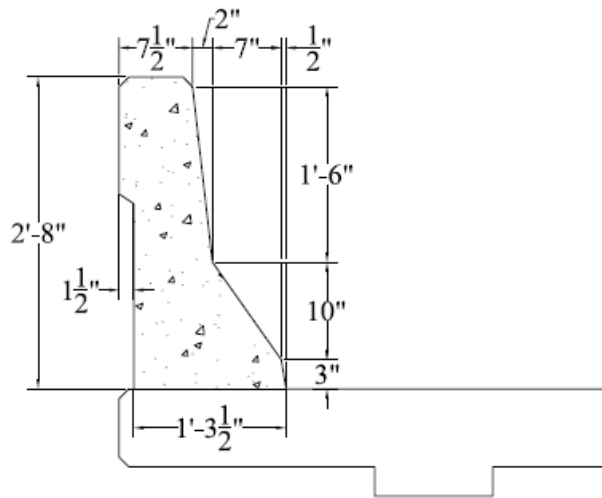


Figure 3-9: Dimensions of T501 cast-in-place rail (TxDOT)

3.2.6 Shear Studs

In composite bridge construction, shear studs are welded to the top flange of the steel bridge girders, and they project into the concrete deck. The primary function of the shear studs is to resist lateral and longitudinal differential movement between the deck and girder. In the case of a full-depth fracture, however, the shear studs are a part of the primary load path for the gravity loads acting on the fractured girder, and they need to resist high tension forces.

The shear studs on the girders used in this project are grouped in threes (Figure 3-8) every 22 in. and are 5 in. in height. Considering the 3-in. haunch, the studs protrude past the top of the haunch and into the deck but do not fully overlap with any of the rebar. The interaction is seen in Figure 3-8, where the top of the shear studs is nearly level with the bottom layer of rebar.

The influence of shear stud interaction with the concrete and rebar of the deck, as well as the tensile pullout capacity, was studied within this TxDOT project. The series of tests run indicate that with a 3 in. haunch and three shear studs across the flange, low tensile strength and very little ductility should be expected (Sutton 2007).

3.3 LIVE LOAD APPLICATION

Current bridge design codes require live load considerations equal to that of one truck, thought to be characteristic of typical loads in length and weight (AASHTO 2004). Because the AASHTO fracture-critical specifications do not clearly state what type, magnitude, or distribution of load must be withstood (Connor et al. 2005), the research team decided with TxDOT engineers that the AASHTO design truck would be an acceptable amount of load.

Because the test specimen was built with the goal of capturing a worst-case loading situation, the variable axle spacing (given as 14 to 30 ft in the AASHTO Specifications (2004)) was set at 14 ft to apply the maximum moment attainable from the truck. The equivalent “truck” was placed 2 ft from the base of the rail, the minimum distance for lane painting as set by AASHTO. Longitudinally, the worst location (in terms of moment induced) was determined using a beam bending equation from the American Institute of Steel Construction (AISC) LRFD design manual (AISC 2001). The manual states:

the maximum bending moment produced by moving concentrated loads occurs under one of the loads when that load is as far from one support as the center of gravity of all the moving loads on the beam is from the other support (pg 3-226).

The bridge specimen was loaded with concrete girders and blocks, representative of the AASHTO HS-20 truck. Using the equation that can be derived from the statement in the AISC manual, the equivalent “truck” was placed with the center axle load 3 ft north of the longitudinal centerline of the bridge. The lighter front axle load was positioned towards the south, 11 ft off centerline; the equivalent rear axle load was placed 17 ft from the centerline. The HS-20 truck is shown in Figure 3-10, and a picture of the concrete girders that provide essentially the same load is provided in Figure 3-11.

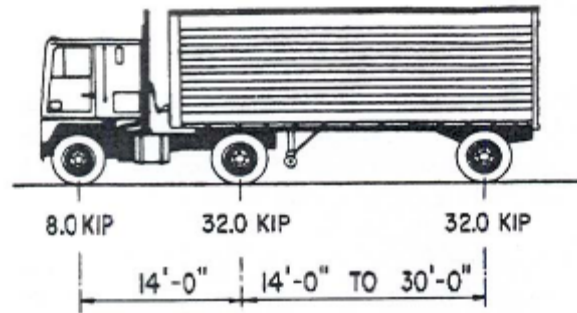


Figure 3-10: Standard AASHTO HS-20 truck (AASHTO 2004)



Figure 3-11: Concrete used to represent the AASHTO truck on the test specimen

3.4 FRACTURE EVENT

A major focus of this research project is to study the response of a steel trapezoidal box-girder bridge during and after a fracture event. The critical step in constructing and running a test is creation and propagation of the fracture.

Most research on fracture uses repetitive loading to mimic the cyclic effects of fatigue: namely, small fatigue cracks at critical locations. Because of the size of the test

specimen and the loads required to create such cracks, creating a fatigue fracture with cyclic loading was not a viable option for this test.

As a relatively easy and repeatable alternative, an explosive charge was placed on the bottom flange of the exterior girder to create a fracture. Although an explosive would cut the steel much faster than a cleavage crack would propagate (by an order of magnitude), both situations create an impulse load over a duration much less than the natural frequency of the bridge, producing a similar fracture load scenario (Williamson 2007, Washabaugh 1994). Once the fracture was initiated, the response of the structure under load in a fractured state could be observed.

3.4.1 Expected Response

The belief of the research team was that the explosive would extend slightly into the bottom of the webs and the increase in stress around the tip of the deformation would propagate the crack through the webs until either the bridge fell or equilibrium was reached. To create an appropriate fracture, the research team worked with explosives consultants from Southwest Research Institute (SwRI), located in San Antonio, to design a test setup. A trial was run with a sample plate and the same explosive intended for the actual test, resulting in a cleanly-cut plate, shown in Figure 3-12. The gold color comes from the copper backing that surrounds the charge before detonation.



Figure 3-12: Cut edge of the trial plate

Because of the shrapnel that results when using such explosives, a containment shield was built around the charge. The day of the fracture event, the area was secured, reducing any chance of injury to persons in the area. The test specimen immediately prior to the fracture event is shown in Figure 3-13. The containment shield, located at the point of fracture, is painted orange.



Figure 3-13: Test specimen, with containment shield in place, 21 October 2006

3.4.2 Actual Response

As expected, the shaped charge had the capacity to cleanly and quickly cut the bottom flange of the exterior girder. What was not expected was the toughness of the web steel and the extra strength that existed in those plates: the fracture did not propagate through the webs. The explosive was designed to cut one inch of steel; this depth was achieved, as both the 0.75-in. bottom flange and 0.25-in. weld were completely severed, as shown in Figure 3-14.



Figure 3-14: Bottom flange, post-fracture

More details of the response of the girders will be given in later chapters; however, it is important to note that the fracture of the bottom flange occurred without the webs fracturing. This fracture event, with the flange but not the webs being severed, is represented in the finite element model detailed in Chapter 5 and influenced the data comparisons given in Chapter 6.

3.5 INSTRUMENTATION

Prior to performing any tests on the specimen, strain gauges were applied on the webs and flanges of the girders and in the deck. A full description of the locations and types of gauges can be found in Barnard (2006), but a brief overview follows.

3.5.1 Girder Gauges

Three cross-sections along the specimen length were instrumented with strain gauges. At two of the cross-sections, there were twelve single-directional foil gauges and six rectangular 0-45-90 rosette gauges; at the third, there were only the rosette gauges. Data were collected on both sides of each plate and then averaged to remove the effects of local plate bending. The cross-sections were located six feet north and six feet south

of centerline. On the south side, both girders were instrumented, whereas on the north, only the interior girder was instrumented. The north cross-section did not include foil gauges. Figure 3-15 shows the longitudinal locations of the three cross-sections; Figure 3-16 illustrates the location around the girder, as well as a sample numbering system for the gauges.

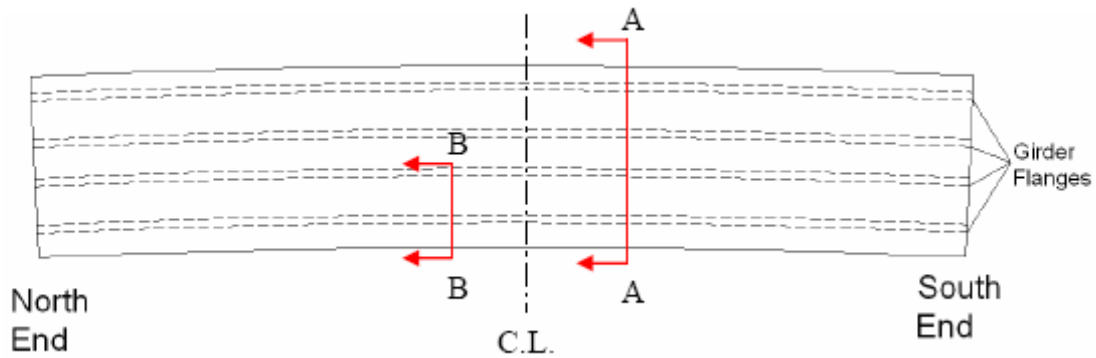


Figure 3-15: Foil and rosette gauge locations, presented in plan view (Barnard 2006)

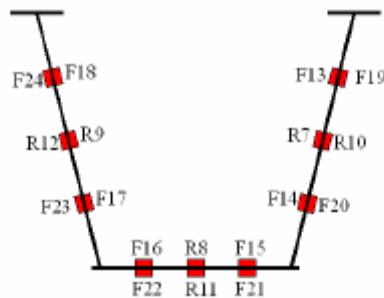


Figure 3-16: Foil gauge (F) and rosette gauge (R) locations within cross-section (Barnard 2006)

Additionally, rosette gauges were placed at the north- and south-end diaphragms in the middle of the plate between the two girders. Two gauges were again used at each location to capture the effect of local plate bending.

3.5.2 Deck Gauges

Prior to casting the deck, members of the research team applied single-direction strain gauges to the reinforcing steel. The gauges were located on the top and bottom layers of rebar, which allows for calculation of the bending forces through the depth of the deck. The gauge locations are shown in Figure 3-17.

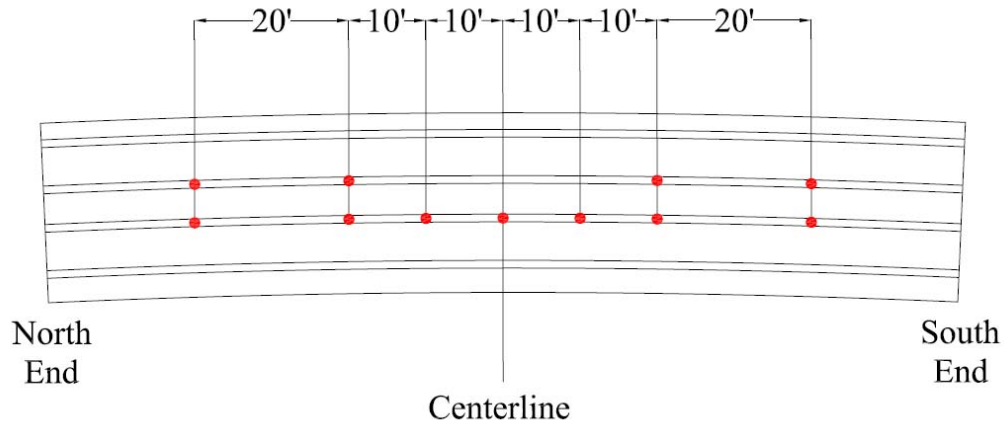


Figure 3-17: Rebar strain gauge locations (Barnard 2006)

Because the shear studs were determined to be a potentially critical detail of the design, there was an interest in gathering tensile data within the studs. These strains were captured using 6-mm bolt gauges that were placed within selected shear studs. The instrumented gauges were located within 22 ft of centerline, with the majority on the exterior flange of the interior girder. The exact locations are given elsewhere, including in Barnard (2006), but the general locations can be seen in Figure 3-18.

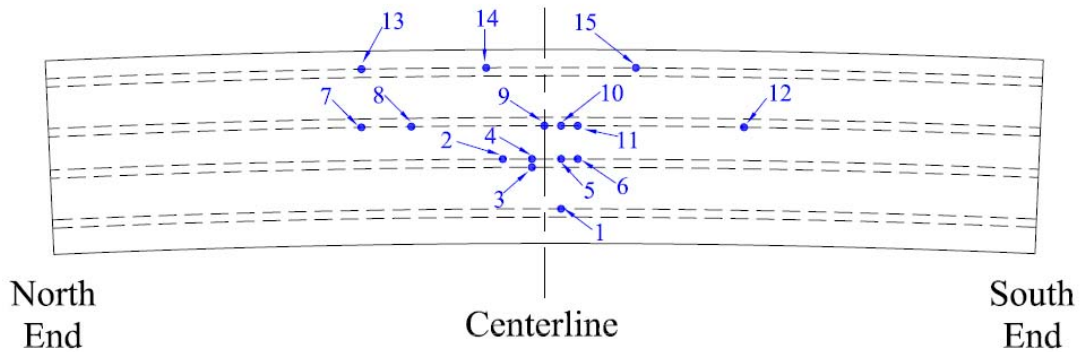


Figure 3-18: Shear stud bolt gauge locations (Barnard 2006)

The correlation between the gauges on the test specimen and elements in the analytical model can be found in detail in Chapter 5. Comparisons of the data from the two sources are in Chapter 6.

3.6 SUMMARY AND CONCLUSIONS

Constructing, installing instrumentation, and testing the full-scale test specimen detailed in this chapter took significant time and expense. Even more so, at the time of this writing, a complete failure state has not yet been achieved, so further resources will be needed to complete the testing plan. Considering the capital needed for a single full-size test, it is clear that repeated trials cannot be performed easily.

Alternatively, a computer model can be used to vary parameters and make predictions of bridge response. During the construction of the test specimen, a finite element model of the bridge was developed in ABAQUS/Standard. Deflections and strains during various stages of construction and testing were compared between the test specimen and the model, verifying the accuracy of the model. The following chapters introduce the finite element analysis program ABAQUS, discuss the formulation of the finite element model, and present the data gathered.

CHAPTER 4

Using ABAQUS for Structural Analysis

4.1 FINITE ELEMENT COMPUTER PROGRAMS

Finite element analysis was developed to estimate the response of a complex structural system under load. While a simple structure can be analyzed accurately using basic mechanics principles, a more intricate problem results in equilibrium, kinematics, and constitution equations that are difficult to solve in closed form. To approximate the response, such a structure can be broken into small, discrete elements whose behavior is well-known (a further explanation of which can be found in Appendix A). Finite element computer programs are designed to combine the effects of the individual elements to estimate overall structural response.

There are several commercially-available finite element modeling packages, including ABAQUS, ANSYS, and LS-DYNA. This project was modeled using ABAQUS/Standard.

4.2 SELECTION OF ABAQUS FOR USE IN THIS STUDY

ABAQUS is a three-dimensional finite element software package consisting of multiple solvers, a graphical user interface, and a post-processor. The programs were developed in their most basic form in the 1980s and have increased in capability since. The most recent large-scale addition occurred in 1999, when the graphical user interface (GUI) ABAUS/CAE (Computer Aided Engineering) was introduced. The programs are in a state of constant enhancement based on feedback from engineers in industry.

One of the primary goals of this project is to develop an accurate model of bridge response that would be reasonable for a practicing engineer to develop. To achieve this goal, many powerful but not widely-used analysis programs and methods were not considered to be viable options. ABAQUS, a commercially-available program that can

run on a Windows-based computer and has been used successfully in other trapezoidal box-girder projects at the University of Texas (e.g. Topkaya 2002) was chosen.

The analyses in this research project were run on a single processor personal computer using ABAQUS 6.6-1, released March 2006, produced by ABAQUS, Inc. in Providence, RI.

4.3 ABAQUS PROGRAMS

There are three main components of the ABAQUS package that work together to process problem statements, run calculations, and present data in an accessible manner: the CAE, the Command, and the Viewer. Each can be accessed from the Start menu on a computer running Windows, as can be seen in Figure 4-1.

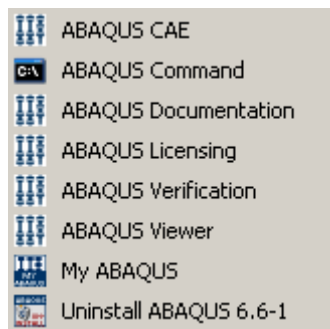


Figure 4-1: ABAQUS menu under Programs in Windows XP (Microsoft 2001)

4.3.1 CAE

The most user-friendly form of ABAQUS is the CAE. The user defines each part of a structure, including material and section properties, then one or more part instances are gathered to form the system. The processor meshes each part based on desired element type and size. The benefit of the program comes from the graphical ability to see each component as it is built.

Behind the visual layer, the CAE assembles an input file that can later be located and modified by the user if necessary. As an alternative, a previously-created input file (.inp) can be imported to the CAE program using File >> Import >> Model. Because the

CAE doesn't have the capacity to handle specific keywords that were desired for this analysis, it was deemed inappropriate for this project.

4.3.2 Command Prompt

There are two solvers available under the ABAQUS heading. ABAQUS/Standard uses an implicit integration method, such as Newmark's method, and is numerically stable for all time step values (although accuracy is lost with large time steps). During each equilibrium calculation, the global stiffness matrix is reassembled, considering material and geometric nonlinearities. ABAQUS/Explicit uses an explicit integration method. Explicit integration considers the contribution of each element individually, thus allowing varying element contributions in each step without iterations. However, explicit integration can be unstable if the time step is not small enough. Further explanation of the difference between implicit and explicit solving can be found in a finite element text such as Belytschko et al. (2006). When using ABAQUS, each solver is called through proper step definitions in the input file.

When running analyses directly from input files, the jobs are started through the ABAQUS Command Prompt, available on the Start menu. The Command Prompt runs like a DOS prompt. The details of running ABAQUS analyses through the Command Prompt are given in Section 4.5.8.

ABAQUS/Standard and ABAQUS/Explicit take text-based input files and run them through a preprocessor and the solver directly. There is no visual representation of the project, so a much more direct knowledge of how the project is defined and how the solver calculates the response is necessary for an accurate and acceptable model. An overview of how to write such an input file can be found in Section 4.5.

4.3.3 Viewer

ABAQUS/Viewer is a subset of the CAE. It does not contain the processing capabilities needed to create a model, but it does include all post-processing options. The Viewer can also be accessed from within the CAE, under the Visualization module.

The Viewer allows for full three-dimensional inspection of the model, graphical presentation of output values at nodes or elements, and animations of response through different load conditions. The calculated values for individual nodes or elements can be found, or the model can be viewed as a whole with ranges expressed through color palettes.

4.4 GENERAL RULES FOR USING ABAQUS

As a starting point towards learning to use ABAQUS, it is a good idea to read through and replicate example problems available in the ABAQUS Example Problem books or study previously written input files on a similar project. When writing code, the ABAQUS User's Manual and Keyword Manual are invaluable tools.

4.4.1 Unit Consistency

ABAQUS has no fixed system of units, requiring the user be vigilant regarding consistency. Establishing a set of units before beginning is important for continuity and accuracy of the model and the results. If starting with an input file that was written by another programmer, it is important to confirm that the units are correct should additions or changes be made.

4.4.2 Project Folder

The ABAQUS solver creates multiple temporary files while running. If using the CAE, these files are generally saved in a temporary folder on the local hard drive. When using Standard or Explicit, the temporary files are located in the same folder as the input file, which is dictated by the user. Of the files ABAQUS writes while running a job, most are deleted when the analysis is complete. There are three important files for monitoring and post-processing, which are detailed further in Section 4.5.9. The first step in running ABAQUS is to create a project folder through which files will be run.

Experience has shown that ABAQUS will run fastest off a local hard drive, so the project folder should not be on a network drive. The folder must also contain an ABAQUS environment file (.env), which can be found on the hard drive of a computer

with ABAQUS installed. Among other things, the environment file defines how much memory the program will ask of the computer. If this amount of memory is less than what the project needs to run, the pre-processor will quit with an error. For this project, it was required to change the default value (512 MB) to a higher value (1024 MB).

4.4.3 Input Files

When using ABAQUS/Standard or ABAQUS/Explicit, the user submits an input file to the solver. The different sections of the input file, described in greater detail in Section 4.5, contain all the specifications of the model and the job to be run. As one character can greatly change an input file (perhaps causing or fixing an error), it is recommended that each draft is saved under a new name. By keeping older drafts, the programmer decreases the chance of losing a functional input file while trying something new.

When keeping each iterative input file, an excellent first step to creating a new file is to distinguish the new version. One way of achieving this distinction is with ***heading**, which assigns a heading to the file that will be printed on all output files and can be used to describe what is being analyzed. The single associated data line can contain up to 80 characters that will be the published heading from the file.

4.5 OVERVIEW OF THE MAJOR STEPS INVOLVED IN USING ABAQUS

Because this project was written and run directly through input files, the methods of writing such a file will be detailed here. This section focuses on the main sections of model definition; specific details and uncommon model keywords for this project will be given in Chapter 5.

To create a physical structure using ABAQUS input files, the main steps are as follows:

- Create a file and folder for the model (described previously)
- Create Nodes
- Create Elements

- Define Section Properties
- Define Material Models
- Define Boundary Conditions
- Enforce Physical Constraints
- Write Load Steps
- Submit the Job
- Monitor Progress of the Job

ABAQUS input files are run using keywords, each of which is prefaced by an asterisk (*) and are marked within this report in **bold**. Each keyword has required and optional parameters that must be included for the program to understand the command. The required parts can be found in the ABAQUS Keywords Manual. Each step discussed below includes keywords that should be used for the necessary definitions.

Certain keywords within a model definition may require certain ordering with others, but in general the preprocessor combines the model information in a way that is compatible with what is needed for calculations. Good programming practice suggests being logical in definitions (for instance, defining nodes before defining elements to connect those nodes), but definitions such as material models can be located before or after elements are created that use the material. The order of sections that follow match those in the input file for this particular project, but they are not necessarily what must be done for the job to run successfully.

4.5.1 Create Nodes

Nodes are defined using ***node**. Especially when analyzing a straight structure, it is generally a good idea to define the model in plane with the global axes. If the global axes are undefined, ABAQUS will use default axes with global 1 being horizontal, global 2 being vertical, and global 3 being into the page. If elements align off the axes, output values will have to be resolved to determine the direct stresses through the element. This situation is shown (for two dimensions) in Figure 4-2. For models where elements do not

align with the default axes, or polar or cylindrical coordinate systems would be more appropriate, the ***system** keyword should be used.

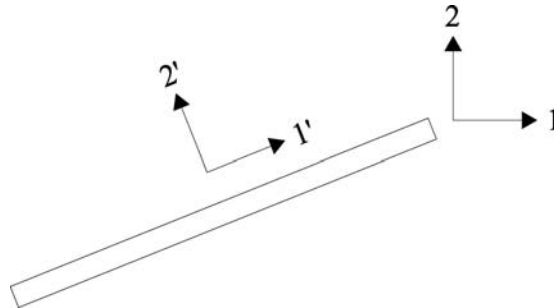


Figure 4-2: Global (1 – 2) and local (1' – 2') axes along an element

In a small model, the coordinates of every node can be included in an input file without much effort or space. However, if the programmer is interested in reducing the clutter in the input file, there are several ways to condense the number of lines needed to define the nodes. One simple and necessary way of grouping nodes and elements is to use the ***nset** and ***elset** keywords to create sets. In creation and manipulation, defining sets removes the need to list every element when defining other properties common to many objects. For node generation alone, ***ngen**, ***nfill**, and ***ncopy** can be used.

4.5.1.1 *ngen, *nfill

The keywords ***ngen** and ***nfill** are used to create nodes based on the locations of certain other nodes. For each keyword command, two nodes or lines of nodes are given, and between them, nodes are created. For instance, the command for ***nfill** might be:

```
*nfill  
line1, line2, 5, 100
```

These lines in the input file would result in five lines of nodes being defined between line1 and line2. The last definition in the card (100) refers to an increase in node number with each additional node. Thus, if the nodes in line1 are numbered 1 through 20, the next rows will be numbered 101 through 120, 201 through 220, and so on. The

location of the nodes will be determined as a percentage of the space between the original nodes, so as to make even divisions.

Both ***ngen** and ***nfill** can define different sets of non-linear nodes – nodes on a circle, for instance, or nodes that geometrically bias towards one end of the set. As one may work better than the other in a given situation, both should be considered.

4.5.1.2 *ncopy

The keyword ***ncopy** copies nodes and is highly useful in the case of a radially swept node layout such as in this project. The first plane of nodes can be defined and then repeated as many times as desired with a given angle between each new plane of nodes. The ***ncopy** command can also be used to extrude an element longitudinally, but ***nfill** requires fewer parameters to do the same thing.

4.5.1.3 *node, input=

One of the optional parameters under the ***node** keyword is the option to input a file of nodes. In a model where many nodes will have to be defined exactly, as opposed to en masse using the previously explained methods, this option can remove hundreds of lines of code from an input file. However, it becomes necessary to maintain an additional file that includes the nodes to be added to the model. A copy of this file must be in the same folder through which ABAQUS will run the job.

4.5.2 Create Elements

Elements are created and generated using ***element** and ***elgen**, respectively. The ***element** keyword parameters include defining the element type and element set. The latter then calls back to section and material definitions, which can be defined anywhere in the input file. It is helpful to gather all material and section property definitions together, rather than with the specific element definition, as each section or material is often used for more than one element set within the model.

There are several different element types available in ABAQUS and most finite element programs. The response of an element type should be considered when choosing

how to model a part of the structure being studied. For more information, see Appendix A, where the response of linearly- and quadratically-modeled beams is presented.

4.5.2.1 *Element Type Nomenclature*

The nomenclature in ABAQUS reflects the type of element and the order of the approximating equation. For instance, a beam element in three-dimensional space (as opposed to planar) with two nodes would be labeled a B31 element (the 1 referring to the linear behavior calculated between the nodes), as detailed in Figure 4-3.

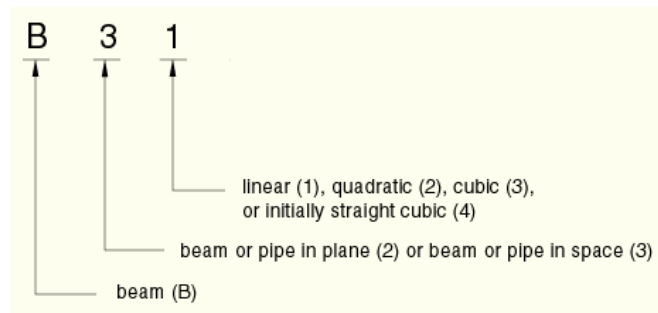


Figure 4-3: Element type nomenclature (HKS, Inc. 2006)

4.5.2.2 *Element Definition*

An individual element is defined using the nodes that comprise it. The most important detail is keeping the order of node definition correct. Incorrect numbering can result in an element that is invalid. Examples of correct and incorrect node numbering schemes are given in Figure 4-4.

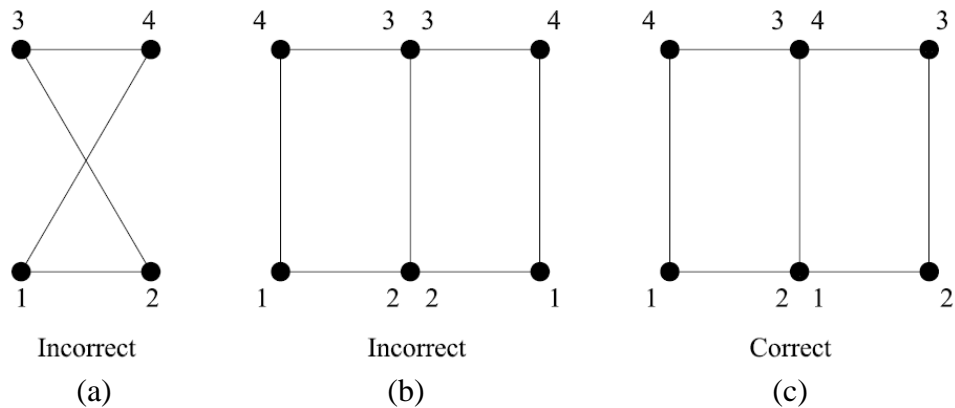


Figure 4-4 Correct and incorrect numbering schemes for a 4-noded element

While Figure 4-4(a) shows clear problems in the defined geometry of the element, Figure 4-4(b) might not be as clear. Both elements defined, while geometrically correct, could cause a problem when applying loads or understanding calculated stresses. Each element type has an “outward normal” associated with it, defined by the node numbering scheme. For beam elements, the normal is perpendicular to the tangent of the element, as shown in Figure 4-5(a). For a shell element defined as those in Figure 4-4(c), the normal comes out of the page.

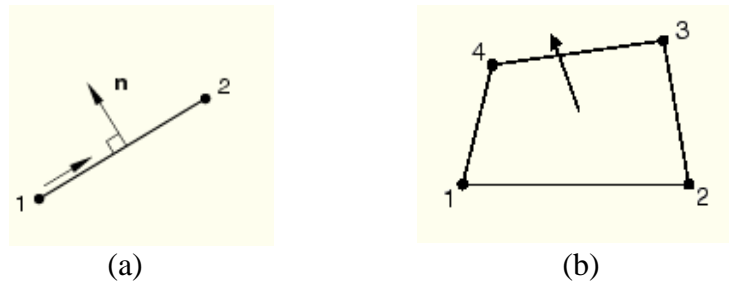


Figure 4-5: Outward normal directions for (a) beam and (b) shell elements (HKS, Inc. 2006)

The normal definitions essentially dictate what direction is considered positive for a certain element. To apply a pressure into the page on the shell elements in Figure 4-4(c), the applied load value would have to be negative. However, for the right-hand element in Figure 4-4(b), the load value would have to be positive. When assigning loads

to a group of elements, consistent normal definitions prevent against alternating global load directions.

4.5.2.3 Element Generation

Once one element is created, it can be copied multiple times with two simple lines of code, so long as the numbering scheme allows for it. It is thus important to determine a logical numbering scheme for nodes and elements. If the numbering scheme is well-established, elements can be generated using ***elgen**. This keyword requires the parent element number, the number of copies desired, and an explanation of how to translate from one to the next through nodes. For instance, consider the following command line:

```
*el gen  
1001, 180, 100, 1
```

This command tells ABAQUS to take element 1001 and copy it 180 times (including the original). The first copy is defined using nodes 100 above those used for element 1001, and the element number of the copy is 1 larger than the original, or 1002. So, if element 1001 was defined using nodes 1-2-3-4, element 1002 would connect nodes 101-102-103-104, element 1003 would connect nodes 201-202-203-204, and so on.

4.5.2.4 Meshing

Unlike when using the meshing tool within the CAE, a written input file requires the user to define individual elements. Thus, to make a ten-foot beam with one-foot elements, the first element would be defined and then nine more generated down the length. When creating the element mesh, it is particularly important for the programmer to consider how many elements will be needed for accurate results.

A model with few elements will run faster than one with a larger number because the total number of degrees of freedom, and hence equations that need to be solved, is a function of the total number and type of elements employed. However, like a circle being drawn with a series of straight lines, fewer elements mean a less accurate approximation of the true response. To confirm that the mesh density is high enough,

multiple trials should be run, each with increasing mesh densities. When successive trials return essentially the same results, the programmer can be satisfied with the chosen number of elements.

It is also important to consider the aspect ratio of individual elements. The aspect ratio compares the longest dimension to the shortest dimension of a given element. For example, a solid element, or brick, with dimensions 2 in. \times 4 in. \times 12 in. would have an aspect ratio equal to 12 in. / 2 in., or 6. If the aspect ratio gets too large, numerical integration of the stiffness matrix will introduce inaccuracies in element stiffness and thus structural response. To prevent inappropriate aspect ratios, when the mesh density is increased in one dimension, it must also be increased in the other dimensions to protect against these numerical inaccuracies.

4.5.3 Define Section Properties

Once an element type is chosen, the section must be defined separately from the element formulation. Section properties are defined using keywords that reflect the type of element assigned to that section. For instance, solids, beams, and shell sections are defined using ***solid section**, ***beam section**, or ***shell section**, respectively. These keywords require parameters such as the material for the section, the element set (***elset**) that contains all elements assigned to that section, and the cross-sectional properties of the section (e.g., area, thickness, or geometry).

4.5.4 Define Material Models

The selection of material models is one of the most critical aspects of defining a structural model for finite element analysis. Especially in cases when loads strain a structure into an inelastic state, it is important to be able to define the material properties appropriately. If doing so is not possible, the results will not accurately predict the response of the real structure, making the model unreliable and of limited use.

That considered, it is also preferable to use materials in their elastic range for computational considerations. An inelastic model requires more time to run than one that

is elastic because nonlinear iterations must be performed, so it is beneficial to only use inelastic material properties when the structure is in fact going to be stressed into this range.

There are no parameters directly required under the ***material** keyword heading. However, the keyword should be immediately followed with others defining the behavior, such as ***elastic**, ***plastic**, and ***density**. Respectively, these keywords define the elastic response, the plastic response, and the density of the material. The lattermost is required if the model load steps will include gravity loading or the inertial effects of self-weight in dynamic analyses. For elements with variations through the depth, as occurs with nonlinearity or composite materials, ***orientation** must be used to define directions for the material and associated elements.

4.5.5 Define Boundary Conditions

Boundary conditions are most often defined using individual nodes (or small node sets). The ***boundary** keyword parameters are the nodes included and the global direction or directions in which a restriction has been placed.

4.5.6 Enforce Physical Constraints

There are other constraints that can come into play in a model besides supports. For instance, springs (defined using ***element**, *type=spring* and ***spring**) are often used to restrict motion while not preventing it entirely.

4.5.6.1 Contact

One of the most calculation-intensive yet frequently necessary parts of a model is the inclusion of contact between surfaces. In a structure, when two surfaces touch one another, forces and stresses develop, and resulting deflections change. Numerically, in a finite element model, planes can pass through each other, unless it is specified by the analyst that they cannot.

The ***contact** keyword establishes boundaries between elements, preventing overlap from occurring. The required parameters are the surface names and an indication

of which surface is the master and which is the slave. Consider a flexible ball hitting a concrete wall: the ball will deflect while the concrete does not. Thus, the concrete wall is the master surface and the ball is the slave. In the case where the two surfaces are of the same material and have equal chances of deforming, it is appropriate to define two matching contact pairs, with each surface acting as the slave and as the master in one. Further discussion on contact pairs can be found in the ABAQUS Theory Manual (2006) or a text such as Belytschko et al. (2006).

4.5.6.2 Multi-Point Constraints

Multi-Point Constraints (MPCs) are most often used in the case of increasing mesh density. Consider the plane where one element comes in from one side, and two go out on the other. For the second side, there will need to be a node in the middle of that plane; for the first there will not. MPCs constrain the midside node so that it moves with the first element, even though the first element does not actively engage the node. This situation is shown in Figure 4-6, where node *p* has been constrained to move with nodes *a* and *b*.

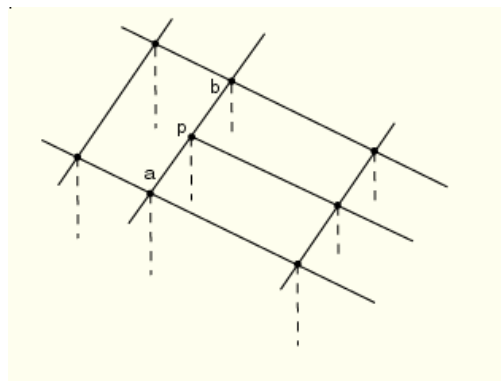


Figure 4-6: Multi-point constraints (type linear) (HKS, Inc. 2006)

To save space in an input file, the MPCs can be written in a separate text file and imported using the *input=* command with ***mpc**. An example multi-point constraint file is provided in Appendix E.

4.5.7 Write Load Steps

The final section of an input file deals with the actual loading of the structure being analyzed. A simple analysis will have one or maybe two load steps; a more complex model could have hundreds, each building off the results of the one before.

The keyword ***step** has several optional parameters. Some of the most important are *amplitude*, *nlgeom*, and *inc*. Both static and dynamic loads can be applied in ramped fashion, or all at once. In modeling, the loading speed is determined with *amplitude=ramp* or *=step*, respectively. “Nonlinear geometry,” or *nlgeom=yes*, indicates that large deflections are expected; the default is *nlgeom=no*. In the case of a load step with a long total time but a small initial time step, *inc=* should be used to increase the total number of increments allowable. The default is 100, and the job will stop at that point, regardless of step completion.

The main keywords below ***step** are the definition of the type of loading, the loads applied, and the outputs. At the end of the step, ***end step** must be included.

4.5.7.1 Static and Dynamic Loading

The first keyword under ***step** should be the way loads are applied; specifically, whether the loads are static or dynamic. Both ***static** and ***dynamic** need initial and total time steps for calculation; if not defined by the user, the program will use defaults. Appropriate time steps are dependent on the model characteristics (such as stiffness and mass) and the response that is desired. The initial and total time steps determine how quickly loads are applied; when non-linear material response is expected, the time step must be small enough to capture all features of the response curve.

In the case where the model cannot converge to a solution with a given initial time step, ABAQUS will automatically change the step in an effort to find a converging solution. The number of times it will sub-increment in this fashion, and the factor by which the time step is decreased, depends on the convergence characteristics of a given case and are problem dependent. The programmer has the option of changing these defaults using ***controls**, if it is necessary.

4.5.7.2 *Load Types*

The most common types of loads are accessed through ***dload**, ***dsload**, and ***cload**, or distributed, distributed surface, and concentrated loads, respectively. With these keywords, an element or node set on which the loads are applied is given, along with a reference direction for the load and a magnitude. In the case of distributed surface loading, a surface is required, which must be defined separately using the ***surface** command. Defining surfaces is one time when the global orientation and proper element node-ordering become particularly important. The former defines what direction positive and negative values refer to, and the latter defines the surface number of an element.

ABAQUS has built in the ability to define certain loads in given directions, such as *BY* being a load in the global Y direction, and *grav* for gravity loading. The load types available are particular to a type of element, and they can be found in the User's Manual definitions of each element. The magnitude and direction of the gravitational acceleration is provided by the programmer, and the solver uses the previously-defined density to apply the correct loads.

4.5.7.3 *Request Outputs*

Upon running a job, multiple files are created. The largest of them, the output database, or .odb file, contains all default outputs available for a given element type, unless it is specified to omit them. However, these results are only viewable through a post-processor like ABAQUS/Viewer. In a load step, the programmer can request certain outputs be written to the data file (.dat). These data can then be accessed directly in a text editor such as Notepad (Microsoft Corp. 2001).

Additionally, simple data collection programs can be written in C++ or another programming language to return desired data from the .dat file. Data will not be written to the .dat file unless directly requested by the user. These requests are made using ***el print** and ***node print**. The required parameters are the element or node set for which data should be returned and the data set desired (such as stresses or deflections in the Y direction).

4.5.8 Submit the Job

When using ABAQUS/Standard or ABAQUS/Explicit, the program is sent to the solver through the DOS prompt shown in Figure 4-7. The simplest manner of doing so is to navigate to the folder where the input file is located (along with all supplementary files, such as the environment file and text files of nodes or MPCs). Then, in the DOS prompt, type:

```
abaqus job=jobname
```

If the job name is the same as the input file (saved as .inp), the solver will automatically read the information from this file. If the job name is different from the input file name, the user will then be prompted for the input file name.

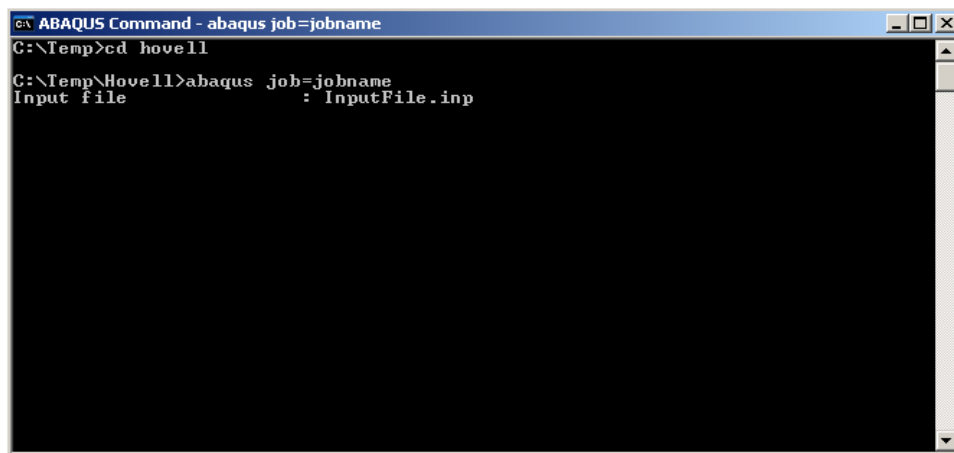


Figure 4-7: ABAQUS Command Prompt window (DOS interface)

4.5.9 Monitor Progress of the Job

While the solver works, there are several files constantly being updated with the progress of the job. Most are illegible to the user, but there are two of importance: the message (.msg) and data (.dat) files. Both can be read using Notepad. The data file details the initial reading of the input file through the preprocessor. If there are problems in the input file, they will be noted here. Additionally, while the solver runs, the data file will be appended with the requested output values. The message file updates with each

iteration within load steps; this file contains information on convergence and completion of the analysis. If the solver aborts with an error, details of the error source can be found in the message file.

4.6 SUMMARY AND CONCLUSIONS

Using a finite element analysis package such as ABAQUS gives an engineer the ability to approximate the response of complex, indeterminate structural systems. This chapter included details of the basic programming information needed to analyze a structure such as a twin steel box-girder bridge. The discussed keywords can be used to define nodes and elements, material models, boundary conditions, constraints, loading steps, and output variables. In Chapter 5, the details of the input file written for this project are given, including material constants, numbering schemes, and load progression.

CHAPTER 5

Details of the Finite Element Model

5.1 INTRODUCTION

When studying system response, multiple full-scale tests are often outside the budget of a single project. Developing an accurate analytical model allows for generalizations and predictions of behavior. In this study, a finite element analysis (FEA) model was programmed in ABAQUS/Standard and calibrated against the full-scale test specimen that was built (discussed in Chapter 3). Once verified, the model can be used to make predictions about the response of other, similar bridges. This chapter details the analysis, including presenting material model definitions, explaining node and element numbering schema, and summarizing the sequencing of the load steps.

Because the long-term goals of this project include creating analysis methods that can be used by an engineer in practice, several restrictions were placed on the FEA design. The first was that the model was to be written in a program that is commercially available and frequently used by engineers. The second was that the analysis would run in a reasonable amount of time (in the range of hours rather than days) on a typical personal computer (PC). A related goal was to model the inelastic material behavior and dynamic load effects simply, so as not to significantly increase the run time of the project or require details of design that are not always easily available. These goals were considered while making decisions regarding modeling techniques, as will be mentioned in the following sections.

5.2 SPECIFICS OF THE ABAQUS MODEL

Two concerns governed the design of the finite element model: appropriate characterization of the real structure and calculation expense, or time needed to run the job. The primary goal was to create a model that would be simple enough to run quickly

on a typical PC, while being complex enough to capture the intricate details of the physical structure. This section explains the model that resulted. The section ordering approximately matches the order of definitions within the final ABAQUS input files. A complete input file can be found in Appendix B.

Significant detail is given in the following sections regarding the numbering methodology for both the nodes and the elements defined in the analysis. The scheme for the nodes was designed to take advantage of ***elgen** in element definition as well as indicate the spatial location of nodes. The elements are numbered to easily identify the part of the structure being defined (webs, bracing, deck, etc.) and again, the spatial location of the element.

5.2.1 Define Nodes

A finite element model is constructed of elements spanning between nodes. The first step in an analysis is thus to define the nodes, or the geometry for each element in the model. In a three-dimensional analysis, each node introduces three or six degrees of freedom, or equations, to the problem. To reduce the number of equations the program must solve, it is desirable to have as few nodes as possible. However, a higher mesh density (smaller elements) requires more nodes. The analyses performed in this research have been designed to reach a balance where the mesh density is high enough to capture an adequate approximation of response while being low enough for the job to run quickly.

In each direction – vertical, longitudinal, and transverse – nodes are defined to replicate the geometry of the full-scale structure and allow for accurate calculations within ABAQUS. The number of nodes needed in each direction and the spacing of each is dependent upon the geometry of the section and the element density required. For instance, nodes were needed along an inclined plane to represent each web, and four to sixteen elements were required through the height of each web to adequately capture bending and fracture response.

The nodes were originally defined using one vertical plane and then sweeping it radially down the length of the bridge using ***ncopy**. When it was determined that the mesh density would have to increase in all directions at the rail gap locations and the fracture site, the programmer switched to individual node definitions: certain nodes were defined in Microsoft Excel (Microsoft Corp. 2003) based on physical position, then the remainder were filled in using formulas in Excel and the ***ngen** feature in ABAQUS.

In the system adopted for this research, individual node numbers are seven digits long, in the form LLLVVTT, where L represents a longitudinal locator, V vertical, and T transverse. The transverse node numbers increase from left to right (with left being the inside of the interior girder) from 00 to 37, as shown in Figure 5-1. Thus, for instance, all nodes on the most interior web will be defined with a transverse node number 08.

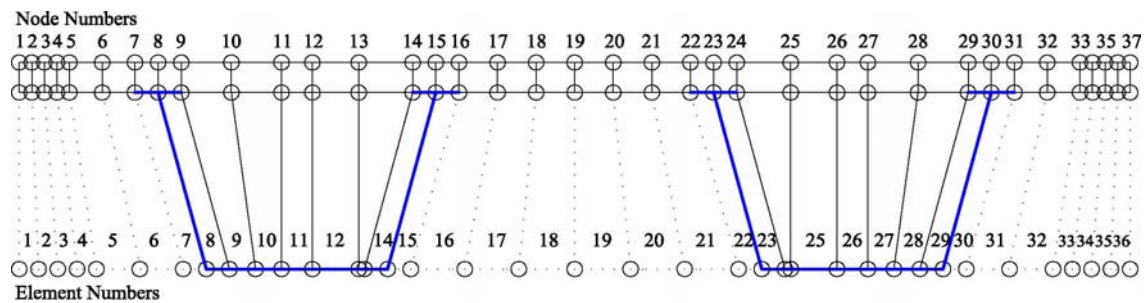


Figure 5-1: Node numbering scheme transverse to the girder profile (girder boundaries marked with a bold blue line)

Vertically, the nodes increase by one hundred with each row through the haunch, deck, and rails. In the girders, the nodes increase by 50, meaning the number in the tens location can also change with vertical location. There are two levels of nodes where the top flanges and deck haunches intersect that to allow for shear studs to be placed between the two surfaces. For example, using this scheme, all nodes with 19 in the vertical placeholders (hundreds) can be found on the top surface of the deck. A cross-section showing some of the boundary lines is given in Figure 5-2.

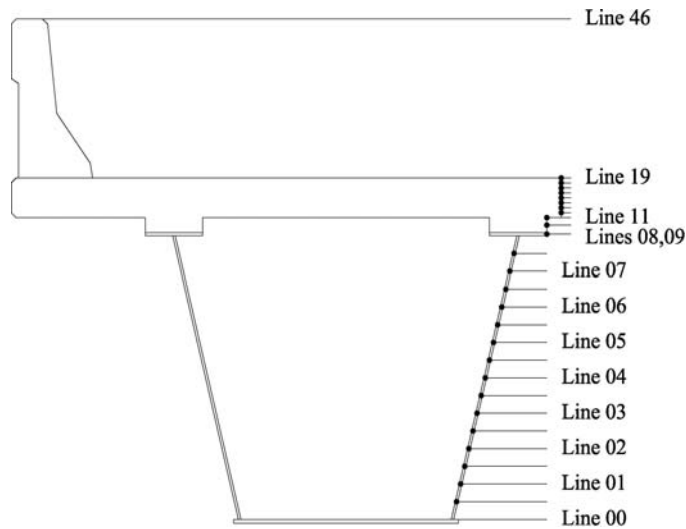


Figure 5-2: Node numbering scheme vertically through the girders, deck, and rails

The longitudinal location is reflected in the first three digits of the node number. In this direction, the node numbering is less straightforward than in the transverse and vertical directions. With each plane of nodes, the node numbers increase by 10,000. Initially, node numbering corresponding directly with length (i.e., node 54xxxx would be located 54 ft down the length of the bridge). As the need for increased mesh density developed, this system of numbering became impractical. With 180 node locations down a 120 ft bridge, the longitudinal locations of each node can be found in Appendix C. Using Appendix C and the numbering schemes given above, a node can still be located using just its number. For instance, node 0710373 is located at 51 ft-0 in. longitudinally, just below halfway up the internal web of the external girder:

LLL = 071, or 51 ft-0 in.

VV = 03, or approximately mid-height

TT = 73, or 23 + 50, indicating the internal web of the external girder, one line of nodes above the 03 line shown in Figure 5-2.

The leading zero does not need to be included; node 0710373 is the same as node 710373.

5.2.2 Restrain Movement

The test specimen is supported on four neoprene pads that allow for rotation and small longitudinal movement. Rather than model the stiffness of the bearing pads exactly, the model is supported on a pin at one end and a roller at the other. This support mechanism allows the modeled bridge to elongate without inducing stresses.

As a precaution against numerical problems due to transverse instability, a horizontal spring (element type *spring1*) connects the outside of the exterior girder with a fixed node in space. The stiffness of the spring is enough to prevent the girder from effectively pushing off its support, without being large enough to draw forces to it.

5.2.3 Assign Section Properties

As described in Section 4.5.3, section properties define the characteristics of a group of elements. In section property definitions, element sets are assigned to a material type and given a common geometry. Thus, solid elements of material *concrete* and *railconc* must have unique section property definitions, as must shell elements of thickness 0.5 in. and 0.75 in.

The finite element model presented here used seventeen different section definitions. Although some could have been combined, keeping the groups separate allows for transparency in the coding: section properties are easily associated with the corresponding elements. The specific section definitions and related properties used in this analysis are given in Table 5-1.

Table 5-1: Section properties definitions

elset	Elements involved	Element Type	Material	Properties
webs	Four girder webs	<i>s4r</i>	<i>steel</i>	$t = 0.5$ in.
botflange	Two bottom flanges	<i>s4r</i>	<i>steel</i>	$t = 0.75$ in.
topflange	Four top flanges	<i>s4r</i>	<i>steel</i>	$t = 0.625$ in.
diaphragms	End diaphragms on both girders, including top flanges and between the girders	<i>s4r</i>	<i>steel</i>	$t = 0.5$ in.
diaphvert	Vertical stiffeners on four end diaphragms	<i>s4r</i>	<i>steel</i>	$t = 0.625$ in.
vert	Vertical stiffeners welded to webs	<i>s4r</i>	<i>steel</i>	$t = 0.625$ in.
deck	Deck elements, including haunches	<i>c3d8r</i>	<i>conc</i>	–
fakedeck	Spacer elements used for accurate deck definition	<i>c3d8r</i>	<i>fakeconc</i>	–
rails	Rail elements	<i>c3d8</i>	<i>railconc</i>	–
fakerails	Spacer elements used for accurate rail definition	<i>c3d8</i>	<i>fakeconc</i>	–
intruss	Interior K-frames	<i>b31</i>	<i>steel</i>	Geometry of steel angle
toptruss	Top bracing frames	<i>b31</i>	<i>steel</i>	Geometry of steel angle
extruss	External bracing frames	<i>b31</i>	<i>steel</i>	Geometry of steel angle
bigtrans	Truss elements accounting for two transverse reinforcing bars	<i>t3d2</i>	<i>rebar</i>	$A = 0.62$ in. ²
smalltrans	Truss elements accounting for a single transverse reinforcing bar	<i>t3d2</i>	<i>rebar</i>	$A = 0.31$ in. ²
botlong	Longitudinal bottom rebar	<i>t3d2</i>	<i>rebar</i>	$A = 0.31$ in. ²

Table 5-1: Section properties definitions (cont'd)

elset	Elements involved	Section Type	Material	Properties
toplong	Longitudinal top rebar	<i>t3d2</i>	<i>rebar</i>	$A = 0.20 \text{ in.}^2$
railrebar	Longitudinal rebar in the rails	<i>t3d2</i>	<i>rebar</i>	$A = 0.20 \text{ in.}^2$
fakedeckrebar	Spacer elements for deck rebar definition	<i>t3d2</i>	<i>fakerebar</i>	$A = 0.01 \text{ in.}^2$
fakerailebar	Spacer elements for rail rebar definition	<i>t3d2</i>	<i>fakerebar</i>	$A = 0.01 \text{ in.}^2$

5.2.4 Define Material Models

This analysis uses three key materials: concrete, steel, and a spacer material. The definitions of each aim to match the true properties of the bridge; details are given in the following sections. A summary of the properties of the material models is given in Table 5-2. The ***elastic** keyword parameters are the elastic modulus of elasticity and the Poisson's ratio. A curve defining the relationship between inelastic stresses and strains is given under ***plastic**, with the first term being stress (in ksi) and the second term, plastic strain. These curves are shown graphically in each material section (Figure 5-3 Figure 5-4). The density of the material is the only parameter given for ***density**. To maintain unit consistency, densities are given in slug/in.³.

Table 5-2: Material model definitions

Material	*elastic (ksi, in./in.)	*plastic (ksi, in./in.)	*density (slug/in ³)
<i>conc</i>	3875, 0.2	3.09, 0 3.77, 0.0004 4.28, 0.0008 4.84, 0.0018 4.50, 0.0027 3.05, 0.0034	2.4576×10^{-7}
<i>railconc</i>	3000, 0.2	–	1.9225×10^{-7}
<i>rebar</i>	29000, 0.3	–	7.33863×10^{-7}
<i>steel</i>	29000, 0.3	50.086, 0 51.0, 0.01804 62.4, 0.03707 70.2, 0.07454 71.5, 0.09284 65.0, 0.4	7.33863×10^{-7}
<i>fakeconc</i>	0.1, 0.2	–	1×10^{-15}
<i>fakerebar</i>	0.1, 0.3	–	1×10^{-15}

5.2.4.1 Concrete

The properties of the concrete used in the full-scale test specimen were obtained using 6 in. × 12 in. test cylinders. During the deck and rail pours, concrete taken from each truck and was used to cast twelve cylinders per truck. The cylinders were then broken at various times after the casting, including after 28 or 29 days. Each cylinder, made from concrete designed to be 4,000 psi in compressive strength, tested above 4,600 psi (Barnard 2006). The modulus of elasticity was calculated from the compressive strength using the equation given in 8.5.1 of ACI 318-05 (ACI 2005):

$$E = 57000 \cdot \sqrt{f'_c} \quad (1)$$

where

E = modulus of elasticity of the concrete, in psi

f_c' = compressive strength of the concrete, in psi

Because reinforced concrete does not behave linear-elastically, with the concrete easily cracking in tension and load being transferred to the reinforcing steel within, there are two general ways of modeling the behavior. The first is to use smeared properties, giving the material strength in compression and in tension that represents the overall behavior, but not the exact response of the concrete or rebar individually. The second is to model each material on its own, allowing the concrete to fail in tension and the rebar to hold the tension forces.

Most simply-supported composite bridges will never have tension in the deck; the neutral axis lies below the top flange of the girder. In the fractured state, however, it is expected that the girder will be completely compromised, moving all response into the deck and rail system. Because the deck will then experience both tension and compression because of localized bending, the stresses in the transverse and longitudinal rebar were a point of interest and thus needed to be modeled individually. Details of the rebar modeling and the material model can be found in Sections 5.2.5.4 and 5.2.4.3, respectively.

Multiple concrete models were evaluated during this research project, including the elastic-plastic model detailed in Table 5-2 and a more detailed, cracked concrete model that used the keywords ***concrete damaged plasticity**, ***concrete compression hardening**, ***concrete tension stiffening**, ***concrete compression damage**, and ***concrete tension damage** in an attempt to capture the cracked response more accurately than the simplified smeared model. The elastic-plastic model was eventually chosen because of the transparency it provided within the input file code. The stress-strain curve defined by the ***plastic** model is shown in Figure 5-3.

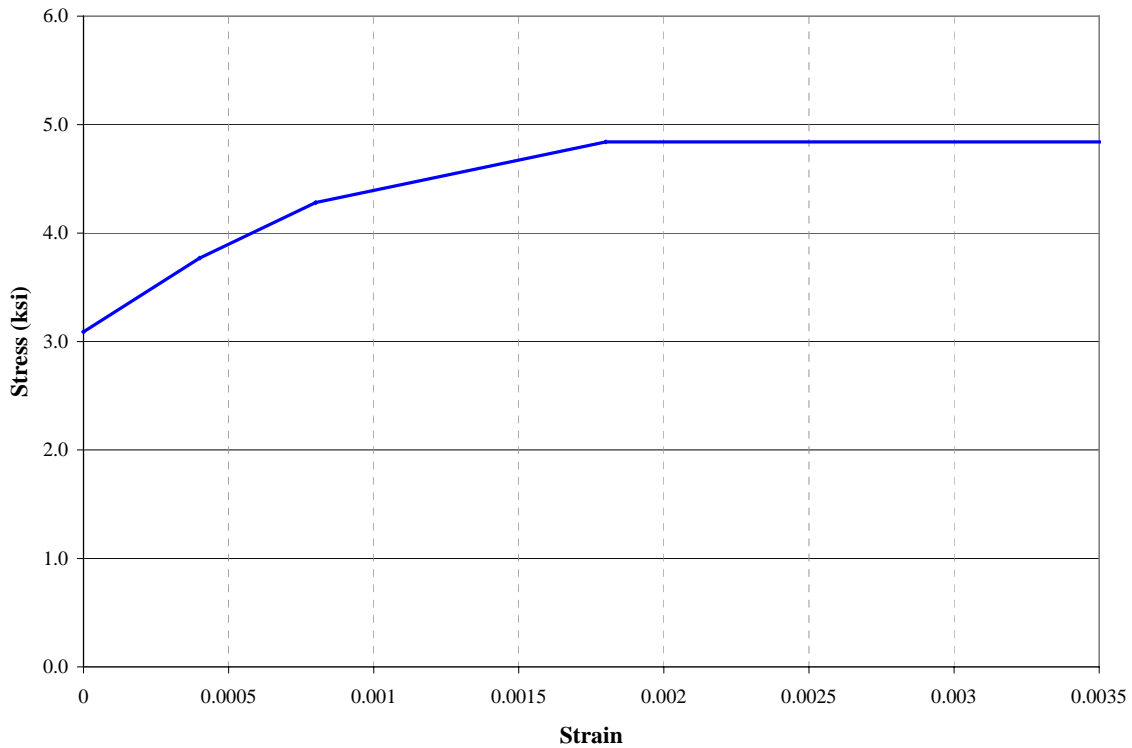


Figure 5-3: Concrete material model stress-strain curve for plastic response

While the plastic behavior shown in Figure 5-3 is a simplified approximation of the concrete response, the zero stiffness that occurs beyond a strain of 0.0018 is appropriate for cracked concrete, which can hold no additional load. The result of using this model for the concrete response will be that the loads can not be resisted by the concrete elements and will be resisted by the rebar, which is the desired phenomenon that the model attempts to capture.

Further study and modification to the concrete model is of paramount importance to this research, as the concrete deck will likely be the contributing component able to provide redundancy for the fractured structure. If the concrete cracks or crushes and the rebar is unable to hold the forces that result, it is doubtful that the structure will remain standing. Continued discussion on the future of concrete modeling within this analysis can be found in the recommendations for future research presented in Chapter 7.

5.2.4.2 *RailConc*

The concrete material model used for the rails is slightly different than the one used for the deck. Rather than using the actual material properties, an adjustment was made to account for geometry differences in the model relative to the actual rail. The actual rail profile, shown in Figure 3.9, is complex geometrically and would require a very fine mesh to capture its intricacies. Instead, the rail was modeled as a rectangular box, as is detailed in Section 5.3.1. However, the goal was to have an overall response equivalent to that of the real rail.

To account for the differences, an equivalent Young's Modulus was assigned to the material *railconc*. The modified modulus was calculated using the stiffness of the real rail (using the true moment of inertia and the true modulus of elasticity) and dividing by the moment of inertia of the modeled rail section:

$$E_{equivalent} = \frac{E_{real} \times I_{real}}{I_{equivalent}} \quad (2)$$

Considering the location of the centroid and the geometries of the sections, the equivalent *railconc* modulus of elasticity used was 3,000 ksi. Like in the deck, the rebar was defined explicitly, as preliminary analyses with an elastic rail showed that cracking was likely around the expansion joints. While it is expected that the rebar will alter the overall stiffness of the rail section, the influence was assumed to be small and was thus not considered in calculating the equivalent modulus of elasticity.

5.2.4.3 *Rebar*

The rebar was modeled using three-dimensional linear truss elements, explained further in Section 5.2.5.4. The material model definition matches that of rebar samples that were tested in the laboratory following the casting of the deck (see Barnard 2006). The modulus of elasticity measured just over 30,000 ksi; a conservative value of 29,000 ksi was used per Section 8.5.2 of ACI 318-05. Inelastic material properties were not considered because the stresses in the rebar were not expected to exceed the measured yield stress of approximately 70 ksi.

5.2.4.4 Steel

Obtaining accurate properties for the steel in the test specimen was more difficult than for concrete, as running tests would involve cutting a sample from the girders. Not wanting to compromise the structural integrity of the bridge, these tests were not performed. Instead, design values for steel strength and plastic response were used. The stress-strain profile defined in the input file is shown in Figure 5-4. The plastic behavior definition comes from a preliminary study of fracture response at the University of Texas.

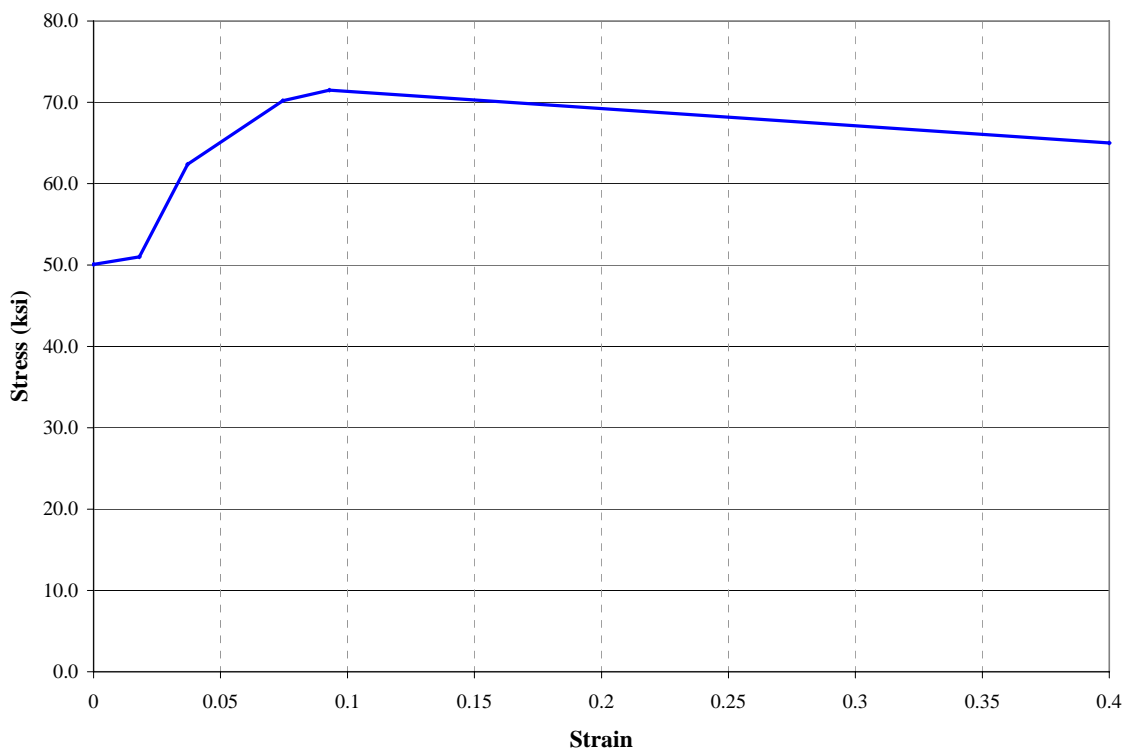


Figure 5-4: Steel material model stress-strain curve for plastic response

Because the inelastic behavior of a steel member varies with the manufacturing and fabrication process (considering, for instance, residual stresses from welding), the plastic properties of the steel in the test specimen are not known exactly. Thus, the steel model in the analysis is not based on the test specimen.

5.2.4.5 Spacer Material

The execution of the analytical model begins with dead load application of the girder upon itself and steps through to the fracture of the bottom flange. In between are steps involving the casting of the deck and rails. Because these elements cannot contribute to the overall stiffness of the structure before the concrete hardens, the elements cannot be in place while the load is applied. However, with no elements in place, the nodes involved in the deck definition do not move with the rest of the structure.

To shift the nodes appropriately, “fakedeck” and “fakerail” elements were used. These elements were defined from the beginning of the model, with the same nodes that define the “real” deck elements. Thus, when the “fake” elements deflected with the girder below, the nodes displaced compatibly with the girder. The material *fakeconc* was defined with almost no stiffness ($E = 0.1$ ksi) and very low density (1×10^{-15} slug/in.³), so that the elements do not influence the response of the structure. Had this step been omitted, upon reactivation, the deck elements would connect the top flange nodes – which moved with the dead load deflection of the girder and deck – with the originally defined nodes. The resulting stretched elements can be seen in Figure 5-5, where the bottom haunch elements reflect the parabolic shape of the deflected girder below.

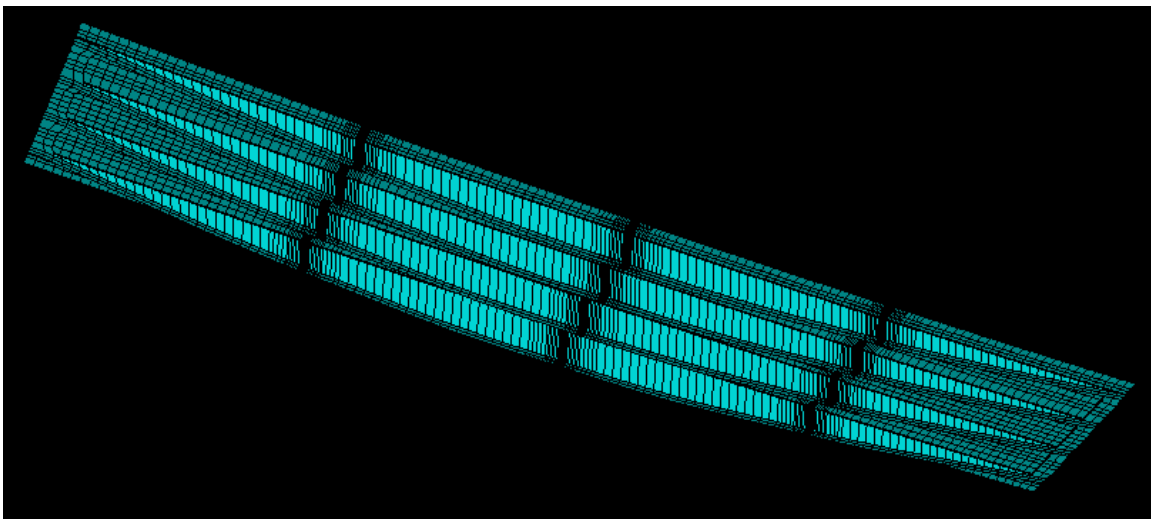


Figure 5-5: Stretching of the deck elements upon reactivation without using fakedeck elements (scale factor = 10)

Alternatively, the model could have been written and run in a series of individual jobs, each outputting the coordinates of each node. For instance, the first job would run through the dead load application of the girders and uncured deck. The displacement values would then need to be post-processed to alter the original node locations and input into the next job (through the curing of the rails). The nodes constituting the deck elements would be extrapolated from the girder nodes by adding the appropriate height differential.

One drawback of this method is the time and attention needed to ensure the nodes are modified correctly. The current model nodes are created using a Microsoft Excel spreadsheet with approximately 100,000 nodes explicitly defined. If even one node is redefined incorrectly, the resulting elemental geometries could cause an error in processing (e.g., if a misplaced node created an element with a zero volume or a distorted geometry). A second drawback is that the second job would need to include the strains accrued during the first job, so as to reach plastic strain levels at the appropriate time. This compatibility concern would again require significant post-processing and additional lines of code.

The fake element system thus becomes a simple way of capturing the response of the bridge during various load stages. To ensure the fake elements were not influencing the data, multiple models were run with and without the fake elements and with various values for the modulus of the spacer material. The deflections and stresses calculated with and without the fake elements, and with multiple values for modulus of elasticity in the *fakeconc* material model were compared, and the method was determined to be acceptable (see Chapter 6).

While not necessary in the deck, where the rebar aligns with existing nodes throughout (and thus with *fakedeck* elements), the rail rebar includes nodes not always used in rail element definition, thus requiring the use of spacer elements for the rebar, as well. The method described above was used again; the material definition “fakerebar” was included, with similar (non-influential) material properties, and assigned to the “fake” rebar elements.

5.2.5 Define Elements

As explained in Section 4.5.2, element sets can be created by defining a single element and then generating additional similarly oriented elements using ***elgen**. This method was used extensively for girder, bracing, and deck element definitions.

One of the more difficult things to recognize upon looking at the input file written by a different programmer is learning the node scheme used. The node numbers were explained in Section 5.2.1; the following sections include the schema for the element sets forming the structure. The longitudinal locations again require referencing the table of locations given in Appendix C. This table will be useful for future data analysis from the output and data files, where results are given in terms of element or node number.

5.2.5.1 Girders

Considering trapezoidal box girders are welded thin plates, using shell elements to represent the girder webs and flanges is an appropriate choice. Both eight- and four-noded elements were considered. Small parametric studies showed deflections varied negligibly between eight- and four-noded elements, so four-noded elements were selected for this study.

One of the drawbacks of finite element modeling is that a continuous section is being represented with a finite number of elements. Consequently, because of this constraint, finite element models are stiffer than the actual structure they represent. In contrast, reduced integration elements, which intentionally introduce numerical inaccuracies in approximating response, underestimate the stiffness of a given element. The underestimation of stiffness introduced by reduced integration occurs in similar proportions to the overestimation of stiffness inherent in all finite element models, and these two phenomena are generally accepted to offset each other (Belytschko et al. 2000). When initial deflection calculations from the model were less than what was observed, the decision was made to switch to *s4r* elements, four-noded shells with reduced integration.

Initial model definitions included two elements across each top flange, four down the webs, and seven across the bottom flange. The webs were soon altered to include seven elements, and then further changed to include a mesh density increase near the fracture site, changing from eight elements at the ends to sixteen in the midsection.

As with the node numbering, each element must be numbered individually. A node and element can have the same number, as the two will be referenced separately. In general, the element numbering scheme includes at least two leading digits that represent the location across the cross-section, then three digits at the end indicating the longitudinal location. This scheme can be represented by TTVVVV, where the T's indicate cross-sectional or transverse location (a top flange element, for instance) and VVV indicate longitudinal location. The longitudinal location numbers are the same as for the nodes, and can be found in Appendix C. It should be noted that Element 001 connects nodes 0 and 1; the element number is reflected in the second node number.

The element numbering longitudinally for the girders increased by one with each element. The numbers vertically and transversely for the interior girder can be found in Figure 5-6. The values given refer to two T's in the definition above. The exterior girder elements are increased by 100,000. For demonstration, an element in the middle of the external web of the external girder 29 ft down the length would be numbered 130034.

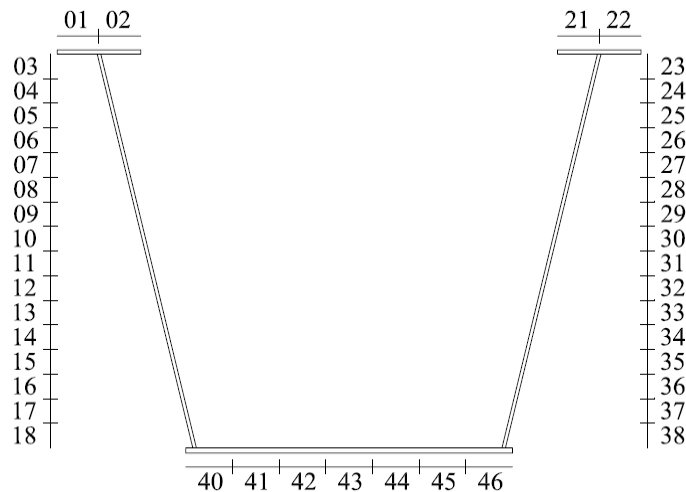


Figure 5-6: Element numbering around internal girder; the interior edge is to the left

5.2.5.2 *Stiffeners and Bracing*

The vertical stiffening plates, being constructed of steel plates welded to the webs, are modeled the same way as the main girder elements, with *s4r* shell elements. The number of elements vertically matches the number of web elements, for continuity in the shared nodes. The same elements were also used for the end diaphragms of each girder and between the girders, as well as the vertical stiffening braces that exist on the diaphragms.

The three brace types – internal K-frames, top lateral bracing, and external braces – are modeled using beam elements. As explained in Appendix A, beam elements should be much longer down their length than in any other dimension, so a single element was used to span between three and seven feet. The cross-sectional dimensions of the angles and T-sections that constituted these frames were used to define beam cross-sections (*section = arbitrary*). While not exactly the same as what exists in construction, this modeling method was considered accurate enough considering the focus of the study was not on the response of bracing, and the beams were not expected to be strained excessively during construction or loading. Truss elements were also considered, as the main loads on the members will be axial. However, truss elements have no out-of-plane stiffness, which could have caused numerical problems during the fracture step. The authors of UTrAp (Popp et al. 2004) chose to create stiffness by including springs out-of-plane at each brace member end; in the analysis presented here, beam elements were chosen to capture more detail of the response of the elements, including bending across the girders and through the depth.

The numbering scheme for the stiffeners and bracing was designed to incorporate location, but more so, to group elements within the same system together. Thus, the internal truss elements begin with 58,000, the top truss elements with 59,000, and the web stiffeners with 60,000 and 61,000. Again, the elements in the external girder used the same numbers, except increased by 100,000. The external brace elements, which exist between the girders, are indicated with element numbers starting with 63,000.

5.2.5.3 Deck

Using previously-written models of similar bridges as a guide, preliminary models of this box-girder system were written using shell elements for the deck. Because of their similar formulation, shell elements would allow easy use of beam elements for the rails and would correspond well with the shell elements forming the girders. When the deck haunch was determined to be a detail of interest, the shells were no longer able to appropriately model the response, and the deck was defined with solid “brick” elements.

As in modeling the girder, both linear and quadratic approximations of deflection through the element were considered. When the girder elements were reduced from eight- to four-node elements, the deck was changed from twenty-node to eight-node bricks, or *c3d8* elements. The two element types (solids and shells) do not use the same order functions to define their edges, so the boundary between the two elements will not correspond exactly without adding constraint equations to the problem. However, by placing nodes at the same location, the deflections at those nodes are the same and the differences along the boundaries are minimized.

To capture the response within the haunch, two elements were used through the three-inch depth. The deck, another eight inches in thickness, was modeled with eight elements. Although this geometry resulted in an aspect ratio as high as 12, the thin solids were used to capture the bending behavior through the depth. Fewer elements would have created a stiffer section that could not bend the way the true deck was expected to deflect under failure loading. At each expansion joint location, the longitudinal spacing of elements was reduced, decreasing the maximum aspect ratio to about 6. The ratio could be decreased further if more elements were added across the width.

Because there would be so many deck elements created (over 50,000), the numbering scheme began with an extra digit for definition. All deck elements begin with a 3 while the associated “fakedeck” spacer elements begin with a 4; the other digits are the same between the fake and real deck elements. Longitudinally, the deck elements increase by 1,000; vertically, they increase by 100, and transversely, by 1. Combining

these rules, a deck element has the form 3LLLVT. The deck element 105 ft down the bridge, on the bottom row of elements, above the innermost flange would be numbered 3165207. The bottom row of deck elements has a 2 in the hundreds spot because the two rows of haunch elements use 0 and 1.

5.2.5.4 Rails

The rails were modeled using *c3d8* elements. Unlike the elements used in the deck and girders, *c3d8* are not reduced integration elements. The change to full-integration elements was made when hourglassing was seen in the rail elements during the fracture steps (Figure 5-7). Hourglass mode shapes occur as a result of reduced integration, where fewer integration points are used to approximate the response of an element than in full integration. With fewer integration points, deformation of the element can occur while the calculated strain is zero, creating a repeating hourglass shape in the elements. Changing the rail elements to *type=c3d8* (full-integration) removed this problem. For more information on hourglassing, see Appendix A or Belytschko et al. (2006).

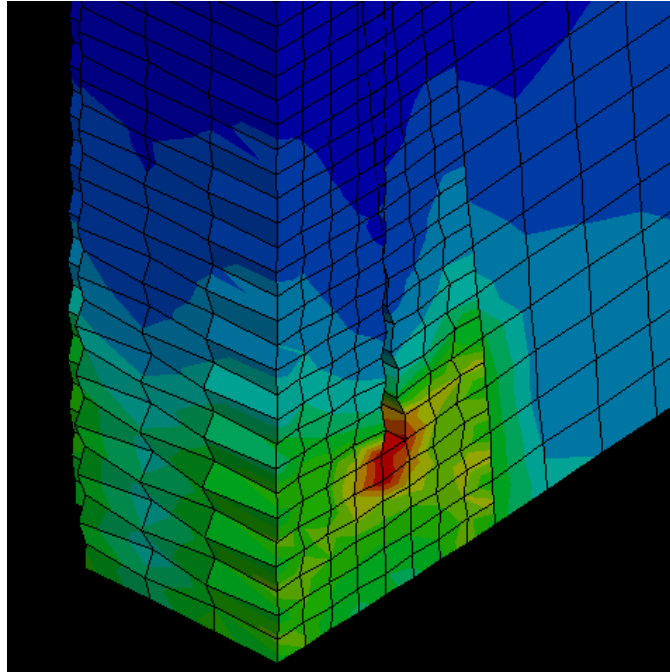


Figure 5-7: Stresses in the rail during fracture, magnified to show hourglassing in the reduced integration rail elements

The rail numbering scheme is similar to the deck, with seven digits defining each element. For the “real” elements, the first digit is always a 5; for the “fake” elements it is a 6. The following six digits are of the form LLLVVT; three to describe the longitudinal location (as used previously, and defined further in Appendix C); two to give vertical position, from 1 to 28; and one for transverse location: 1 through 4 for the interior rail and 5 through 8 for the exterior rail.

5.2.5.5 Rebar

The rebar layers defined within the concrete deck – longitudinally and transversely, top and bottom – are three-dimensional linear truss elements. Almost all of the rebar elements shared nodes with the deck elements they are “embedded” in, but for those that use unique nodes, ***embedded element** constrains the response of the two materials, ensuring compatibility. The interaction between the rebar and concrete is thought to be perfect; there is no slip.

The top and bottom longitudinal rebar is placed at all but four interior nodes transversely, resulting in 31 bars across the width. Considering the design called for 32, the area of the modeled bars was modified by 32 over 31; the bottom #5 bars have an area of 0.32 and the top #4s have an area of 0.206. Transversely, rebar was placed at approximately 6-in. intervals near the rail expansion joints and at 12-in. intervals elsewhere. The design called for 6-in. spacing, so at the 6-in. spacing locations, the rebar dimension matches the design. The rebar spaced at 12 in. has an area twice that called for in design to compensate for having fewer bars.

The numbering scheme for the rebar is similar to other element sets. The first digit indicates which rebar layer is being considered (top or bottom, longitudinal or transverse). The next three digits indicate the location longitudinally and correspond to associated nodes; because not every node line has rebar attached to it, not every value from 0 to 180 is used. The final two digits indicate location transversely. Again, the number indicates the nodes involved. For example, the first transverse rebar connects nodes ending in 3 and 4, so the first element number would end in 03.

“Fake” rebar elements were defined in the same fashion as with the deck and rail elements. The numbering varies by 50,000. The “real” rebar elements are removed and reactivated with the rail elements; the “fake” rebar elements are in place from the beginning and removed with the reactivation of the “real” elements.

5.2.5.6 Rail Rebar

As in the deck, the rebar within the rails was defined explicitly. While the model does not indicate plasticity in the rail (with the exception of immediately surrounding the expansion joints), a full-depth web fracture in a bridge with a differing geometry could experience such plasticity. The seven #4 bars ($A = 0.20 \text{ in.}^2$) are modeled in a similar geometry in the model as was constructed in the test specimen. The greatest variation is in placement horizontally, as the uniquely-shaped rails were modeled with rectangular elements in the model. Vertically, the placement is accurate within 0.5 in., which is within reasonable construction tolerance.

The rail rebar elements are defined as the deck rebar elements are, as truss elements connecting two nodes and constrained to the rail elements using ***embedded element**. The interior rail six-digit element numbers begin with 9 and indicate the longitudinal location in the next three digits and the vertical and horizontal in the last two, respectively (1 through 4 for vertical, 2 and 3 for horizontal). The external rail rebar element numbers are the same, preceded by a 1. The “fake” rebar elements are numbered 50,000 larger than the corresponding “real” element.

5.2.6 Compile Load Sets

While element and node sets were defined through the input file as necessary, there are other, more specific subsets needed, generally for loading and output requests. In this section of the input file, ***surface** is used to define loading surfaces, ***nset** is used to create sets of nodes of particular interest for output variables, and ***elset** is used to create element groups for actions like gravity loading or element removal.

5.2.7 Define Load Steps

The analytical model consists of fourteen load steps. Each step has been written to capture a certain stage of the construction process, from applying the self-weight of the girder to the removal of the exterior cross-bracing. Each step is detailed here:

- Step 1: Remove deck and rail elements
Use ***model change** to remove all elements that were not in place when the girders arrived at the testing facility, including the deck, rebar, and both rails.
Apply gravity loading (self-weight) to the girders and bracing.
- Step 2: Apply dead load of deck to girder flanges
Use ***dsload** to apply a distributed surface load to the top flanges of the girder equivalent to the dead load of the wet deck (deck casting).
- Step 3: Reactivate real deck elements, strain free

Use ***model change**, *add=strain free* to replace the real deck and rebar elements in a zero-strain state.

- Step 4: Remove applied flange load, turn on deck gravity load, remove fakedeck elements

Modify previously applied surface loads (on flanges) to zero.

Apply gravity loading to deck and rebar elements.

Use ***model change** to remove the *fakedeck* and *fakedeckrebar* elements. While they could have been left in place, this removed the possibility of the fake elements affecting the response of the system.

- Step 5: Apply dead load of inside rail to edge of deck

Similarly to Step 2, apply a distributed surface load to the inside edge deck elements equivalent to the dead load of the wet rail (first rail casting).

- Step 6: Reactivate real inside rail, strain free

Same as Step 3, but for the inside rail.

- Step 7: Apply dead load of outside rail to edge of deck

Same as Step 5, but for the outside rail (second rail casting).

- Step 8: Reactivate real outside rail, strain free

Same as Step 3, but for the outside rail.

- Step 9: Remove applied rail loads, turn on rail gravity loads

Same as Step 4: remove the distributed surface rail loads and apply gravity loading in the rail elements. Also remove *fakerail* and *fakerailrebar* elements

- Step 10: Apply truck loads

Apply distributed surface loads to certain deck elements to represent the concrete-block “truck” placed on the test specimen.

- Step 11: Remove external cross-braces

Use ***model change** to remove the external brace elements (end of construction phase).

- Step 12: Remove bottom flange elements
Fracture event. Use ***model change** to remove a strip of elements from the bottom flange of the external girder.
- Step 13: Remove web elements
Fracture event. Same as Step 12, but removes elements from both webs of the external girder from bottom flange to top flange.
- Step 14: Remove truck loads
Modifies the previously applied distributed surface loads to remove the equivalent truck from the bridge.

The motivation behind using so many steps was the desire to replicate expected stresses and deflections as accurately as possible. To capture these effects, the dead load of the deck had to be applied before the deck cured; the deck elements could not be in place with a full-strength modulus. As was explained in Section 5.2.4.5, this effect was achieved using “fake” elements to take the space of the real elements to come and to translate the associated nodes appropriately. Once the real elements were in place, such as in Steps 3, 6, and 8, the spacer elements could be removed (as in Steps 4 and 9).

For later models, where the general response was of interest but the exact value of stress was not needed, some of these steps were condensed. For instance, both rail loads were applied in one step, rather than individually.

5.3 AREAS OF SPECIAL FOCUS

Finite element analysis of trapezoidal box girder bridges is not a new field of study; programs like UTrAp (Popp et al. 2004) already exist to easily calculate the response of the girders under load. The current project strives to capture the effects of details that were not previously considered. More specifically, the finite element model includes a step where the girder is fractured while under service loads. Current belief states that a bridge in a fractured state will collapse, as discussed in Chapter 2; this

research project is focused at verifying or disproving this belief, arguing that the twin girders could work as a system, allowing for adequate load transfer.

During construction of the test specimen and the analytical model, certain details came into light as possibly being crucially important in stabilizing a fractured girder. These details included the presence of rails (and expansion joints within those rails), the shear stud pullout strength, and the presence of the haunch in the deck. Simplified calculations or models were made to consider these details; more importantly, specific attention was paid in the development of the ABAQUS model to capture the response of these details accurately.

Additionally, it was important to represent the fracture itself accurately, this event being the crucial load step in the model. Various methods were considered and tried before the keyword ***model change** was decided upon. The ***model change** keyword allows the programmer to remove elements during a load step; in this case, the elements that constituted the fracture. The details of the rail and shear stud modeling and the fracture load step are given below.

5.3.1 Modeling of the Rails

Current design practice does not consider the structural advantages cast-in-place composite rails give to a bridge. Thus, for the purpose of design, they are in place to prevent cars and trucks from going off the bridge, not to reduce deflections and stresses. However, in the case of a fractured girder, the presence of such rails could lend significant strength to the system as a whole, providing a compression member far from the neutral axis.

Additionally, preliminary tests showed that the presence of expansion joints – which were, until recently, mandated by TxDOT – changed how the rails resisted bending. Specifically, the joints create a discontinuity in the stiffness provided by the rails. Based on these findings, it was decided that the model needed to not only include the rails but include the expansion joints as well.

The modeling of the rails began with a decision about element type. Beam elements were considered; however, they were dismissed when the deck was modeled with solid elements. As explained earlier, an eight-noded solid element uses linear shape functions to predict behavior; the responding deflections will vary linearly between any two nodes. Beam elements, however, even if only constructed with two nodes, use cubic shape functions, and the deflections will respond in that manner. The problem that exists lies on the surface of the two elements, where mathematically, the sections move independently, even potentially passing through each other. This effect could be neutralized using constraints, but to do so would mean adding layers of equations that would slow down the analysis. It was less computationally expensive to add solid elements to model the rails, even if thousands more elements were needed than if beams were used.

As was explained in Section 5.2.4.1, the geometry of the rails is complex, with multiple exposed surfaces. Because the rails were not the primary focus of the study, it was impractical to model them with the complexity the geometry may have dictated. Instead, the rails were modeled with a simplified rectangular solid, 27 in. in height and 13 in. in width. Between expansion joints and at the ends of the bridge, one element was used through the width and seven through the height. Nearing the joints, the mesh density was increased to 2×14 and then 4×28 . An elastic modulus was then calculated to compensate for the altered geometric properties, to create an effective section with a similar influence on overall stiffness, as described in Section 5.2.4.2. The rail section can be seen in Figure 5-8.

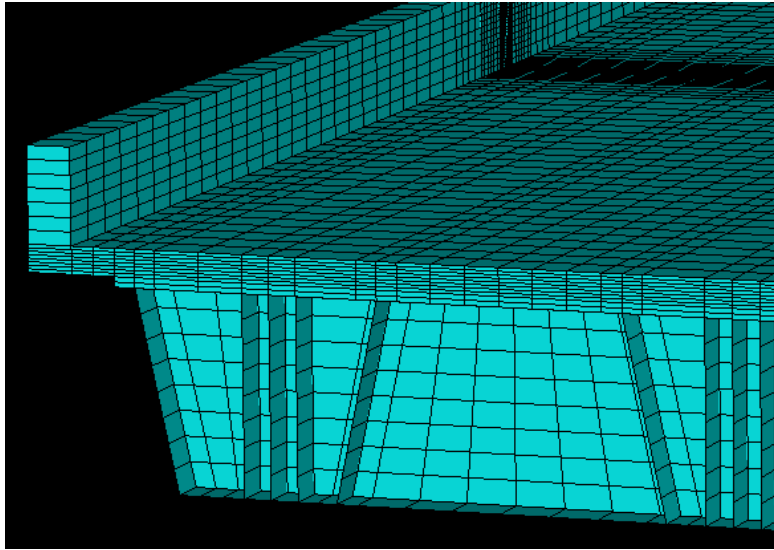


Figure 5-8: ABAQUS view of the end of the modeled bridge, showing block railing

Once it was determined that the expansion joints could influence the response of the structure, a strategy for adding them was determined. The modeling of the gaps began by decreasing the node spacing at the three expansion joint spacer locations to allow for a small gap to be created. Iterative versions were run, testing the numerical response to smaller elements. Through these versions, it was learned that decreasing the size longitudinally alone was not enough; vertically and transversely, there would need to be more elements as well. More nodes were added, resulting in elements at the gap dimensioned at 1 in. \times 1.5 in. \times 2.25 in. This change was reflected through the entire depth of the girder model. The gaps in the rails on the bridge were designed to be between 0.25 and 0.75 in. The modeled gaps are 1.5 in., as fewer mesh density reductions were needed to achieve this spacing. Although the larger gap decreases the chance of contact occurring, it presents a greater area of lower global stiffness at the centerline of the bridge.

Because more elements mean more degrees of freedom and more time for calculation, these small elements are not ideal for the entire length of the bridge. The full-size rail elements of acceptable size between the joint locations were subdivided slowly, as mesh density increases must occur gradually. Vertically, the transition is from

seven to fourteen to twenty-eight elements; transversely, from one to two to four. The constraints required to increase the mesh density are explained further in Section 5.3.1.2.

5.3.1.1 *Contact Constraints*

With the addition of the expansion joints in the rails came the need to establish contact. Although not expected under normal loading, in the case of catastrophic failure, the 1.5 in. spacing between the two rail parts could close. As explained in 4.5.6, numerically, ABAQUS will allow these surfaces to pass through one another. In reality, contact occurs between the two sides. The ABAQUS model defines the surfaces at each gap and has a pair of contact definitions: one with each side as the master, and one with each as the slave surface.

By defining the contact twice, neither side of the contact pair is stronger than the other. Because both sides are made of the same material, each has an equal chance of deforming under contact loading (unlike, for example, a rubber ball hitting a concrete wall). Further information on contact problems and modeling can be found in Belytschko et al. (2006).

5.3.1.2 *Multi-Point Constraints*

The ***mpc** keyword is used to establish compatibility at mesh density increase points in the rails (and in similar mesh density changes in the webs, detailed further in Section 5.2.5.1). The shell web elements use type *linear*, which connects a single node on an edge with the two that make up that edge. The solid rail elements use type *bilinear*, which restricts a node in the center of a surface to the four nodes creating that surface. For instance, consider this line of code, from a rail ***mpc** file:

```
bi l i near, 1504535, 1504737, 1504333, 1503933, 1503937
```

This code constrains node 1504535 (a node 92 ft down the length of the bridge, 4 in. from the top of the exterior rail) to nodes 1504737, 1504333, 1503933, 1503937, the four nodes that make up the front surface of the next element down the rail. Figure 5-9 illustrates the bilinear constraint, with node p being linked to a, b, c, and d.

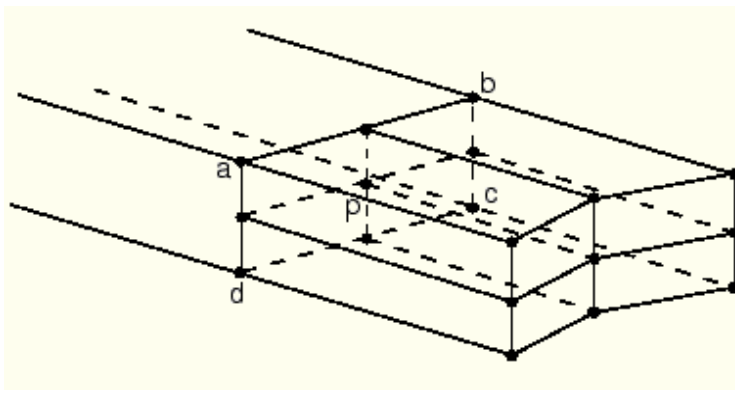


Figure 5-9: Use of the bilinear multi-point constraint (HKS, Inc. 2006)

5.3.2 Modeling of the Shear Studs

The research team predicted that, once fractured, the bridge would respond by losing nearly all capacity in the fractured girder. The fractured steel girder would be left essentially hanging from the concrete deck. The question arose as to whether the steel shear studs that connect the two, designed to resist shearing between the two materials, not to hold load in tension, would be able to withstand this kind of sudden loading. Because of the sensitivity of this detail, it was necessary to include the shear studs in the ABAQUS model.

The simplest way to model a connection between two nodes is using spring elements. Being one-dimensional, each spring adds two terms along the diagonal and two terms off the diagonal in the stiffness matrix, meaning they are computationally cheap. In contrast, a three-dimensional beam connection would contribute to the stiffness matrix for twelve degrees of freedom. In developing the box-girder analysis program UTrAp, Topkaya and Williamson (2003) showed good correlation with test data using one-dimensional spring elements. Considering this previous success and the minimal impact on the stiffness matrix, spring elements were chosen for shear stud modeling.

The first step in creating the interaction between the girder and the deck was to separate the two bodies geometrically. To do so, a second line of nodes was defined at essentially the same location (0.01 in. apart vertically). The bottom line of nodes is used

in the definition of top flange elements; the top line of nodes bounds the bottom of the haunch elements. The two lines are connected using the springs that represent the shear studs.

The second step was to determine how many springs would be needed and where they would be located. On the physical structure, three shear studs exist transversely on each top flange, each triplet spaced at 22 in longitudinally. The shear studs extend five inches into the concrete, which results in the head being approximately even with the bottom mat of reinforcing steel in the deck.

The model features three shear studs in each direction located every 12 in. down the length, or approximately twice as often as exist on the full-scale specimen. This spacing was used to correlate shear studs with element boundaries. To compensate for the greater number of studs, the shear stud stiffness was decreased by 50% relative to the actual case to adequately capture the system response. If shear stud pullout becomes a concern for fracture models, the studs should be redefined to exist at the correct spacing, as the change in loading that could occur with each stud failure could be enough to cause instability in the structure.

The third step was to determine an appropriate spring stiffness. J. Sutton, a member of the research team, explored the capacity of the shear studs further, questioning specifically whether there was any interaction between the reinforcing steel and the shear studs and what level of pullout capacity the shear studs had, as described briefly in Chapter 3. The test results for three studs with a 3-in. haunch showed very brittle behavior and a pullout strength of approximately 17 kip (Sutton 2007). The load-deflection behavior can be seen in Figure 5-10.



Figure 5-10: Load-deflection curve for test specimen shear stud geometry (Sutton 2007)

Using average values for load and deflection from the two tests run with the 3-stud, 3-in. haunch geometry, the stiffness provided by the stud group is approximately 2000 k/in. In the analytical model, the springs are positioned every twelve inches (or almost twice as often as on the test specimen). The vertical springs were thus given a stiffness of 1000 k/in. Springs are also defined in the two other directions (global 1 and 3), to ensure stability of the structure and have an assigned stiffness of 200 k/in. The stiffness value is approximately 1/100th the horizontal stiffness of a beam element of similar dimensions to one shear stud:

$$k = \frac{12 \cdot E \cdot I}{L^3} \quad (3)$$

where

k = stiffness of the shear stud

E = Young's modulus (29,000 ksi)

I = moment of inertia (~7 in.⁴)

L = length of the beam (5 in.)

At this point in this research project, the springs do not have a failure load associated with them. Thus, the bridge cannot fail through shear pullout. Strain values in the springs that represent the studs were monitored, however, during the flange and web fracture simulations and are discussed in greater detail in Chapter 6.

The numbering scheme for the shear studs is similar to other elements, containing an aspect of location longitudinally as well as transversely. Each element has a seven-digit number. The first digit indicates which degree of freedom the spring is associated with, 7 being transverse, 8 vertical, and 9 longitudinal. The next three digits represent the longitudinal location (0 to 180, see Appendix C). The fifth digit is always a 0. The final two indicate the transverse location, starting at 01 to 03 on the innermost flange and increasing to 09 to 12 on the outermost flange.

5.3.3 Modeling the Fracture

The most critical step in this analytical study is that of replicating the fracture of the bottom flange and then predicting the fracture of the web. There are many programs that can analyze structural loads on an unfractured girder, such as the previously discussed UTrAp, and programs that can analyze a small fracture event, such as WARP3D (Computation Fracture Mechanics Research Group 2007), developed at the University of Illinois. The unique part of this study is in the modeling of a fractured girder and the system response of the structural system.

5.3.3.1 **model change*

The fracture in this model occurs using ***model change**, which allows the programmer to remove and re-add element sets. This same keyword was utilized in previous steps to remove deck and rail elements during the construction stages, then re-add them strain-free at the point when the concrete would have hardened.

The ***model change** keyword is used in two ways: to remove and to add elements. The keyword requires one of those two mutually exclusive parameters be given: *remove* or *add*. Under *add*, the elements can be reactivated *strain free* or *with strain*, depending on the desired element state. The single data line contains the element set involved in the removal or reactivation. Multiple element numbers or sets can exist on one line, and the line can be repeated as necessary.

At the beginning of the step including ***model change**, the removed elements are not considered when developing the global stiffness matrix. Thus, the surfaces bounding the fracture are less constrained, and stresses cannot be transferred through the gap. There is no consideration of the dynamic effects of quickly releasing the elements, as equilibrium is established before and after, but not during, the removal of the elements (discussed further in Section 5.3.3.4).

5.3.3.2 Fracture Path

In defining the fracture, the programmer must dictate the fracture load and the fracture path, as well as the timing of the fracture event. Other ABAQUS keywords, such as ***fail strain** and ***fail stress**, allow some automation of the event, but only work with linearly elastic material models (HKS, Inc. 2006). Additionally, the keywords do not induce material degradation, but rather indicate to the user that the material has reached a failure state. While using these keywords might be useful for determining the onset of failure, these keywords did not perform adequately for this study. ABAQUS also allows the use of fracture elements, which will fail at a given point. However, decisions regarding when such elements fail is still at the discretion of the programmer. The fracture elements, which are much more computationally expensive than using ***model change**, were not thought to be appropriate for this study in which the post-fracture behavior and not the fracture itself was of critical importance.

In an attempt to avoid creating an unrealistic fracture, multiple analyses were run, each involving an extra row of elements up the web of the girder, from zero to the sixteen that are defined at midspan. The elemental von Mises stresses at the tip of the fracture were considered, and if greater than the limit of 50 ksi, the fracture would be extended in the next job.

This method has one major drawback involving the mesh definition around the crack tip. In a real crack, the tip would be very small and very sharp (acute). The element definitions around the crack location in this analysis do not have a density appropriate to create this kind of crack. Rather, using ***model change** results in a

fracture with a square front, as shown in Figure 5-11(a). The square corners, while not realistic, also create stress concentrations from the abrupt geometry change. A typical stress profile (von Mises) around the crack tip with some web elements removed is shown in Figure 5-11(b). Ultimately, the analysis was run with a full-depth web fracture as an absolute worst-case scenario.

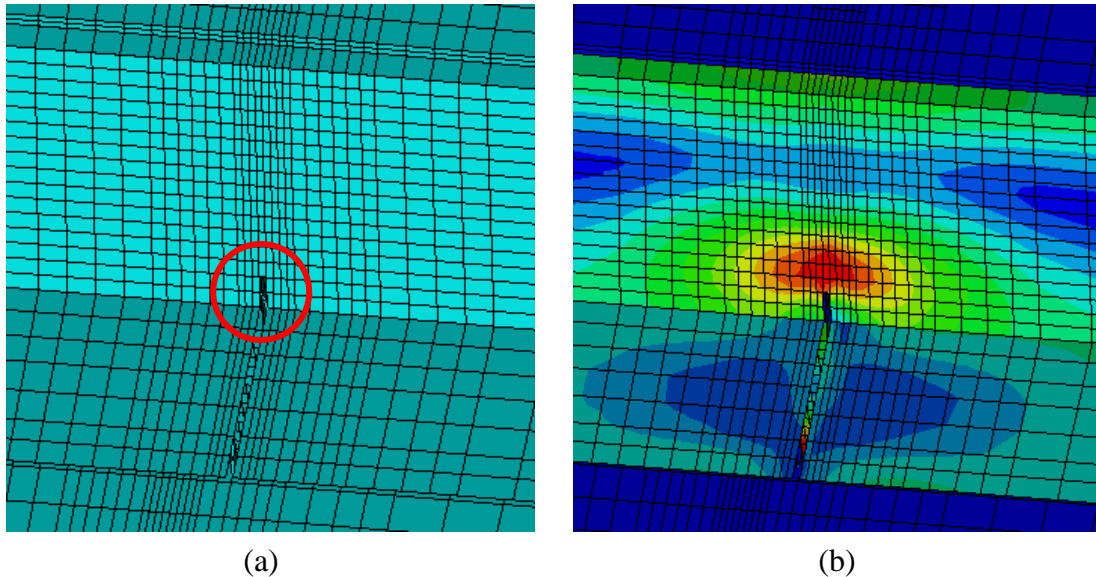


Figure 5-11: (a) Square tip of fracture path using *model change, (b) stress concentration that results

For prediction of a full fracture event, the fracture through the web was programmed to occur vertically from the bottom flange fracture location. While it is possible that a real fracture would not follow this exact path, the overall effect of a fracture on the system, and thus the total system response, should be similar to what was modeled. Further research could consider variable crack paths, but doing so would likely require remeshing the elements around the fracture.

5.3.3.3 Alternative Fracture Methods

The fracture method presented here (using ***model change**) has both benefits and drawbacks. Positively, the method is quick and simple, taking little time to run. It is also very straightforward and clearly indicates what occurs during the modeled fracture. On

the other hand, as mentioned, the crack tip is not representative of a true crack tip and as a result, inappropriate stress concentrations form. It also does not allow for consideration of dynamic effects (explained in more detail in Section 5.3.3.4). Future research could feature other fracture modeling methods, some of which are described here.

The analysis run in this project was also designed using two overlapping sets of nodes along the centerline. Each node connected to elements on one side – north or south of centerline – but not to the elements on the other side. The intention was to apply edge loads on each boundary element that would be equivalent to those experienced during each load step. Then, at the step associated with the fracture event, the loads would be suddenly released, similar to what would be expected during the failure of the steel.

The main problem with this method occurs in the defining of the loads. As was explained in Section 4.5.1, the global axes do not necessarily align with the local axes of an element. The difference may not be very influential in a bridge with a large radius, such as the one analyzed here, but it can be very important in a bridge with a small radius. To apply representative loads, the values output by the program must then be resolved into the appropriate values for reapplication. Considering that there are three edge loads (normal, shear, and traction, seen in Figure 5-12) to be applied to each of the seventy-eight elements surrounding the full fracture for each of fourteen load steps, calculating these values can take significant time by the programmer. This method was attempted, applying loads through only the first step of the analysis, with little success or consistency with earlier models. Although a cylindrical coordinate system might seem more appropriate for this kind of load application, it is not possible in ABAQUS, where cylindrical coordinates are transformed into Cartesian locations upon definition (HKS, Inc. 2006). The comparisons are presented in more detail in Chapter 6.

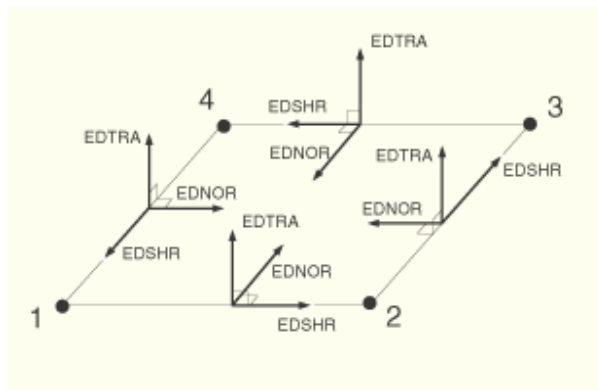


Figure 5-12: Edge loading directions and nomenclature for four-noded shell elements (HKS, Inc. 2006)

Another possible method of modeling fracture, which was not tried, would be to treat the fracture as a substructure, analyzed in a smaller analysis. In that case, only the fracture and some of the elements in proximity would be considered. The resulting change in stresses at the boundaries would be applied to a large-structure analysis as loads and pressures on surfaces and edges. By replicating the fracture step in the analysis as a simple load step, the total analysis time should decrease considerably.

The substructure analysis could be designed in ABAQUS, which would ease data transition from the small analysis to the large. Alternatively, the finite element analysis program WARP3D (Computation Fracture Mechanics Research Group 2007), available from the University of Illinois at Urbana-Champaign, specializes in modeling fractures, with meshing tools designed to make the sharp crack tip expected during an in-service fracture event. For this study, the specifics of the crack tip and crack propagation were considered of lesser importance than the overall system effects, and so the simplified, blunt-end fracture was adequate.

5.3.3.4 Dynamic Effects

Studies run using simpler models have shown that ***model change** does not consider dynamic effects the way adding or removing a load directly would. However, one goal of this project is to remove the need to analyze a dynamic event in a dynamic

fashion, instead mimicking the worst-case response of the structure using increased loads. Once the dynamic load increase is understood, a simplified model that can run statically will likely run faster than the dynamic step required to capture dynamic load applications directly. This approach is considered appropriate for the current project in which a major objective is to develop simplified modeling guidelines that can be used by designers to estimate the system-wide response of a steel bridge that experiences a fracture.

The standard method of considering dynamic effects is to double the loads applied (United Facilities Criteria 2005). The maximum dynamic stresses and deflections are generally smaller than what results, so the analysis is considered to be conservative. However, an analysis gets more complicated when considering loads that push a structure into an inelastic response, as energy is dissipated through yielding.

In progressive collapse analyses, only the loads coincident with a removed structural component are increased to represent dynamic effects, such as the bays surrounding a disabled column (United Facilities Criteria 2005). In the current study, the loads applied within two times the depth of the girder in either direction from the fracture location (approximately 100 in. [8 ft-4 in.] on either side of midspan) are multiplied by either 1.5 or 2.0 during the fracture step.

5.4 CORRELATION WITH TEST SPECIMEN

The finite element model for this project was developed with the intention of predicting the response of a box-girder bridge during a fracture event. To do so, the researcher must have confidence in the accuracy of the results predicted under certain loads. Results from the model were thus compared at various stages with deflections and strains measured on the full-scale test specimen; these comparisons are detailed in Chapter 6. During the programming of the model, however, care was taken to recognize where and in what way the model corresponded with the gauges on the test specimen. An overview of key elements along the bridge is given in the following sections.

When comparing strain measurements, the type of strain measured and calculated should be considered. In this project, the data gathered was post-processed to give engineering strain, or

$$\varepsilon = \frac{L_f - L_o}{L_o} \quad (4)$$

where

L_f = final length

L_o = initial length

The default strain calculation in ABAQUS is Green's strain, or

$$\varepsilon_G = \frac{L_f^2 - L_o^2}{2L_o^2} \quad (5)$$

However, for the element types used in the girder, this strain was not calculated directly. Instead, logarithmic strain was given by ABAQUS and then used for data comparison. Logarithmic strain is defined as

$$\varepsilon_L = \ln \frac{L_f}{L_o} \quad (6)$$

For small-deflection analyses, the strain equations converge to the same value. However, for larger strains, the specifics of the calculation become important, as shown in Figure 5-13. The strains experienced in the girders during the live load and fracture tests, given in more detail in Chapter 6, were on the order of 10^{-4} , or much smaller than would be needed for error to exist. In the case of a full-fracture event, the strains could reach higher levels.

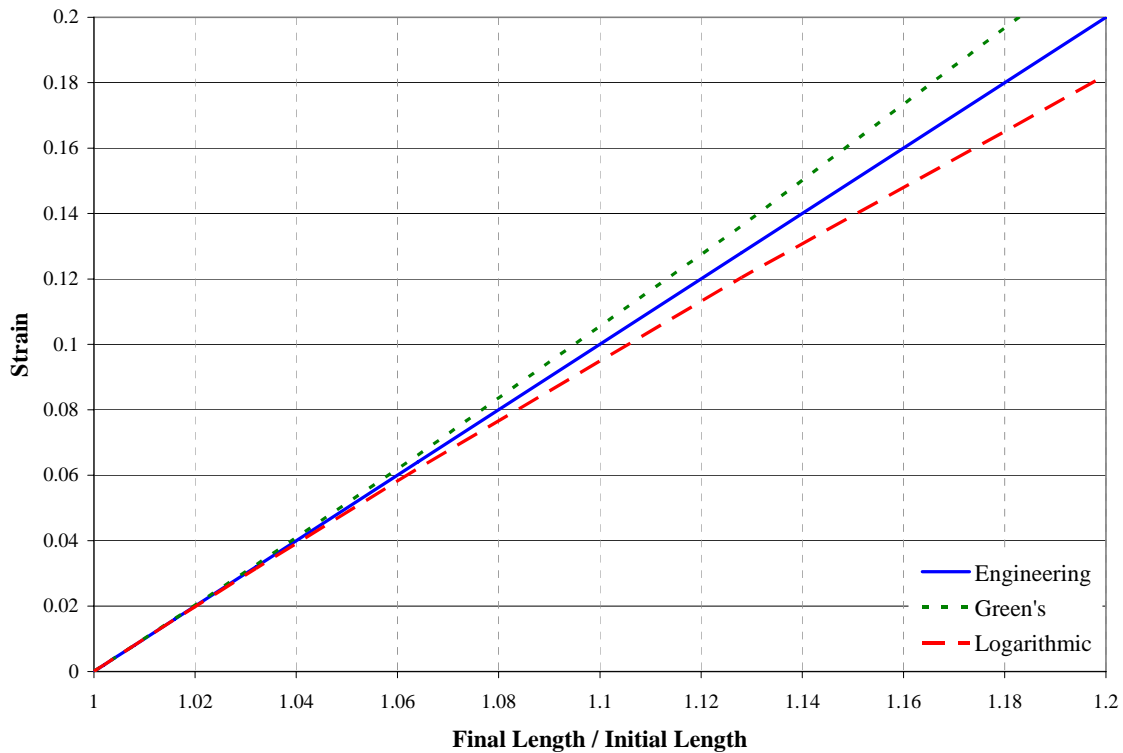


Figure 5-13: Variation in strain using different strain equations

5.4.1 Girder Instrumentation

The strain gauge locations along the bridge were considered when defining element boundaries. Further programming revealed that what became most appropriate within the model did not exactly match the instrumented locations. Because the instrumentation was in place by the time this discrepancy was realized, the data from the model had to be manipulated slightly before being compared to measured results. The gauge and corresponding element numbers are tabulated in Table 5-3, indicating which element responses must be included for direct comparisons.

Table 5-3: Element numbers corresponding to foil gauges and rosettes on the test specimen

ROSETTE GAUGES		FOIL GAUGES	
Gauge Number	Element Number	Gauge Number	Element Number
1 & 4		1 & 7	6075 7075
2 & 5		2 & 8	14075 15075
3 & 6		3 & 9	41075
7 & 10	30075 31075	4 & 10	45075
8 & 11	43075	5 & 11	34075 35075
9 & 12	10075 11075	6 & 12	26075 27075
13 & 16	30106 31106	13 & 19	106075 107075
14 & 17	43106	14 & 20	114075 115075
15 & 18	10106 11106	15 & 21	141075
19 & 20		16 & 22	145075
21 & 22		17 & 23	134075 135075
		18 & 24	126075 127075

The foil gauges measure single-directional strains and were oriented down the length of the bridge. The longitudinal direction corresponds with the Global 3 axis in the model and the local 22 direction within the girder shell elements. The measured strain was compared with the logarithmic strain calculated in ABAQUS, or LE22, for each element.

The rosette gauges are three-dimensional and capture maximum and minimum principle strains. These values were compared with the calculated maximum and minimum principle logarithmic strains. Discussion of the data comparisons can be found in Chapter 6.

5.4.2 Deck Instrumentation

With the rebar elements being defined uniquely, it is again straightforward to make data comparisons. The most important part is knowing which element in the model corresponds with the gauges in the bridge. There are eleven rebar gauge locations in the deck: five on each side of centerline and the last at the centerline of the bridge. On the test specimen, two gauges were placed at each location, on the top and bottom layers of rebar, to capture the bending response through the deck. In the ABAQUS model, the top and bottom rebar mats are defined individually and there are two elements across the top of each flange, so each gauge location corresponds with four elements in the model, given in Table 5-4.

Table 5-4: Element numbers corresponding to deck rebar gauges on the test specimen

Gauge Location	Element Numbers
40 ft north, interior	516012, 516013 616012, 616013
40 ft north, exterior	516020, 516021 616020, 616021
20 ft north, interior	512012, 512013 612012, 612013
20 ft north, exterior	512020, 512021 612020, 612021
10 ft north, interior	511012, 512013 611012, 612013
Centerline, interior	509012, 509012 609012, 609013
10 ft south, interior	507012, 607013 607012, 607013
20 ft south, interior	506012, 506013 606012, 606013
20 ft south, exterior	506020, 506021 606020, 606021
40 ft south, interior	502012, 506013 602012, 602012
40 ft south, exterior	502020, 502021 602020, 602021

5.4.3 Stud Instrumentation

As with the defining of element boundaries, the shear stud gauge locations were considered when defining the location of shear stud springs in the model. Using more, weaker springs allowed for a better correspondence between stud gauges and available elements. Although easier for model definition, this modification should be considered in data comparisons and analysis. Considering the representation of one shear stud with two springs (based on the spacing along the length) and the small and variable strains

measured during the fracture event, strains measured at neighboring shear studs should be considered and possibly averaged during data comparison. Given the element numbers in Table 5-5, nearby gauges can be found longitudinally by varying the second through fourth digits, and horizontally by varying the final two digits (the exact numbering scheme was given in Section 5.3.2).

Out of the fifteen stud gauges placed on the test specimen, only two do not line up with a shear stud spring element in the model; all of the element numbers are given in Table 5-5. The LE11 strain from these elements as computed by ABAQUS can then be compared to the direct strain measurements made during the live load tests and the fracture event.

Table 5-5: Element numbers corresponding to shear stud gauges on the test specimen

Gauge Number	Element Number
1	8080003
2	8105006
3	--
4	--
5	8080006
6	8076006
7	8122007
8	8116007
9	8090007
10	8080007
11	8076007
12	8056007
13	8122012
14	8107012
15	8065012

5.5 SUMMARY AND CONCLUSIONS

This chapter has detailed the development of a finite element model of a steel trapezoidal box-girder bridge. The specifics given include geometries, material models, and numbering schemes, so as to enable a future researcher to make modifications as necessary. The main logic governing this model, such as the use of the fake deck element system and the ***model change** keyword, can also be used to build models of other bridges with varying geometries or boundaries.

The model in this project was designed to match the full-scale test specimen detailed in Chapter 3. The model also includes load steps capable of removing the entire web of the girder to study a full-depth fracture event, with the intention of predicting the response of a bridge in this condition. Details of the verification process, using measured strains and displacements, can be found in the next chapter. Additionally, Chapter 6 presents expected deflections and strains after a full-web fracture event and in the case of alternate geometries (e.g., a three-span structure).

CHAPTER 6

Results and Comparisons

6.1 INTRODUCTION

The finite element model described in Chapter 5 was developed to create a predictive tool for the response of twin trapezoidal box-girder bridges in a fractured state. Response parameters computed with this model that are of particular interest in assessing the stability of the tested bridge in its post-fractured condition are the deflections and the stresses in the bottom flange of the unfractured girder.

In order to be confident about the predictive capabilities of the analytical model, data were gathered on the full-scale test specimen and compared with calculated values from the finite element model. Considered responses include deflections under dead and live loads, strain changes in the girders during live load testing, and the change in strain and deflection states during the flange fracture event.

Additionally, during the developmental stages of the model, comparisons were made between various modeling methods. Included in these tests are studies on mesh density through the length, width, and depth of the girders; load application methods for the construction load of the uncured concrete; and element type options for the concrete deck, rails, and haunches. Analyzing the structure using multiple methods and returning the same results suggests the accuracy of those results and gives a good foundation that can be used to compare against experimental data.

This chapter focuses on two methods of verifying the predictive capabilities of the developed models and concludes by presenting the computed results for a full-depth web fracture event. The model recommended for analysis can also be modified to consider bridge geometries other than that of the full-scale test specimen.

6.2 PRELIMINARY VERIFICATIONS

During the development of the finite element model, certain decisions were made regarding modeling techniques. Some, such as the switch from shell elements to solid elements in the deck, allowed for specific details of the structure to be included. Others, such as increasing the mesh density near the fracture point, aided in establishing a convergent state during the load and fracture steps. Whenever possible, the researcher made comparisons between two techniques (such as using shell and solid elements), often by comparing deflections along the length. Comparable deflections gave reliability to both modeling methods and their accuracy in reflecting the true response.

6.2.1 Mesh Density

High mesh density, the benefits of which were explained in Chapter 5, has the drawback of requiring greater computation times due to the increased number of degrees of freedom over models with coarser mesh densities. To capture the response surrounding the expansion joints in the rails and the fracture location where stresses and strains change rapidly over a small area, a greater number of elements are needed relative to other locations over the length of the bridge where the changes in the response parameters are less abrupt.

Adding elements at locations where stresses and strains change rapidly, and thus increasing the total number of longitudinal elements from 120 to 180, provided the ability to verify the accuracy of the original mesh density. For the dead load application steps, neither the expansion joints nor the fracture were in place, so the additional elements were not needed for convergence. A comparison of dead load deflections calculated using 60- and 120-element models is given in Figure 6-1. The deflections indicate those expected during deck casting, with essentially no stiffness added by the deck. At midspan, the percent difference between the two curves is 0.30%. This minor difference indicates that sixty elements down the length of the bridge were adequate to capture the response of the real structure for this uniform load case. The final model has 180, the additional elements being located at the three expansion joints in the rails.

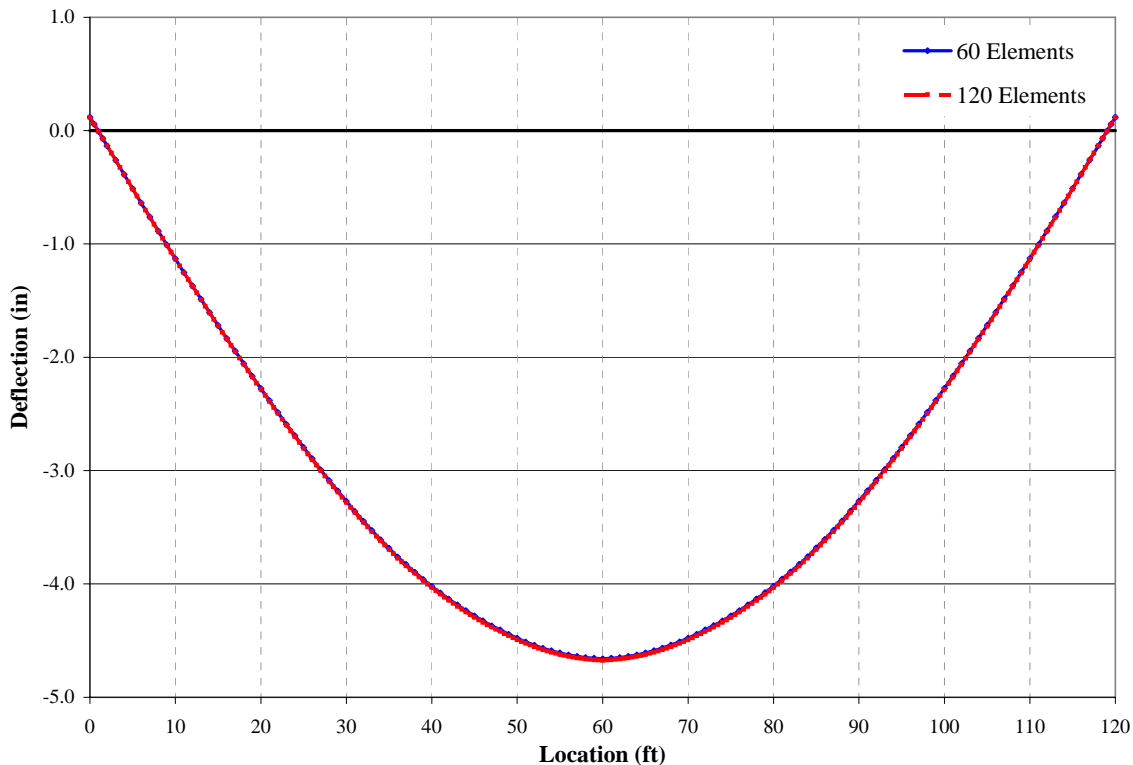


Figure 6-1: Comparison of dead load deflections with 60 and 120 elements down the length (curves overlap)

6.2.2 Deck Element Type

The earliest versions of the analytical model featured a shell-element deck. For general loading and composite response, shell elements provided enough detail while limiting the number of elements and thus minimizing the number of equations that needed to be solved. However, upon realizing the possible importance of the haunch on the deck response and considering the possibility of cracking in the deck during the fracture event, the model was modified using solid elements for the deck, rails, and haunches.

In each case, deflections under dead load were compiled using a gravity loading scheme. Unlike in the mesh density comparisons, the deck was in place and stiff during loading, so the deflections are much smaller. The overlapping curves can be seen in

Figure 6-2. At midspan, the variation in deflection between the two element types is 0.005%. The final model uses solid elements through the haunches, deck, and rails.

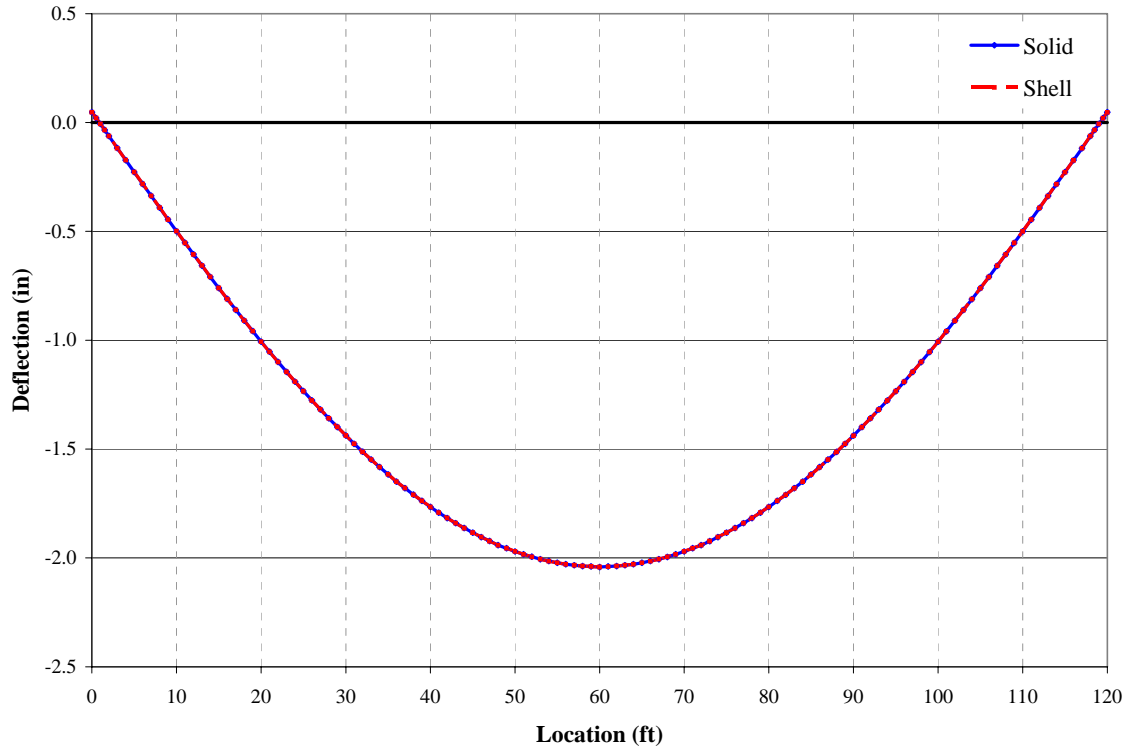


Figure 6-2: Comparison of dead load deflections using solid and shell deck elements (curves overlap)

A second point of comparison for the element types is in the reaction forces. If each element is able to similarly represent the same loads on the structure, the response in the reactions should also be the same. A representative sample of comparative reaction forces is given in Table 6-1. In the set of twenty nodes and thirty reaction forces (twenty vertical and ten horizontal), none varied by more than 0.5 kip.

Table 6-1: Comparison of reaction forces under dead load using solid and shell deck elements

Node No.	Solid Elements (kip)	Shell Elements (kip)	% Difference
20112	28.95	28.69	-0.90%
20113	11.42	11.58	1.37%
20114	19.46	19.01	-2.36%
20115	11.47	11.77	2.54%
20116	31.58	31.88	0.95%

6.2.3 Concrete Load Application

In an effort to capture the true stresses that are experienced by a steel bridge from fabrication through service, the construction sequence needs special attention. In the early stages of construction, the steel girders do not have the stiffness or rigidity that is later gained through casting and curing of the solid composite deck. Thus, to calculate the correct deflections and stresses, the load steps have to begin with zero stiffness in the deck.

The deck stiffness was developed using ***model change**, as described in Section 5.3.3. During the construction step, the dead load of the wet deck was applied to the top flanges of the girder, where the stay-in-place metal pan decking would be attached. The next steps reactivated the deck elements (with an appropriate value for Young's modulus), disabled the applied flange load, and activated gravity loading.

To ensure the applied and gravity loads were equivalent, deflections considering each scenario were gathered and compared. Additionally, the change in deflection across the load steps where the deck elements were reactivated and loaded was monitored to confirm that appropriate loads were applied considering the dimensions and density of the deck. Figure 6-3 shows the deflection curve down the length for the applied and gravity load scenarios (applied load referring to the case where the dead load is applied on the top flanges). As with the previous graphs, the two curves are coincident, with percent differences on the order of 0.05%.

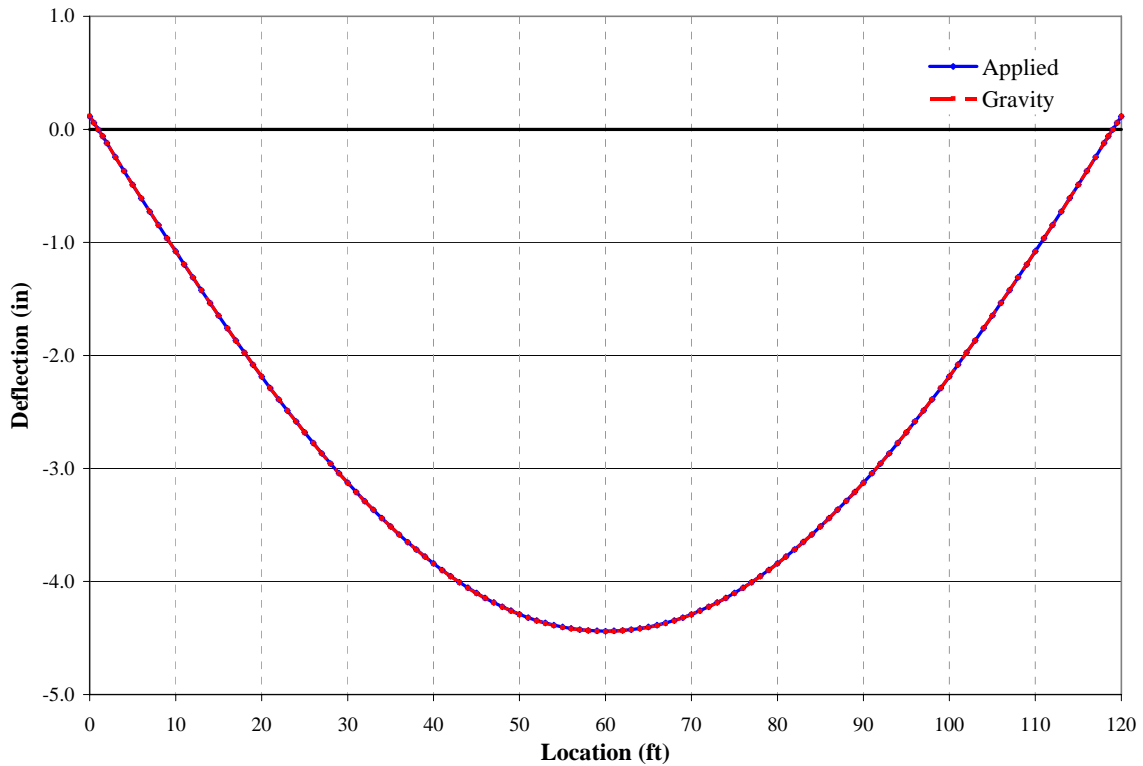


Figure 6-3: Comparison of dead load deflections while applying deck load as a surface load on the top flange (applied) or as a gravity load

The same method of removing and reactivating elements was used in the rail pour steps, with each rail considered individually and in a corresponding manner to the construction of the test specimen. A typical deflection profile through the first ten load steps – girder erection through external cross-brace removal – is shown in Figure 6-4. The switch in deck loading leads to a change in deflection of 0.01%, while the switch in rail loadings change the deflection by 0.8%.

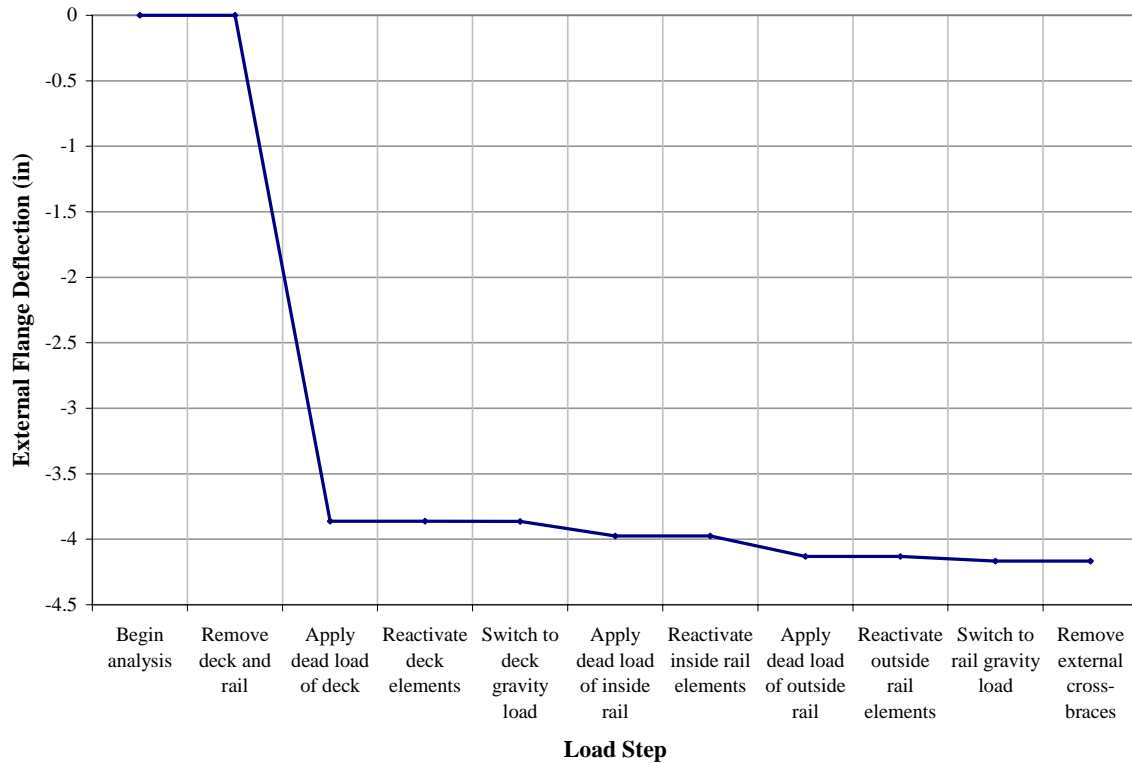


Figure 6-4: Deflection profile for a midspan node on the external girder from girder erection through external cross-brace removal

6.3 COMPARISONS TO MEASURED DATA

During construction and testing, deflection and strain data were gathered from the test specimen. The data were then compared to calculated values obtained from the ABAQUS analyses. Included in the comparisons are:

- deflection measurements from dead and lives loads,
- strain changes during live load testing, and
- strain changes during the fracture event.

These comparisons are presented in the following sections.

6.3.1 Deflections

The bottom flange deflections of the girders on the test specimen were measured during each step in the construction process, as detailed in Barnard (2006). Similarly, the

stepped process of analysis in the ABAQUS model allowed for the separation of individual load step deflections. To help evaluate the accuracy of the analytical model, the measured and ABAQUS values were compared after the deck was poured (thus capturing the deflection experienced from the dead load of the deck). Additionally, the same deflections were calculated in UTrAp. A comparison of the deflection curves for the exterior bottom flange are shown in Figure 6-5. At midspan, the difference in deflection between the three curves is less than 0.15 in. Considering the accuracy of the laser level used for measurement (± 0.06 in.), the curves are nearly coincident at that point.

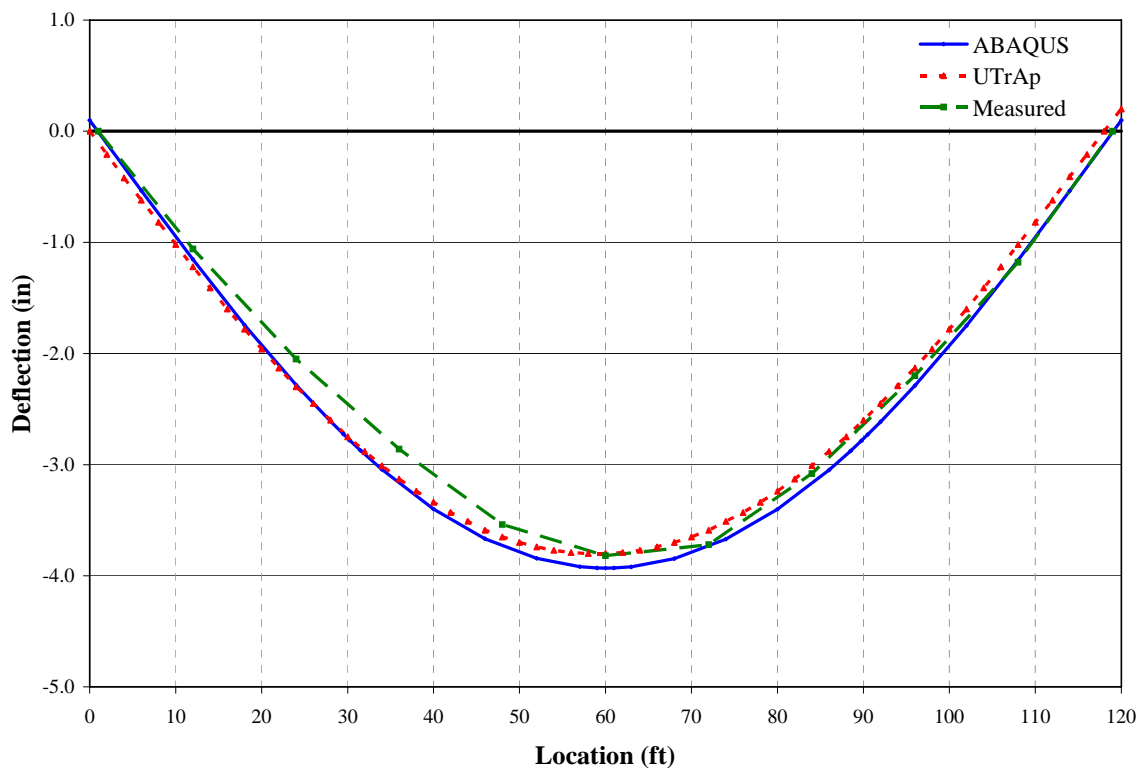


Figure 6-5: Deck load deflection comparison using ABAQUS, UTrAp, and measured data

The similarity in data between the ABAQUS model and the measured values continued to reinforce the strength of the “fake element” method for applying the deck loads (described in Chapter 5). If the “fake” deck elements had added significantly to the

strength of the system during deck casting, the ABAQUS model would have resulted in deflections less than the measured values. The larger deflections that were actually calculated suggest that the use of reduced-integration elements throughout the girder overcompensated for the extra stiffness in the model. Figure 6-6 shows how the measured data generally falls between the response of full- and reduced-integration elements. To the south of centerline (the left on Figure 6-6), the correlation between measured and calculated values is not as good as it is to the north of the centerline. This discrepancy was most likely caused by imperfections in the geometry of the girders that were present at the time of construction or error in the deflection measurements. Further data regarding the shape of the girders through the construction phases can be found in Barnard (2006).

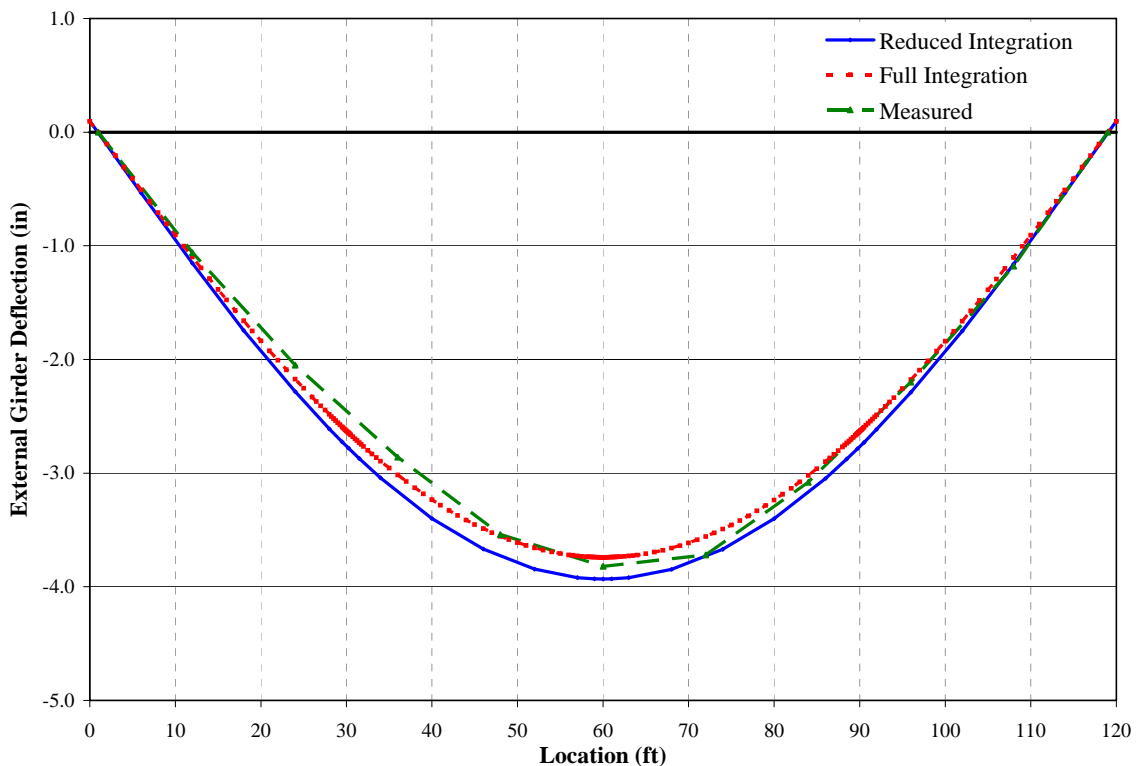


Figure 6-6: Deck and girder dead load deflection comparison using reduced- and full-integration girder elements (*s4r* and *s4*)

While the deflections of the south end might be better approximated with full integration elements, reduced integration was used for two reasons. First, the computation time for reduced integration elements is less than for full integration elements. Secondly, the higher deflections that result present a conservative approximation of response, which the full integration elements cannot do at all locations.

6.3.2 Live Load Testing

During the fracture event, the bridge was loaded with an equivalent HS-20 truck, approximately 76 kips spread at 14-ft intervals. The loading was achieved using concrete blocks, as described in Section 3.3. Before the fracture event, the changes in strain experienced during the placing of the blocks were measured; after the fracture event, the changes during unloading were measured. Similarly, steps are included in the ABAQUS analysis that mimic the placing and removing of the surface load on the bridge. Strain changes across those steps were calculated and compared with the measured values, as shown in Figure 6-7.

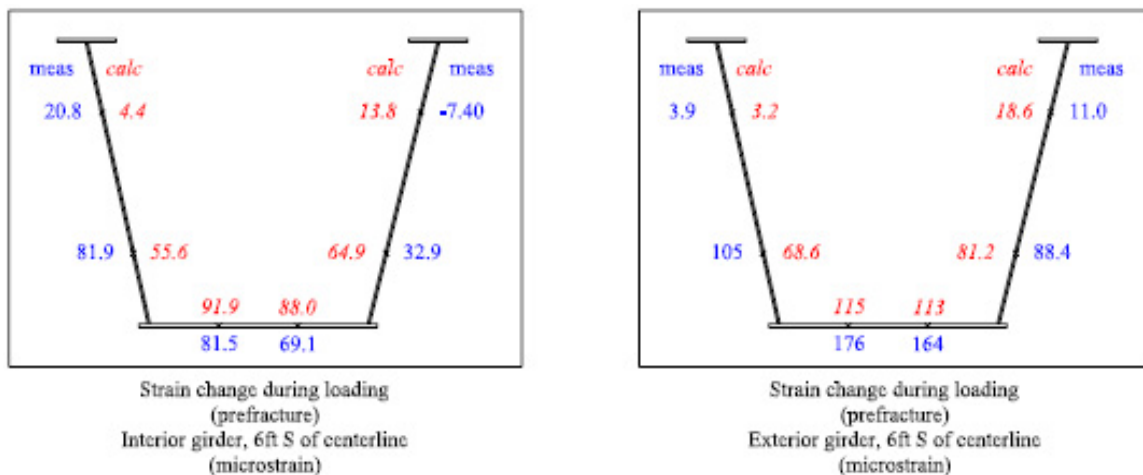


Figure 6-7: Measured and calculated strain changes in the girders during loading. Measured values are on the exterior of the girders in blue; calculated values are on the interior in red italics.

It is important to note the magnitudes of the strains shown in Figure 6-7. While those near the top of the webs may seem to have large variation between measured and

recorded values, the values are very small, as the gauges are situated close to the neutral axis of the structure. The comparisons on the bottom flange, which are of larger strain values, present a more suitable look at the accuracy of the model.

Additionally, initial imperfections in the girders would influence the measured strains. By definition, the bridge in the finite element model has no superelevation or initial twist, and thus all loads are applied vertically and uniformly. The test specimen is known to have a slope longitudinally which would influence the exact direction and magnitude of the dead loads. Any initial transverse rotation would also alter the loading, as the wet concrete would favor the lower side during casting.

Figure 6-8 presents strain comparisons at the same locations during unloading, after the flange was fractured. Again, the most accuracy is found on the bottom flange, where the strain change is the greatest.

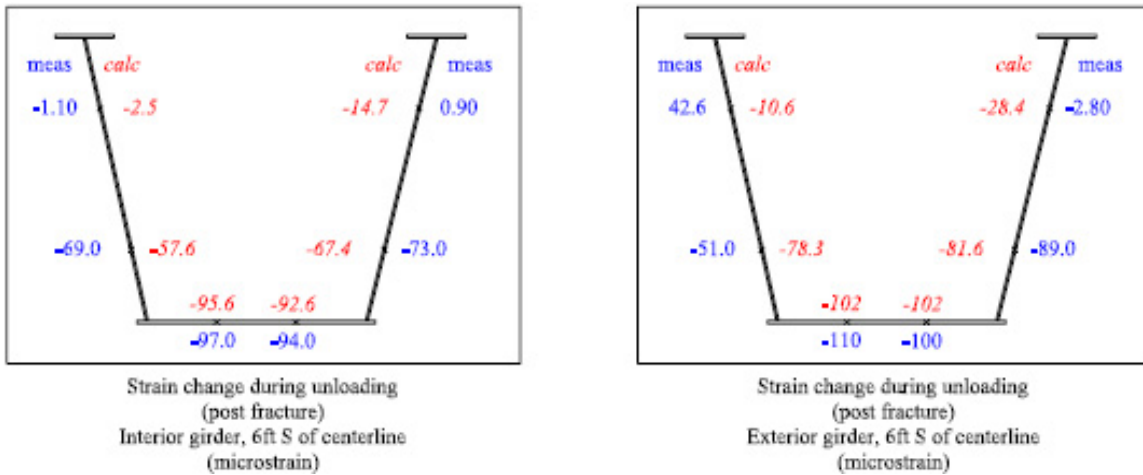


Figure 6-8: Measured and calculated strain changes in the girders during unloading. Measured values are on the exterior of the girders in blue; calculated values are on the interior in red italics.

6.3.3 Fracture Event

During the fracture test, there were strain gauges on the girders, the rebar within the deck, and the shear studs. Data processing after the event showed essentially negligible changes in the rebar strains; there was not enough bending induced in the deck to register outside the range of noise and with any believed accuracy in the rebar gauges.

The rosette and foil gauges on the girders, however, as well as the stud gauges, did return strain values indicative of the transfer of forces after the fracture event. These values were compared to calculated values for strain in the analytical model in an effort to verify the accuracy of the model.

6.3.3.1 Deflections

During the flange fracture, the girders deflected 0.25 in. (± 0.06 in.) at midspan. The analytical model predicted a change in deflection of 0.252 in. A comparison of the measured and calculated change in deflections due to the flange fracture can be seen in Figure 6-9. While the maximum measured change in deflection was not at midspan, the total deflection was greatest at the fracture location. Considering the deck gravity loading and the weight of the truck, as well as the influence of the fracture, the difference between the total measured and calculated deflections was 0.1 in. at midspan.

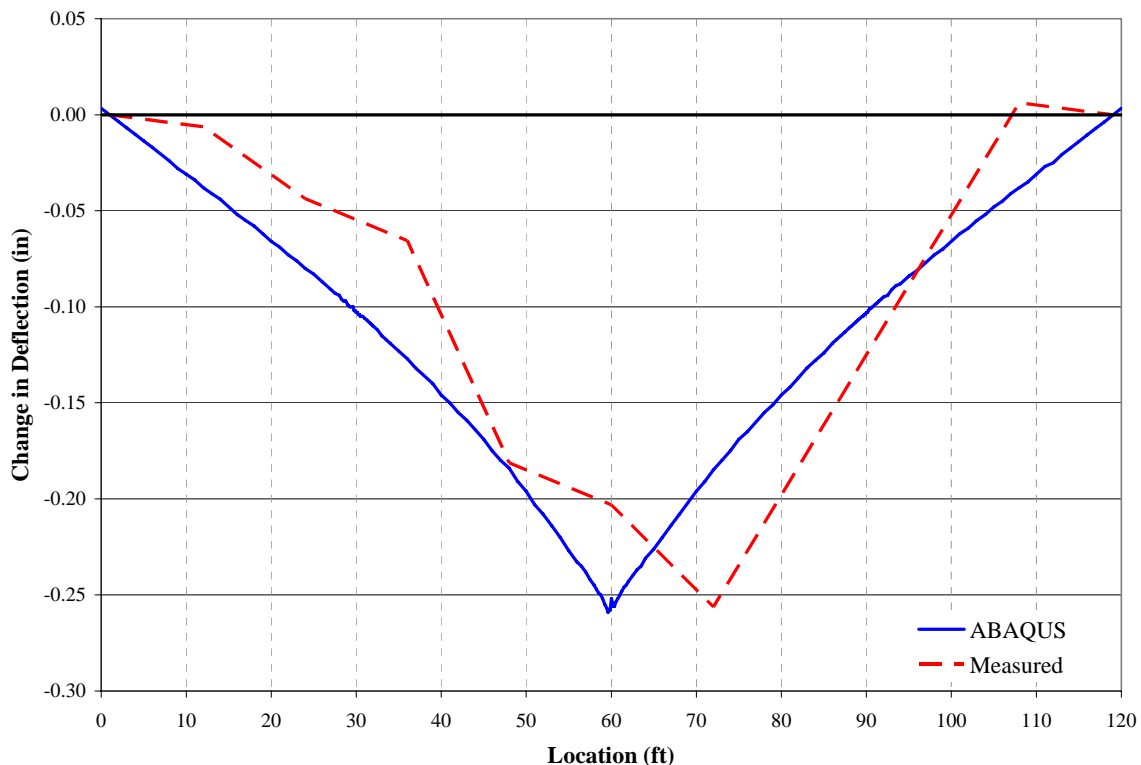


Figure 6-9: Comparison of the change in deflections calculated in ABAQUS and measured on the test-specimen using a laser-level

The smaller deflections calculated by the model, especially in comparison with the larger deflections calculated pre-fracture, imply that the model responded in a stiffer manner than the test specimen. The stiffness could come from the strength attributes given to the deck or the static load application method. Further study of response during the live load testing and the full-depth fracture of this bridge and fracture events on other test specimens would continue to validate the modeling methods presented here.

6.3.3.2 Girder Strains

As with the live load testing, the foil gauge readings were compared with the longitudinal directional (LE11 and LE22) strains measured in certain elements in the web and flange. Because the analysis was run statically and the fracture event happened dynamically, the calculated strains were compared with the final-state strain change measured on the girder. The peak strains measured are compared in Section 6.5 with dynamic load-effect-modified analyses.

Figure 6-10 shows the calculated and measured strains. There are four locations where the gauges failed, most because the wires were severed by shrapnel from the explosive event. The calculated values are displayed even without the comparison to measurements so as to show the trends through the full girder cross-section.

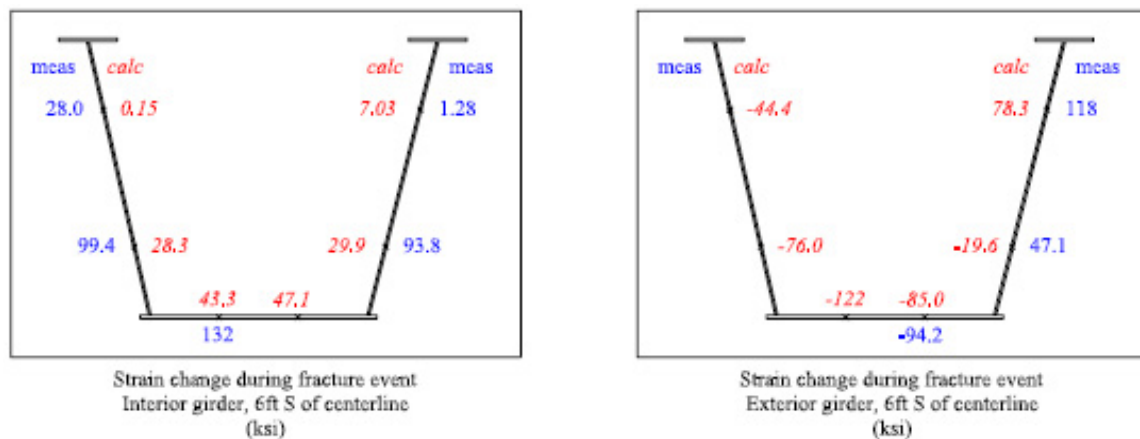


Figure 6-10: Measured and calculated strain changes in the girders during fracture event. Measured values are on the exterior of the girders in blue; calculated values are on the interior in red italics. Blank spots indicate broken gauges.

Some of the gauges, especially along the bottom flange, show very good correlation with the calculated values, while others do not. Even for the cases involving the largest differences, the error is on the order of a 2 ksi stress (assuming elastic response). The differences between the two could come from a variety of sources including the element size and location considered on the model and the placement of the gauges on the girders. The strains gathered were aligned with the longitudinal edges of the elements, which were horizontal at the beginning of the analysis. If there was a slight angle off horizontal in the gauges, the measured strain would actually contain components from each directional strain. Considering the calculated vertical and shear strains were smaller by only one order of magnitude, the predicted influence on strain readings would be important.

Differences in sign could be caused by incorrect element-gauge location correspondence. The gauge that measured -19.6 microstrain could have been placed lower on the web than the element that measured 47.1 microstrain. To some extent, this source of error could be confirmed by measuring the exact locations of the gauges on the girders to ensure the location is known. However, the size of the elements in relation to the size of the strain gauges also means the element is measuring strain over a larger area that might not be centered on the gauge. Initial imperfections in the girder placement and loading should also be considered, as explained further in Section 6.3.2.

Keeping in mind that the displayed strains are *changes* in the strain in the members, general trends can be observed. In the fractured (exterior) girder, the increase in tension through the top of the web indicates the neutral axis has shifted upwards, as was expected after the loss of stiffness in the bottom flange. The strain at the other points decreased due to the transfer of stresses through other pathways because the bottom flange can no longer hold load. Fracture theory predicts an ellipse of near-zero stress to form around a fracture; this effect is seen both in the data shown in Figure 6-10 and in the ABAQUS plot shown in Figure 6-11.

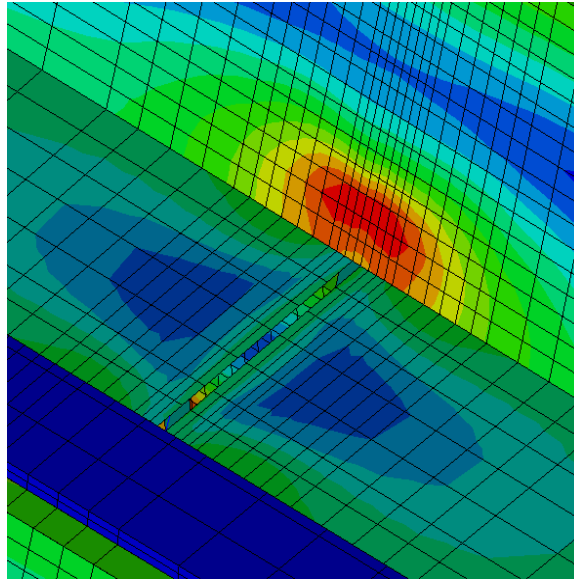


Figure 6-11: Ellipse of near-zero stress surrounding the flange fracture (blue is low, red is high)

All gauges on the interior girder showed an increase in tension in the web and bottom flange. This increase correlates with the expectation that some of the loads from the exterior girder would be transferred to the interior girder. With the additional loads on the interior girder, one concern is the possibility of yielding in the bottom flange if the loads get too high. Both the measured and calculated strains show very little change: 40 to 130 microstrain, or, if the steel remains elastic, less than 4 ksi of added stress. Considering the pre-fracture stresses were calculated to be in the range of 20 ksi, yielding of the interior bottom flange is not likely. However, these calculations do not consider the fracture of the exterior girder webs. Also neglected are the initial residual stresses that are caused by welding the plates of the box together. Full fracture response predictions are presented in Section 6.4.

6.3.3.3 *Shear Stud Strains*

Strain gauges were placed within selected shear studs to measure the vertical forces transferred to the slab through the studs from the dead weight of the fractured girder. Seven of the fifteen gauges returned useable data, and the elongations were

compared to deflection differentials through the spring element shear studs in the analytical model.

The overall difference in length in individual shear studs measured was on the order of 10^{-5} in. across a 5 in. tall stud (this value being calculated from the measured engineering strain and the initial length), with five of the seven gauges indicating elongation. The ABAQUS model accuracy was limited to five decimal places and thus barely captured any change between load steps. However, the values that were calculated corresponded in sign and magnitude with the measurements during the fracture event.

To further validate the modeling method, it would be beneficial to perform tests that create higher loads in the studs. With such small values, gauge precision and placement become highly influential. For instance, if the gauge was not placed exactly vertically within the stud, shear forces transferred between the deck and girders could influence the reading. As for precision, the readings need to be high enough to be outside the tolerance of the gauge, where the reading is not dictated by noise but by the changing load paths of the structure. A full-depth web fracture test should be able to create these strains, which can then be compared to the predicted values gathered by the model. This scenario is investigated analytically and is presented in part in Section 6.4.1.3. If the spring elements are found not to represent the response adequately, the stiffness and placement of the springs could be changed to improve correlation or a different modeling method could be used.

6.4 PREDICTION OF FULL FRACTURE RESPONSE

This project was designed with the goal of creating a predictive tool for the behavior of trapezoidal box-girders that experience a fracture event. The intent was to build a full-scale test specimen concurrently with an analytical finite element model. Data gathered from the fracture test would be compared with those calculated by the model, verifying the accuracy of the model. However, testing of the full-scale test specimen failed to fracture the web, so the finite element model could only be evaluated to that point.

The model was still run through a full-fracture event, as that response is still of interest. Without verification, however, it is difficult to assess the validity of the predicted response, especially when considering certain assumptions made in creating the model and the variability between calculated and measured values during the flange fracture event.

Included in those assumptions is the behavior of the concrete in the deck and rails. The non-linear and complex failure behavior of concrete is difficult to model, and it was eventually simplified to an elastic-plastic model as described in Chapter 5. A more complex material model including the cracking behavior of concrete was not used because local failures in the deck and rail caused non-convergence in the model. The elastic-plastic model assumes that the concrete failures will be localized and the rebar embedded in those members will be able to withstand the stresses without the confining concrete.

6.4.1.1 Deflections

Twin box girders are not classified as redundant structures because there are less than three primary load-carrying members. The expected response of the bridge under fracture does not give credit to the system effects that come from having two connected girders. While one can fracture, the other can still hold load. The two behaviors are seen most clearly looking at a plot of the deflections of each bottom flange. Figure 6-12 shows the change in deflection down the length of the bridge from pre-fracture to post-full-depth web and flange fracture. The exterior girder, with no continuity at the midspan, shows hinging effects: a sharp change in rotation occurs at the fracture site (the jump in displacement visible at midspan is caused by the unsymmetrical interior bracing and the location of the truck loading with respect to the fracture site, and is discussed further in Section 6.6.1). The interior girder, however, which is still intact, responds in bending, to a much smaller extent.

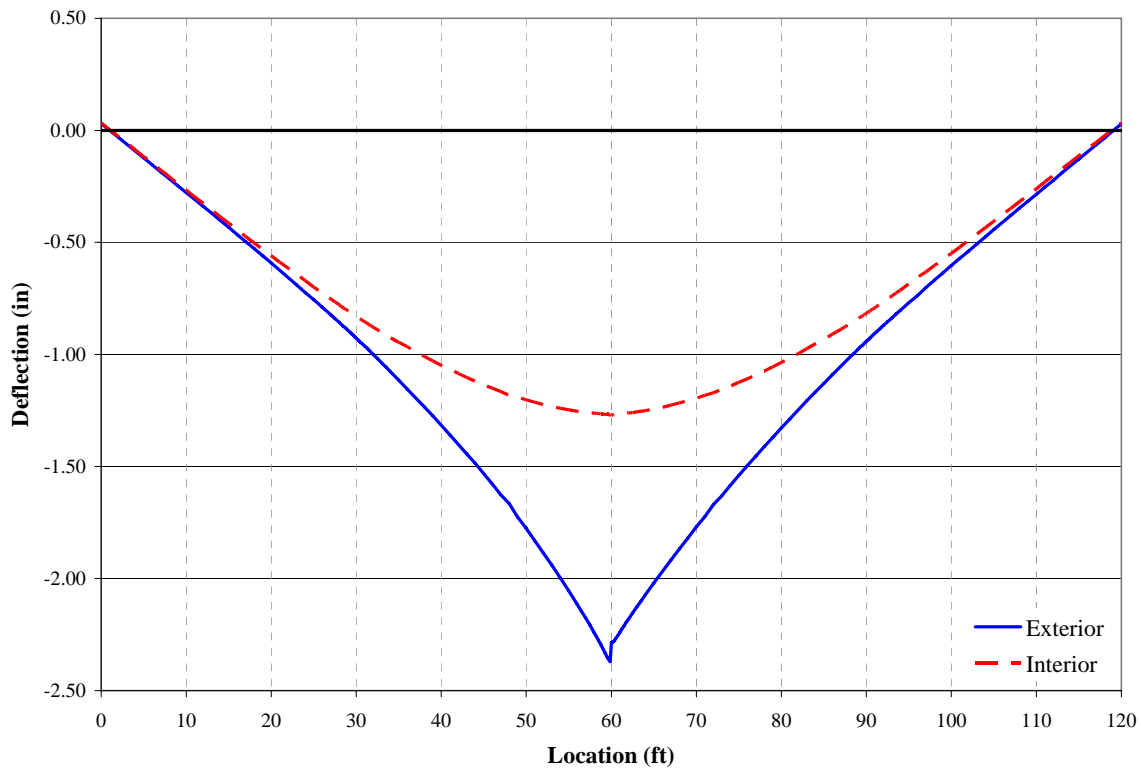


Figure 6-12: Change in deflections of the interior and exterior flange during a simulated full-depth flange and web fracture

The stability of the structure then becomes dependent on four additional factors: (1) the stresses in the bottom flange of the interior girder, which could be high enough to cause yielding; (2) the stresses in the shear studs, which are expected to pull out of the concrete deck if the load is too great; (3) the strain in the rebar of the deck and rails; and (4) the presence of uplift at the supports, which could cause the bridge become unstable due to a lack of proper restraint. The first three factors are considered in the following sections; the reaction forces are discussed further in Section 6.6.1.3 in conjunction with bridges of variable radii.

6.4.1.2 Interior Girder Stresses

As mentioned in Section 6.3.3.2, there is a possibility of yielding in the interior girder due to the increased load that occurs after failure of the exterior girder. Using the

von Mises failure stress criterion (Salmon and Johnson 1996), no yielding is expected in the bottom flange as a result of a full-depth fracture. The maximum calculated von Mises stresses are in the range of 40.0 ksi at midspan of the interior girder, which is less than the assumed design yield stress of 50.0 ksi. The actual uniaxial yield stress of the steel in the girders is unknown, as no coupon from the girders was tested. During deconstruction of the test specimen, it would be beneficial to perform this test. The stresses are presented in more detail alongside those from alternate bridge geometries in Section 6.6.1.2.

6.4.1.3 *Shear Stud Strains*

The elongations calculated in the shear studs during a full fracture event were between 1×10^{-5} in. and 2×10^{-4} in. The loads calculated from these strains are between 0.01 and 0.5 k, which is much less than the expected 17 k failure pullout load found by Sutton (2007). While the accuracy of the shear stud modeling was not verified during the flange fracture event, the axial load on one shear stud can be approximated by considering the dead load each will need to carry if the girder below is fractured.

Considering solely statically applied dead loads, six shear studs (three on each top flange) will need to support a tributary width of 22 in. of girder below. The weight of that girder can be found by considering the volume of steel and the unit weight of steel (0.490 k/ft^3):

$$Load_{onestud} = \frac{1}{6} \cdot \gamma_{steel} \cdot L_{trib} \cdot A_{steel} \quad (1)$$

where

$$\gamma_{steel} = \text{unit weight of steel, } 0.490 \text{ k/ft}^3$$

$$L_{trib} = \text{tributary length, } 22 \text{ in. or } 1.83 \text{ ft}^2$$

$$A_{steel} = \text{area of steel in girder cross-section, } 0.76 \text{ ft}^2$$

The result is 0.11 k, which is again much less than the experimental limit load, and approximately equal to those calculated from the ABAQUS model.

The more damaging impact could be that caused by the dynamic change in geometry. Sutton showed the shear studs to have very little ductility, meaning no plastic behavior is expected. Additionally, the tests were run with static loads; it is unclear if dynamic loads will increase or decrease the pullout strength. The combination of increasing the expected strains and decreasing the pullout strength could result in an unbuttoning response of the shear studs: the set nearest to the fracture fails, thus more heavily loading the set 22 in. away, which quickly fail, and the process repeats down the length of the girder. The results from this model do not indicate this progression as a likely mode of failure.

6.4.1.4 Rebar Strains

In the model, the rebar was defined explicitly for two reasons: the first was to account for the failure of the surrounding concrete without losing all capacity in the deck; the second was to allow for data comparison with the rebar gauges. During the flange fracture event, the rebar gauges indicated so little change that there were no meaningful comparisons to be made. However, the analytical model does still have predictive capabilities for a full web fracture event. The total stresses expected in the rebar after girder fracture are presented here.

The analysis was run with a perfectly elastic rebar model, as the stresses were never high enough to indicate imminent plasticity. The rebar was modeled using truss (axial) elements, so the direct stresses (S11) were considered. Figure 6-13 presents a schematic of the stress value data shown in Figure 6-14 and 6-15.

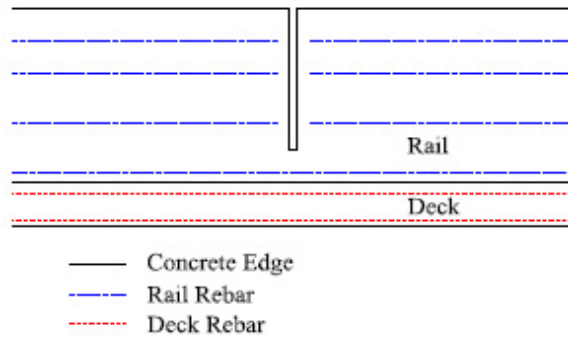


Figure 6-13: Schematic of the rebar stress figures shown in Figures 6-14 and 6-15

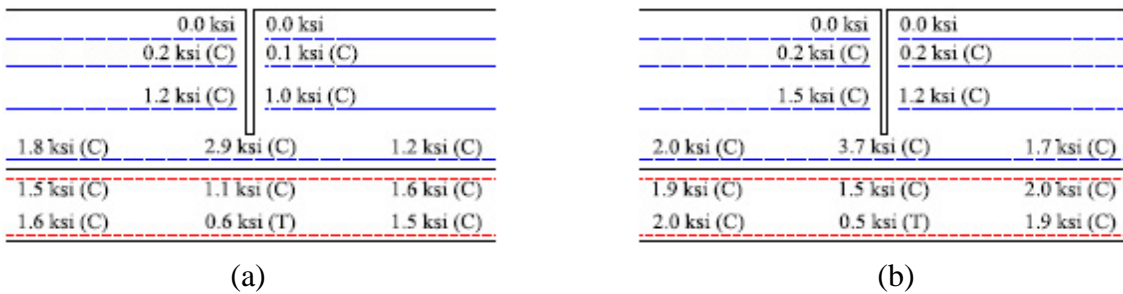


Figure 6-14: Predicted total stresses from live load in (a) interior and (b) exterior deck and rail rebar at midspan

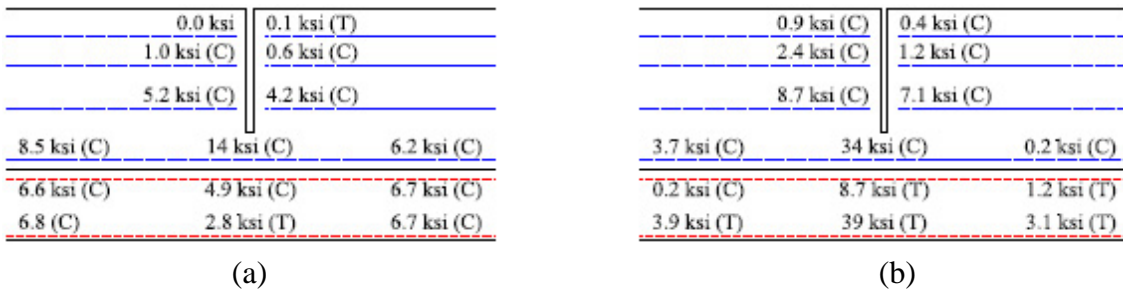


Figure 6-15: Predicted total stresses after a full-depth flange and web fracture in (a) interior and (b) exterior deck and rail rebar at midspan

The general trends include high stresses right near the central expansion joint, which coincides with the induced fracture. Additionally, the full-depth fracture results in the neutral axis being located much higher at midspan, which is expected due to the lack of stiffness in the external girder. The high stresses calculated in the rebar were very

localized, remaining within three feet of midspan and of the external edge of the deck. In all cases stresses were not large enough to indicate yielding of the rebar.

6.5 EFFECT OF DYNAMIC LOADING

Dynamic response calculations are made through a series of iterations that capture the behavior at many points through a load step. Because each iteration means solving the governing system of equilibrium equations, dynamic studies take significantly more time to run than static ones. As such, in an effort to limit computation time, it is useful to mimic the behavior experienced from a dynamically-applied load using statically-applied loads.

In 1989, the National Cooperative Highway Research Program released a report discussing redundancy ratings for two-girder steel bridges (Daniels et al.). In it, loads were applied statically, but the standard truck loadings were increased by 30% to account for dynamic impact. However, the dynamic effects of the fracture are not considered explicitly. Instead, further studies increased the truck load until “failure” was reached (according to serviceability concerns, or the ability of a truck to cross the bridge safely).

In an effort to capture dynamic load increase effects for the present study, an analysis was defined using a method similar to that used for progressive collapse modeling of structures. The Unified Facilities Criteria Guidelines (2006) state that, to consider the dynamic effects of the failure of a column, the loads in the surrounding bays should be magnified by a factor of two. As there are no bays on the bridge, this method was modified slightly. Instead, the gravity and truck loads within two times the depth of the girder (or approximately 96 in.) in either direction from the fracture location (midspan) were multiplied by two. While there are recommendations in recent literature to use a magnification factor of 1.5 (Ruth et al. 2006), the guidelines still advise using 2.0, so that was the value used for this research project. Each 50% increase added approximately 70 kip to the total load on the bridge, increasing the total load from 600 kip (no amplification) to 670 kip ($\times 1.5$) to 740 kip ($\times 2.0$).

The UFC Guidelines state that 1.2 times the dead load and 0.5 times the live load should be magnified. The decrease in live load reflects the probability of having the full design load at the time of failure. In this study, the “live” truck load was considered as dead load, as it was known to be on the bridge at the time of the fracture. In a real fracture situation, a load would have moved across the fracture location during some part of the fracture event; the truck used here did not. The impact of the truck on the response of the bridge was thus more similar to a dead load, and as such, the truck loads were also amplified in the dynamic load study.

The effects of dynamically applied loads are felt during the first moments of the event. The difference in static and dynamic responses can be seen in Figure 6-16, where the dynamic load (applied at Time = 1.00) creates a peak value approximately two times the final value from a static load. The statically calculated values with dynamic amplification factors were thus compared to the peak change in strain in the gauges, not the overall change (as has been previously considered).

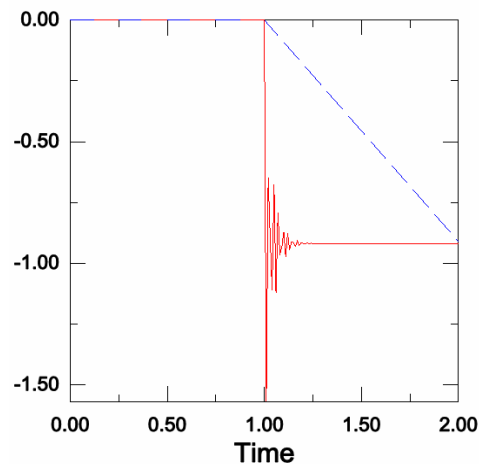


Figure 6-16: Example of the difference in peak values from static (blue dashed line) and dynamic (red solid line) load application

The expectation was that the peak strains measured would fall between the strains calculated using a 1.5 and a 2.0 amplification factor. Of the eight foil gauges that returned good results from the flange fracture test, only two fit this trend. The other six

registered strains greater than even the 2.0 amplification factor would suggest. A comparison of each gauge reading and calculation can be seen in Figure 6-17.

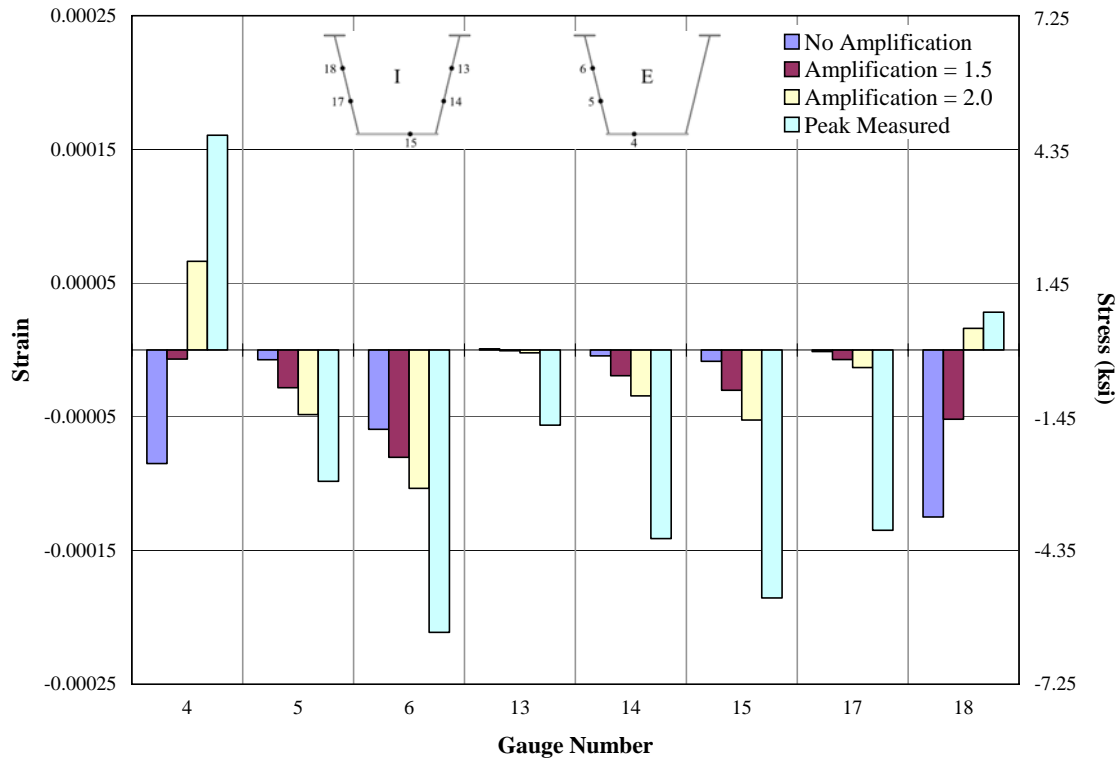


Figure 6-17: Measured peak and calculated base and amplified strain values during fracture event at locations indicated on inset (6 ft south of centerline)

The higher peak strains could indicate several things. Most simply, the area over which the loads were amplified in the models was possibly not large enough. More load would certainly increase the calculated strains. However, to arbitrarily increase loads without reason is not a good analysis decision, as it cannot be repeated with confidence for other geometries. Additional load amplification areas, such as the entire length of the bridge, as there are no additional supports between the fracture and the ends, could be tried and compared to the gathered data to find a better method of capturing the dynamic response. However, true verification of any load scheme would require data from multiple bridge geometries to show that the same loading method works independently of geometry.

One critical detail when considering dynamic loads is the length of time over which they happen. If the peak strains were felt in the bridge for just a millisecond, the impact of that load both locally and system-wide could be minimal. In an effort to remove the change of a high peak value skewing the data, an alternate method could be used where the values recorded in the first milliseconds of the test (for instance, 50 ms) are averaged to get an effective “peak” value. If the gauges read high for just an instant, the timed average would lessen the effect of that maximum on the recorded data. Further study and comparisons based on additional data are needed to better understand appropriate static loads to mimic dynamic response.

6.6 ALTERNATIVE GEOMETRIES

One of the goals in designing this model was to be able to make predictions of the behavior of other bridges. The bridge studied here had three details whose influence was of particular interest. First, the bridge has a very large radius of curvature, which, relative to a bridge with a small radius of curvature, minimizes the amount of torsional stress on the bridge during a fracture event. Second, researchers are presently debating the merits of keeping or removing the external cross-braces used during construction. Currently, as in this study, they are removed after the deck is cured because there is concern that they may help initiate a fracture at a critical location. Conversely, they may benefit a fracture-critical bridge by providing additional load paths to transfer forces from one girder to the other. Lastly, the test specimen in this study was simply-supported and thus lacking redundancy that could come from multiple spans. The base input file was modified to consider these three variables. The following sections present comparisons in the response of the system with these varying geometries.

6.6.1 Variable Radius

The AASHTO Guide Specifications for Horizontally Curved Steel Girder Highway Bridges (2003) is written for bridges with a minimum radius of curvature of

100 ft. Considering the length of the bridge in this study is only 120 ft, studying a radius that small was not necessary. Section 4.2.2 of the specification states that

the effect of curvature may be ignored in the determination of vertical bending moment in box-girder bridges when ... the arc span divided by the girder radius is less than 0.3 radians (AASHTO 2003).

Using the arc length of the bridge and rearranging the equation to solve for R ,

$$R = \frac{L_{arc}}{0.3} = \frac{120 ft}{0.3} = 400 ft \quad (2)$$

The minimum radius of curvature considered was thus chosen as 400 ft. An intermediate value of $R = 800$ ft was also used as a middle geometry. All three of these geometries are still considered to be essentially straight; further study should include tightly-curving bridges where the AASHTO limit given above is exceeded. For the geometries considered, the deflections and bottom flange strains from each bridge were compared, as were the reaction forces at the ends. These three variables are general indicators of performance and are useful in assessing the system-wide stability of the structure. For instance, uplift reaction forces at the ends could indicate instability of the bridge in the form of possible rollover.

6.6.1.1 Deflections

The bottom flange deflections of the bridge give an idea of the magnitude of deformation that occurs during a fracture event. Most of the deflection comes from the fractured girder sinking as the stiffness approaches zero at the centerline. The rotation of the girder towards the outside of the curve – where the load is placed, and where the structure is weak – also adds to the deflection of the exterior girder. Figure 6-18 shows the change in displacement of the bottom flange of the exterior girder along the length of each bridge from before fracture initiation to after the web is completely cut. As expected, the smallest radius girder ($R = 400$ ft) has the most deflection, at 2.64 in.

However, this deflection is not significantly greater than what is expected for the near-straight case ($R = 1365$ ft), which deflected 2.37 in, or 10% less.

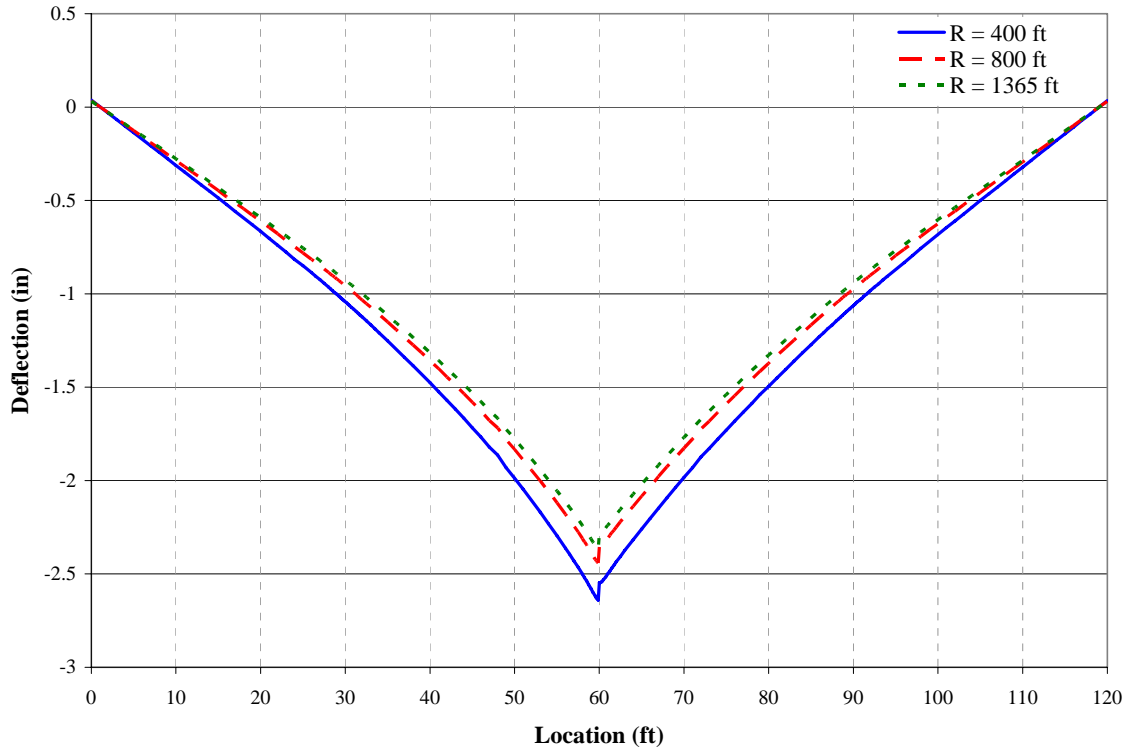


Figure 6-18: Change in displacement of the exterior girder during a full-web fracture with variable radii: blue solid line is 400 ft radius, red dashed is 800 ft, and green dotted is 1365 ft

It should be noted that at the point of fracture ($x = 60$ ft), there is a jump in the calculated deflection. The fracture was modeled just south of centerline, or between 59 ft-10.5 in. and 60 ft. The difference in deflection on either side of the centerline is almost 0.1 in. for the $R = 400$ ft case. Possible causes of this difference include the greater truck load that is applied on the south end of the bridge, or the presence of internal stiffeners on only the north side of the fracture. The result is the formation of a hinge at the fracture location. Prior to the fracture, the bottom flange held the highest moments in the structure, but after, is unable to hold any.

The effect of the hinge can be seen in Figure 6-19 and Figure 6-20. The former shows the deflection in the bottom flange of the exterior girder after the flange has been

fractured but while the web is intact. The latter shows the total deflection after the web has failed. The shape of the curve in Figure 6-20 shows how the hinge has formed: the girder bends very little between the support and midspan.

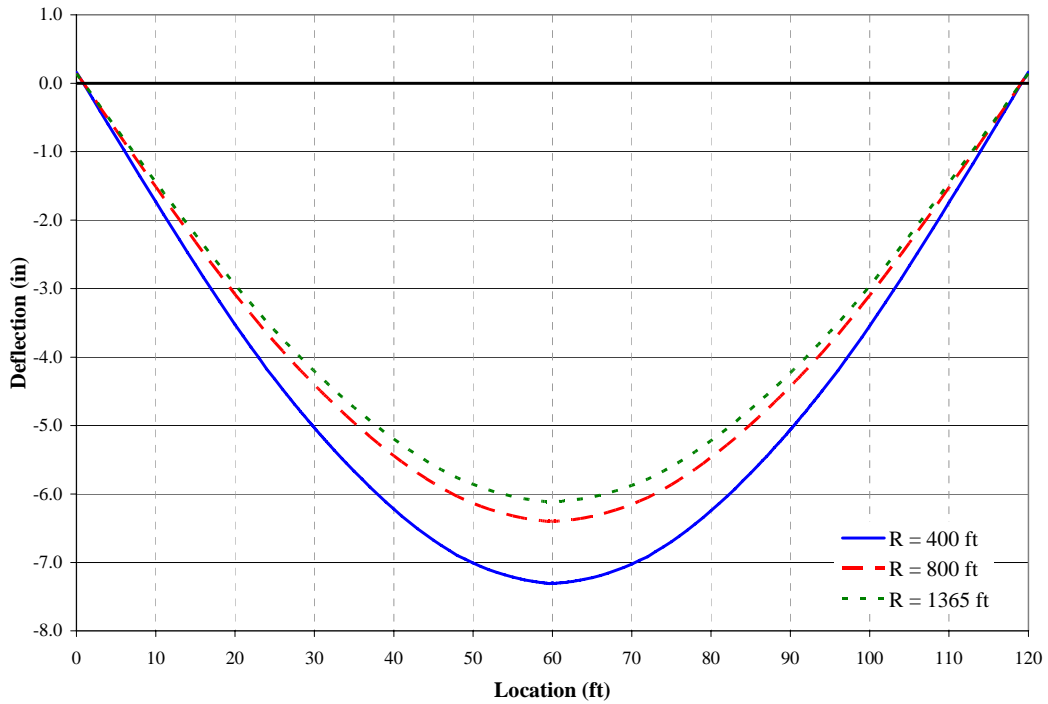


Figure 6-19: Deflection of the bottom flange of the exterior girder after flange fracture

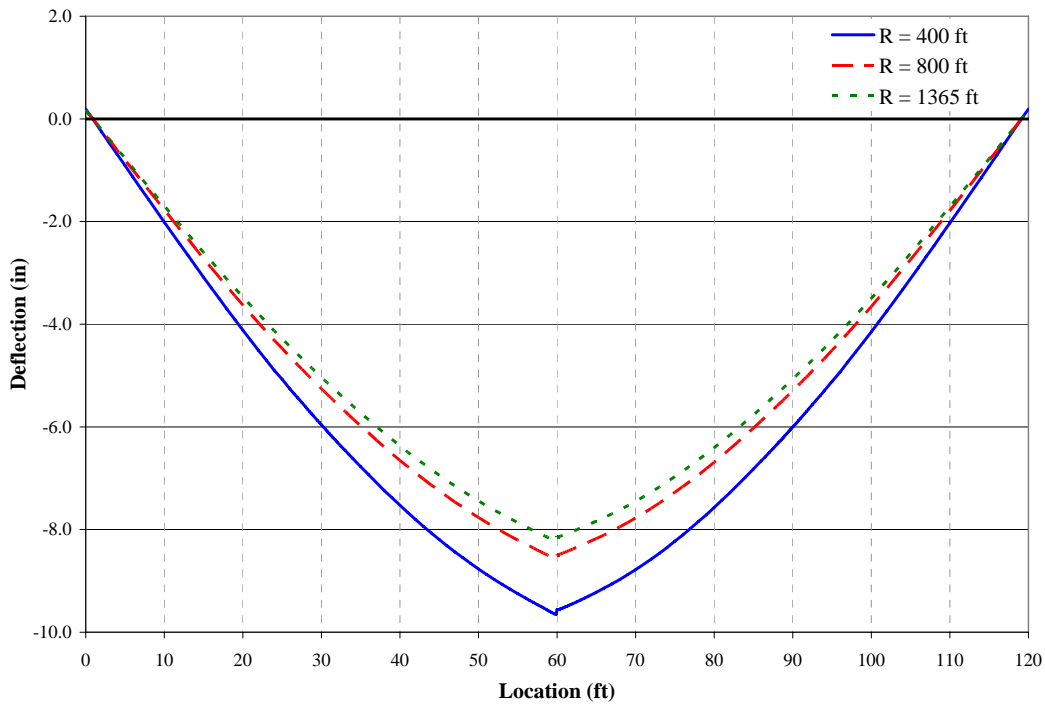


Figure 6-20: Total deflection of the bottom flange of the exterior girder down the length of the bridge, post-web fracture

The hinging effect is present in all three geometries, without much variation in response. However, in all three cases, the web fracture was dictated to progress through the web to the top flange. An actual fracture event might occur differently in the three bridges due to the varied magnitude and distribution of service-load stresses, so results suggest a worst-case scenario.

6.6.1.2 Bottom Flange Stresses

Upon fracture of the exterior girder, load is expected to transfer to the interior girder through the shear studs and deck. Assuming the shear studs and deck have the ability to transfer this load, the interior girder must have the capacity to withstand the resulting increase in stresses and strains. The maximum bottom flange stresses for the three different bridge geometries considered are presented in Figure 6-21. For each geometry, the maximum stresses in the bottom flange of the interior girder occurred at

the intersection of the web and flange on the outside of the horizontal curve of the bridge (towards the fractured girder). The element at midspan (in the same longitudinal location as the fracture), as well as one element north and south of midspan, are shown in the figure. The stresses in the interior girder flange pre-flange fracture are within two ksi of the stresses shown post-flange fracture.

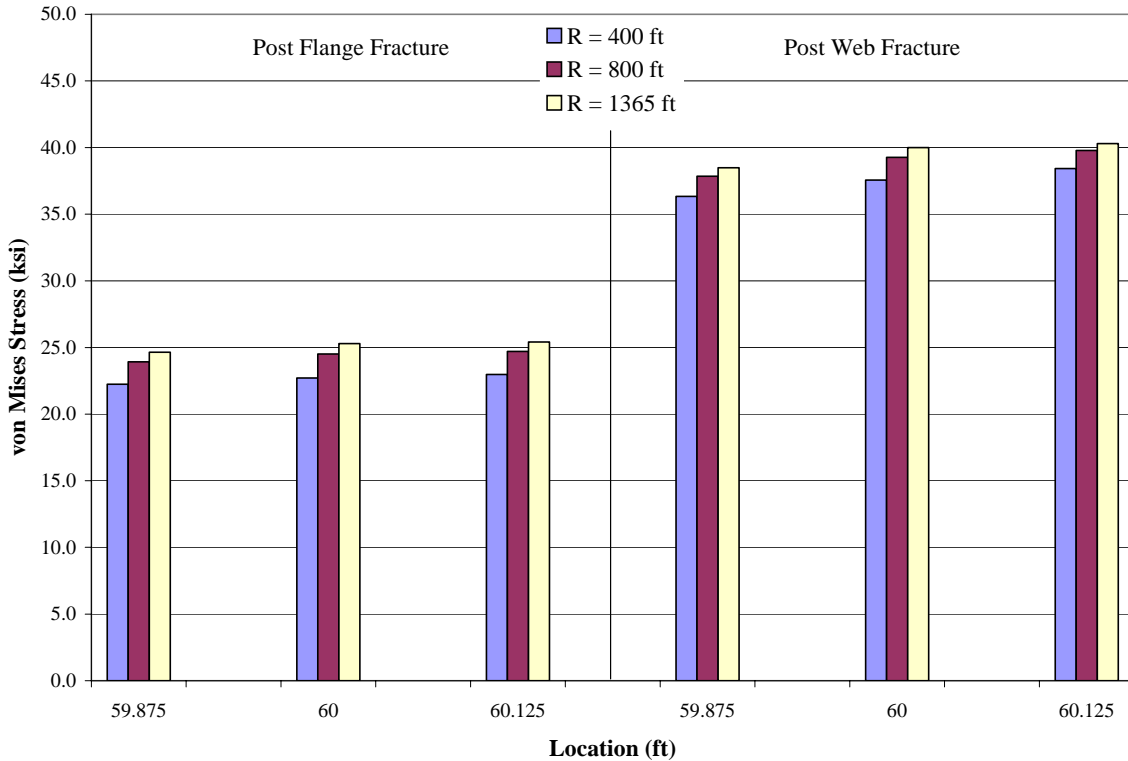


Figure 6-21: von Mises stresses calculated in the bottom flange of the interior girder after each stage of fracture for three different geometries ($R = 400, 800,$ and 1365 ft)

The clear trend with the variable radius is an increase in stress as the radius is increased. This increase is likely due to rotation across the width of the bridge that is experienced more with the smaller radius, where the interior girder is actually lifting slightly, thus reducing the amount of tension experienced by the bottom flange. Achieving a failure through flange yield during a fracture is thus more likely in a straighter bridge. However, for all three geometries considered, the stresses did not reach the von Mises yield criterion, which was defined as 50.0 ksi for the steel used. The

interior girder thus remained elastic and has reserve capacity to withstand load transferred from the failed exterior girder.

6.6.1.3 Reaction Forces

Curved bridges must be designed to resist torsion both within the members and as a system: loads on the exterior edge of the bridge must not be able to tip the girder off its supports. Neither elastomeric or pot bearings have any tensile capacity, which means uplift cannot be resisted. For this study, the fracture was initiated in the exterior girder, as the exterior girder is normally instrumental in securing the system-wide stability (i.e., it represents a worst-case scenario). The reaction forces were calculated at each of the sixteen support nodes: four on each girder, at each end. The forces are referenced in the graphs by a letter and number. The letter determines the location across the bottom flange (shown in Figure 6-22), and the number indicates the end of the bridge, with 1 being the south end (roller support) and 2 being the north (pin support).



Figure 6-22: Support locations and lettering scheme

Figure 6-23 shows the total vertical reaction forces at each of the sixteen support nodes after a full web and flange fracture event for the three different geometries. While the geometries were different, the total load on each bridge was within 0.5 kip of one another (0.1% of the total load of 600 kip). Only the 400-ft radius bridge experienced any uplift (negative reaction values), and neither instance spanned the entire width of the support. The trend was for the girders to lean on the supports toward the outside of the curvature of the bridge, which is expected for a curved bridge.

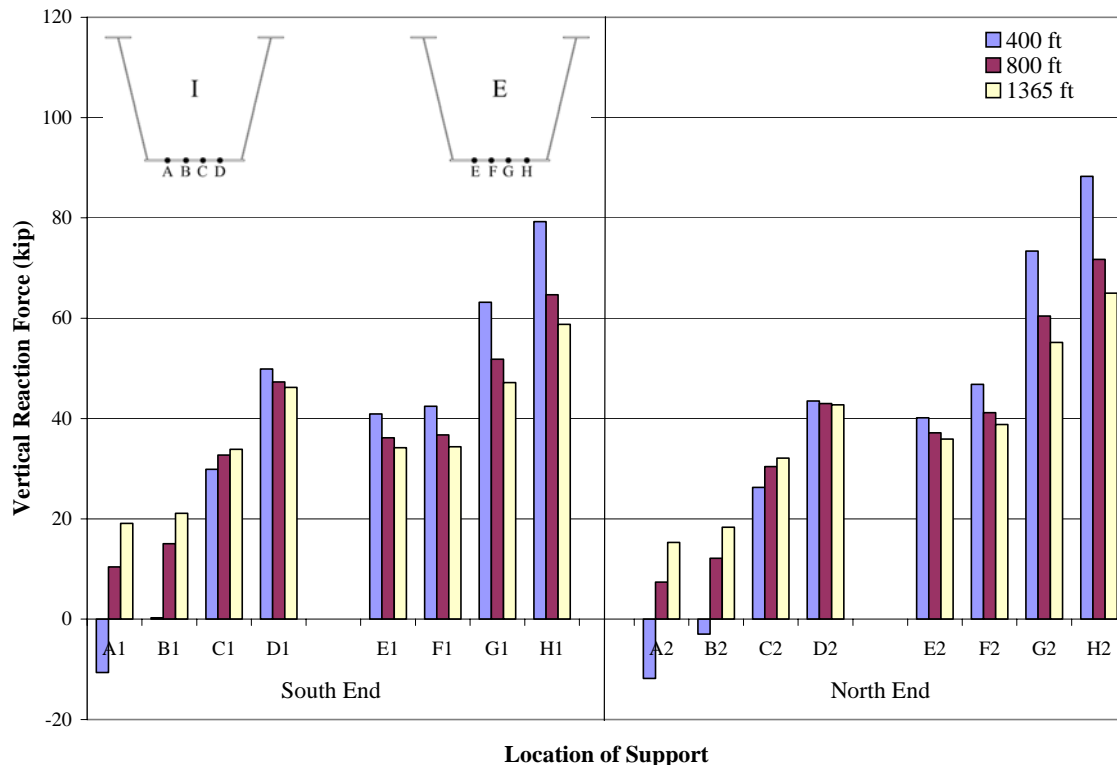


Figure 6-23: Total reaction forces after a full web and flange fracture event for three different geometries ($R = 400, 800,$ and 1365 ft)

The total load on each bearing can be calculated by summing the reactions at the four constitutive nodes. The reaction forces calculated before and after the fracture event are presented in Table 6-2, along with the difference between the two steps. The analyses predict that transversely, the loads will shift from one support to the other, in amounts of 4 to 10 kip. At the south end, the loads increase on the interior support and decrease on the exterior. At the north end, the loads increase on the exterior support and decrease on the interior. This difference in response could be due to the decreased stiffness in the exterior girder, which would cause rotation of the bridge towards the outside support, and the hinging of the fractured girder, which would lift the end of the girder off its support. The hinging effect dominates over the overturning effect at the south support because the majority of the truck load is south of centerline.

Table 6-2: Variation in reaction forces at each of four supports for three bridges of different radii

Location			Loads (kip)		
			Pre-Fracture	Post-Fracture	Change
R = 400 ft	South	Interior	60.2	69.4	9.3
		Exterior	235.0	225.8	-9.1
	North	Interior	59.8	55.0	-4.7
		Exterior	244.0	248.7	4.6
R = 800 ft	South	Interior	96.8	105.5	8.8
		Exterior	198.1	189.4	-8.7
	North	Interior	97.4	93.0	-4.4
		Exterior	206.2	210.5	4.3
R = 1365 ft	South	Interior	111.7	120.3	8.5
		Exterior	183.0	174.5	-8.5
	North	Interior	112.7	108.5	-4.2
		Exterior	190.8	195.0	4.2

The change in vertical reaction force from pre- to post-fracture (using two static load steps) was also calculated and is shown in Figure 6-24. These forces again show the rotation of the girders on their supports, decreasing the load towards the inside and increasing the load towards the outside. The exterior girder supports on the south end are almost entirely negative, showing a decrease in the reactions across the entire girder. This decrease could be due to the effective hinge that forms in the bridge when the fracture is formed, as was shown in Figure 6-20. The difference in response between the north and south ends could be a result of the placement of the fracture, which is just south of centerline in the model, and the placement of the truck, with the majority of the load south of centerline.

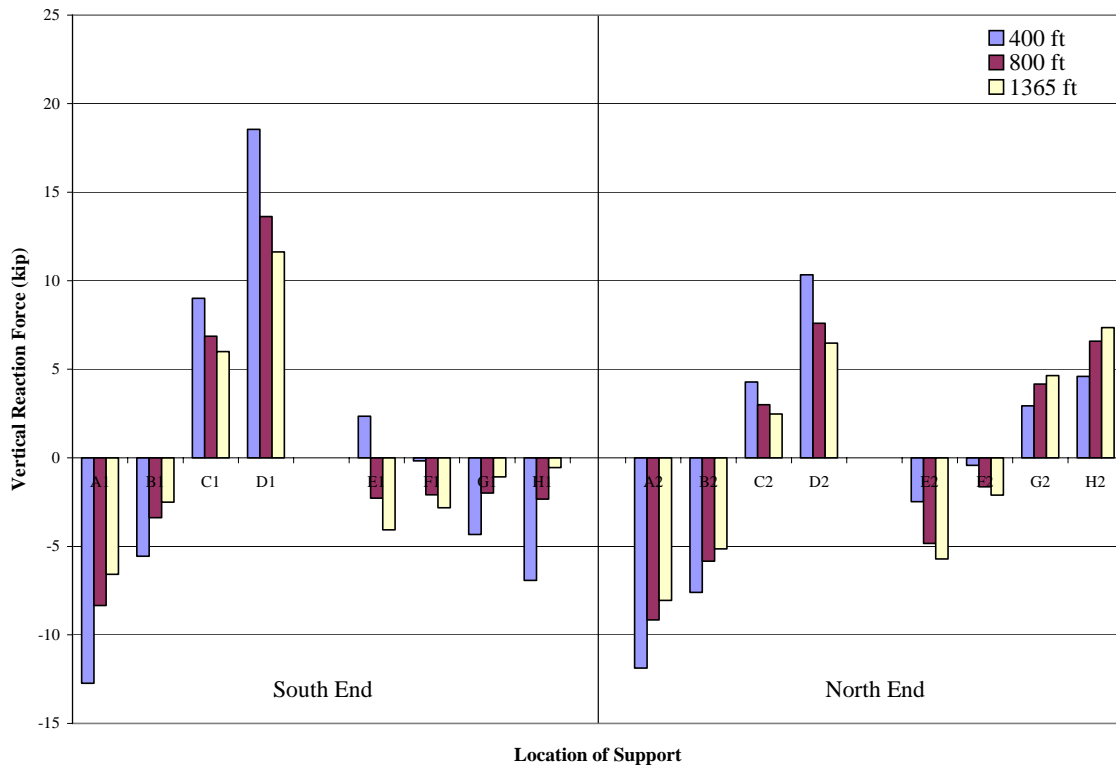


Figure 6-24: Change in support reactions during a full web and flange fracture event for three different geometries ($R = 400, 800, \text{ and } 1365 \text{ ft}$)

At three of the four supports, the response across the bearing is the same for all three bridge geometries. For the exterior girder at the south end, each responds slightly differently. The 800-ft radius bridge shows a uniform decrease in reaction forces across the width of the bearing (nodes E1 to H1). The 1365-ft radius bridge follows the trend of the other three supports, with the uplift being smallest towards the exterior of the curve of the bridge, indicating some roll of the girder towards the outside. The 400-ft radius bridge, however, varies in the opposite direction, increasing in uplift towards the exterior of the bearing. These variances are most likely due to the hinging at midspan and the truck load placement. Further study is warranted considering bridges of larger and smaller radii and different load schemes to determine the true cause of the response.

The data presented in Figure 6-23 and 6-24 and Table 6-2 can also be used to consider the moments produced within each bearing pad. The larger radius bridge has

less variation in reaction forces between the interior and exterior girder, and across each individual bearing. As the bearings were all modeled with the same width (22.75 in.), the moment around the centerline of the larger-radius bridge bearings are thus less than in the smaller-radius bridge. The change in moment during the fracture is also smaller. The total moments for each of the bearings before and after the fracture event are presented in Figure 6-25. Of the four bearing locations on each bridge, only one responds differently: the southern support on the exterior girder. This support is the same one discussed previously. As the moments are calculated from the reaction forces, the same factors would influence the response (truck loading and hinging at midspan).

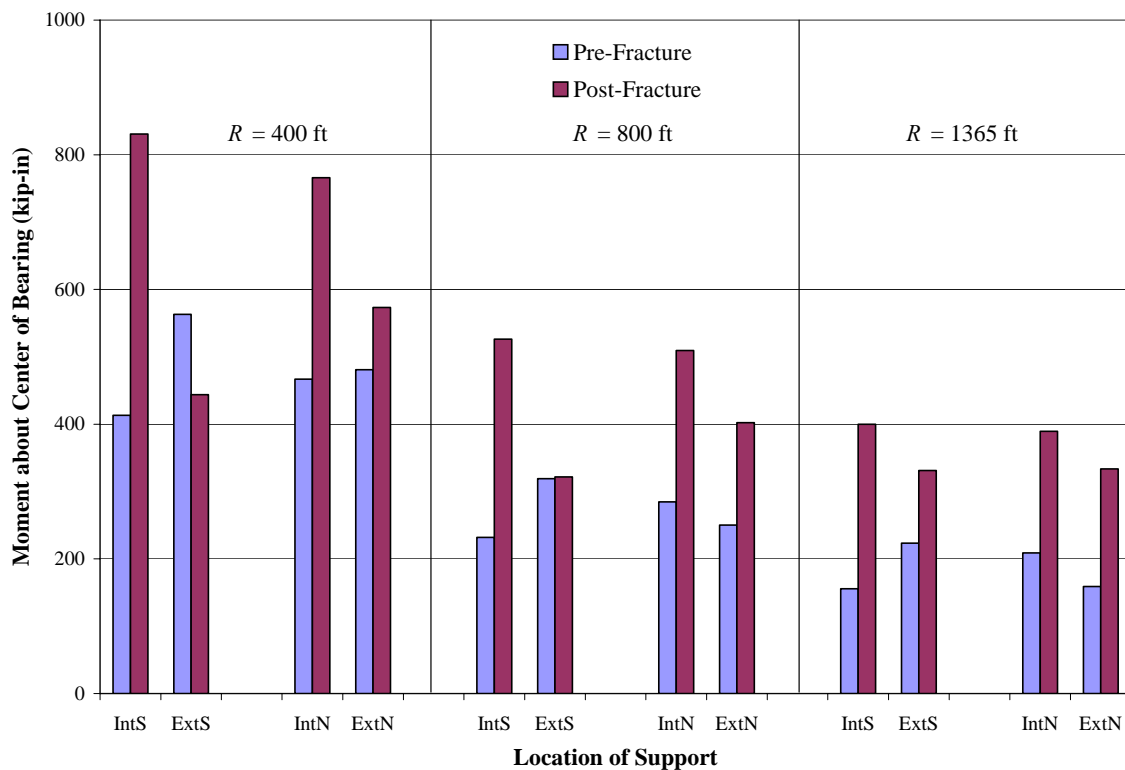


Figure 6-25: Moment about the centerline of each bearing pad for three bridges of different radii. The bearings are located beneath the internal and external (Int and Ext) girders at the north and south ends of the bridge (N and S).

In a case where rollover is of concern (as may be for the 400-ft radius bridge), bearings that include uplift prevention mechanisms are warranted. Although more

expensive, if this minor modification to the design could prevent collapse in a fracture event, it would be practical to use it.

6.6.2 Influence of External Bracing

In the construction of the full-scale test specimen, the external bracing frames were removed after construction was complete, as is standard in Texas box-girder bridges. In general service life, the braces hold very little load but can be a source of fatigue crack initiation. However, in the case of a fracture event, the braces might have the ability to transfer load from the fractured girder to intact components of the bridge. A model was run with the braces left in place during the two fracture events (flange and web removal). The external braces were able to aide in transferring load from the fractured girder to the remaining one but did little to restrict rotation and independent movement of the fractured girder. The model predicts a decrease in deflections during the web removal step of approximately 0.07 in., as summarized in Table 6-3. The overall shape of both girders post-fracture was the same with and without the braces.

Table 6-3: Maximum change in deflection at midspan of the fractured girder with and without external cross-bracing

	Change in Deflection (in)	
	Flange Fracture	Web Fracture
Without bracing	0.26	2.16
With bracing	0.26	2.09

The stress gained in the external braces during the flange fracture was less than 1 ksi in each individual member. Removing the flange and web resulted in a total stress of up to 7.3 ksi in tension and 6.6 ksi in compression, as shown in Figure 6-26 (the larger stresses in the south brace are likely due to the location of the fractured elements, just south of midspan). Considering the areas of the members (6.31 in² for the horizontal T-shapes and 6.1 in² for the inclined double-angles) and assuming pinned connections at both ends, the critical buckling stresses are one to two orders of magnitude greater than

the induced compression stresses, and none of the calculated values near a 50 ksi yield stress.

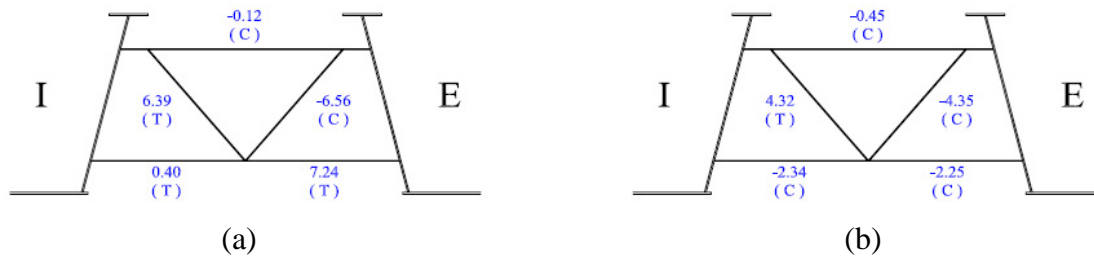


Figure 6-26: Total stresses calculated in the (a) south and (b) north external brace elements after flange and web removal (actual braces connect at girder web; drawn for clarity in data presentation)

The external braces are generally removed because of fatigue concerns at the connections with the web plates. Any weld that holds tension forces is susceptible to flaw growth from fatigue. However, the estimated life for a member (in terms of cycles of load) is dependent on the stress range in that member. The stresses accrued in the members during service (before the fracture event) were calculated to be between 0.01 and 1.5 ksi, which could be small enough to classify the connection as having an “infinite life” and thus need not be considered during fracture-critical inspections.

Concerning global stability, the bottom flange stresses in the unfractured girder are of importance. By transferring more of the forces from the fractured girder, the external braces slightly increased the stresses induced during the fracture event. The differential, shown in Figure 6-27, is greatest on the outer edge of the interior girder flange. Considering the positive difference on the inner edge (meaning the model without cross-braces calculated higher stresses), the cross-braces are causing rotation of the interior girder towards the exterior girder. As the cross-braces add points of contact between the girders, this rotation should be expected as the fractured girder deflects more significantly than the unfractured girder.

The external cross-braces modeled match those designed for construction stability purposes on the test specimen but not for load-transfer capabilities. Further study should

include using stiffer braces that are designed for the purpose of transferring the dead load of the fractured girder to the unfractured interior girder.

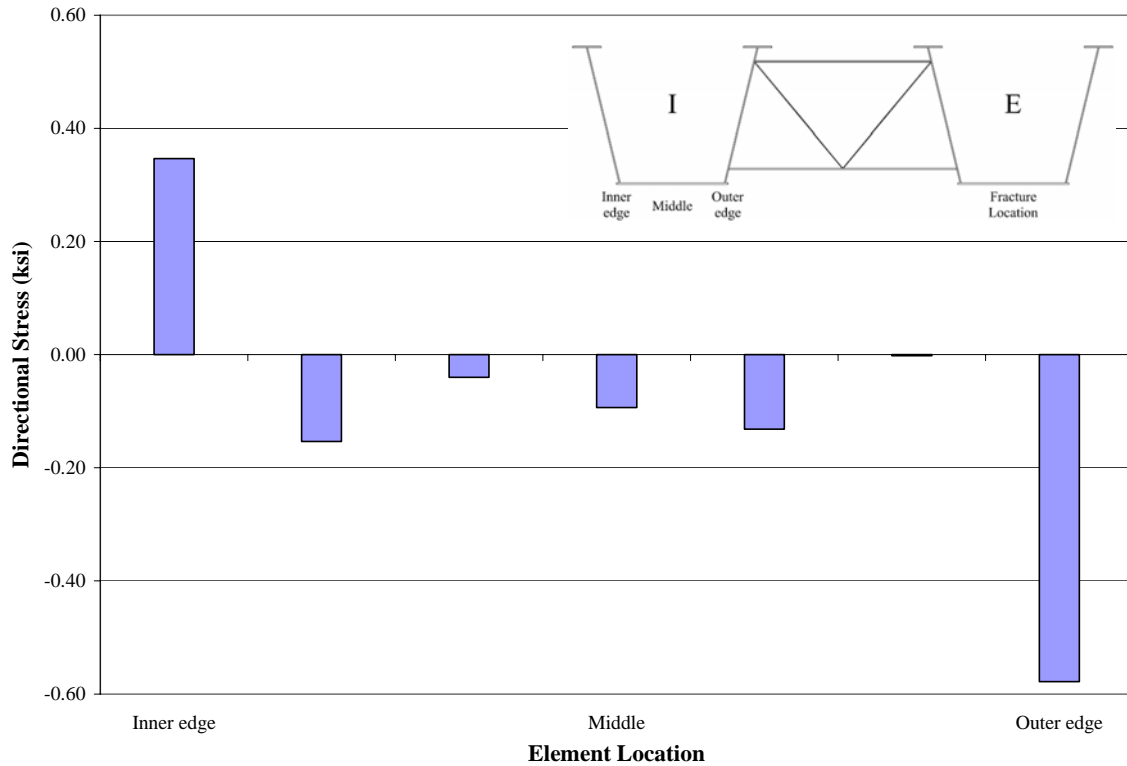


Figure 6-27: Difference in average midspan stresses across the seven elements of the interior girder bottom flange with and without external braces after a full-depth fracture. Negative values indicate the stresses with the braces in place were higher.

6.6.3 Benefits of Structural Redundancy

All of the previous recorded fracture incidents involved bridges with multiple spans. As was explained in Chapter 2, the indeterminacy of such a structure could provide redundancy to an otherwise non-redundant two-span girder. The 120-ft long bridge initially modeled was thus tripled in length to form a three-span continuous structure to evaluate the role of structural redundancy in a fracture event.

The modeling was accomplished in the same fashion as the previously designed model, with elements being defined through a greater length than for the original model. At the intersections of the spans, elements were defined more explicitly to capture the

non-sequential numbering at that location. Another option would have been to use the ABAQUS keywords ***part**, ***instance**, and ***assembly**, which allow for one object to be defined (such as a single span) and then copied into the model multiple times.

The geometry of the multi-span structure is very similar to that of the previously-modeled bridge. There are three spans, each 120 ft in length and containing bracing identical to the original model. Two external braces are in place on each span through deck casting, then they are removed. Two fracture scenarios were considered: in the first, the midspan web and flange elements of just the center span are removed during the fracture steps. However, the pre-fracture deflections and strains of the continuous beam indicated that the worst case would be a fracture in one of the end spans. Thus, the second test featured a fracture at midspan of an exterior span.

The expansion joint that would exist in the rail at the central supports (as per former TxDOT requirement) is not included as to do so would require increasing the mesh density significantly at the end of each span. Considering the expected response, with a negative moment region across the support, a continuous rail could add benefit to the structure. In a more detailed analysis, the expansion joint could be included based on the expected bridge design; since the initiation of this project, TxDOT has removed the requirement for expansion joints as were used in this study.

At the other joint locations, contact was only considered for the gaps in the rails of the fractured span. While the fracture event may cause a closing of the space in the railings, the closure is expected to be small enough to not require contact considerations. This assumption was validated by considering the simply-supported case, where the gap closed less than 0.5 in. between element re-activation and web fracture. As contact constraints add significantly to computation time, it was beneficial to limit the number of contact locations considered.

To limit the contact considerations further, the shear studs were not included in this study. Instead, the deck and flanges were designed as fully composite; the two elements share nodes at their joint. While the spring element shear studs themselves do not add significant computation time, the contact constraint between the haunch and

flange was found to double the time for analysis in the simply-supported case. Because the changes in deflections were not expected to be large, and the strain in the shear studs of the simply-supported model were so small, this assumption was appropriate and allowed for great savings in computation time.

An additional inaccuracy in this model is that the deck loading occurs all in one step, with each span having “wet” and “dry” concrete at the same time. During construction, this timeline is not practical and thus the induced stresses before fracture are not likely to correspond precisely with what would be expected in the field. This error could be removed by adding more load steps in which different sections of deck are cast and cured separately, accounting for the change in stiffness due to the hardened deck; to do so would add time to the computational effort. Additionally, the stress in the girders from dead load is generally significantly less than those added during the fracture, and thus the calculations of response were considered acceptable with the simultaneous casting of the decks.

Lastly, the deck and rail rebar were not included in this study. The study was originally written with rebar considerations; however, the memory needed for such a large study was not available on the personal computer used for the rest of the analyses in this project. Considering the additional calculations that come from added elements (the rebar) and constraints (embedding the elements), the estimated time to run the study was also found to be impossible considering the computing limitations. The University of Texas does, however, have a high-level computing facility available to researchers within and outside of the UT program, the Texas Advanced Computing Center (TACC). If the rebar is considered to be of great importance (such as in near-failure cases), resources like TACC can be used to conduct additional analyses. Analyses of such large size do not meet the project goal of being able to be run in a design firm facility, and so the rebar was removed for these studies.

The expectation in considering a multi-span bridge is that the post-fracture deflections and stresses would be less than those in the simply-supported case. This belief is based on principles explained more fully in Chapter 2: removing a central

element from a continuous bridge forms two cantilevered structures, which, with the proper support mechanisms, can support the additional load. The deflections and support reactions from the multi-span geometry were thus considered and are presented here.

6.6.3.1 Deflections

All of the deflections presented in this section are from full-depth web fracture events; the changes calculated during the flange fracture step were on the order of 0.05 in., and thus not considered to be significant. The deflections along the length of the continuous bridge after a fracture event were compared to both the pre-fracture deflections and to those calculated for a simply-supported structure with a fracture.

The deflections from the first test, with the fracture located in the central span, are shown in Figure 6-28. Two things can be seen in this plot. First, the fractured span deflection changes are much smaller than those from the simply-supported case, measuring under 0.5 in. Second, the end span deflections in fact decrease during the fracture, as load patterns shifted to make the more cantilevered response discussed in Chapter 2.

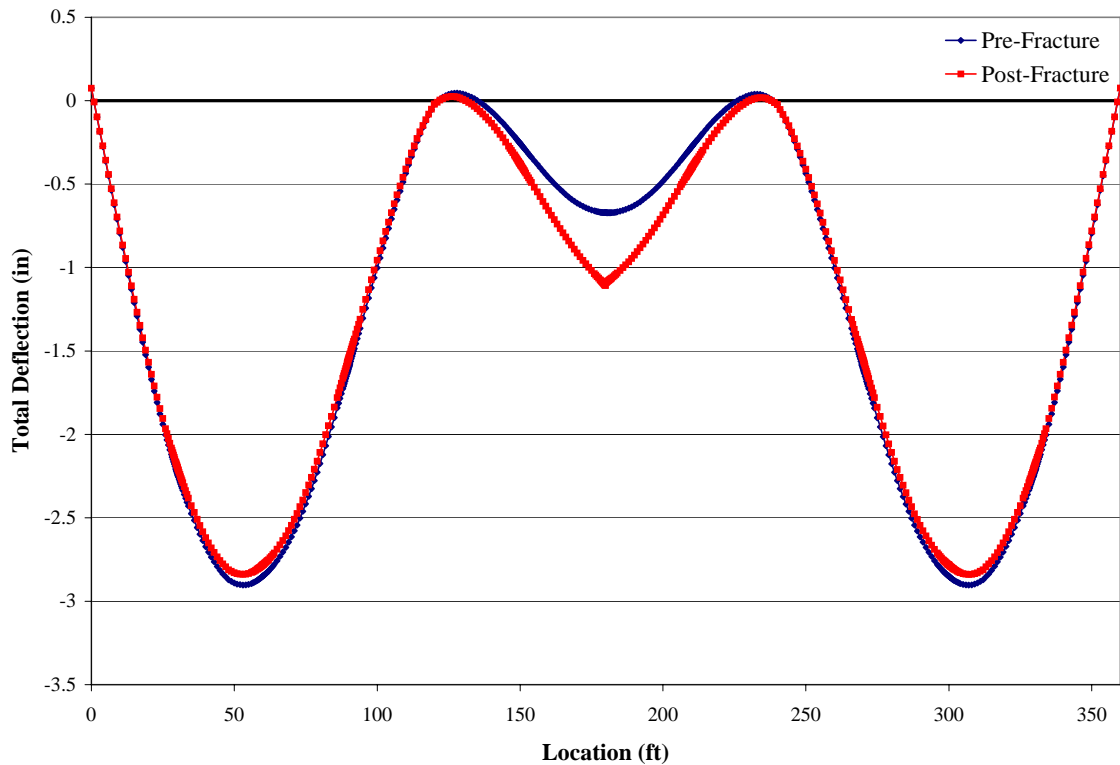


Figure 6-28: Total vertical deflections of the exterior girders before and after a full-depth web fracture at the centerline of the middle span

Analyses conducted for the first scenario also highlighted the need to consider a fracture in the exterior spans, where the pre-fracture deflections (and stresses) are significantly higher than the central span. An exterior span can only benefit from continuity on one side; the other end is more akin to the simply-supported case. The expectation is that the response will be a combination of the two geometries.

The second fracture scenario moved both the truck load and the fracture to the first span of the bridge. It is expected that, due to the symmetric nature of the design, fracturing the third span would cause the same response. The truck load was placed in the same location within the length of the span as in the previous study, which is not necessarily the location of maximum moment. The total deflections along the entire length of the three-span bridge before and after the fracture event are shown in Figure 6-29. As expected, the event causes the fractured girder to deflect significantly, by

approximately 1.0 in. The center span deflections are reduced due to the cantilevered behavior towards the end span. The far span shows almost no change, deflecting less than 0.05 in. The minimal response indicates that a two-span continuous bridge might also hold the same redundancy as a three-span bridge. However, further study considering two- and three-span bridges with varying length ratios is needed to clearly indicate the redundancy in such structures. Additionally, the truck load should be relocated to maximize the moment in the bottom flange of the end span.

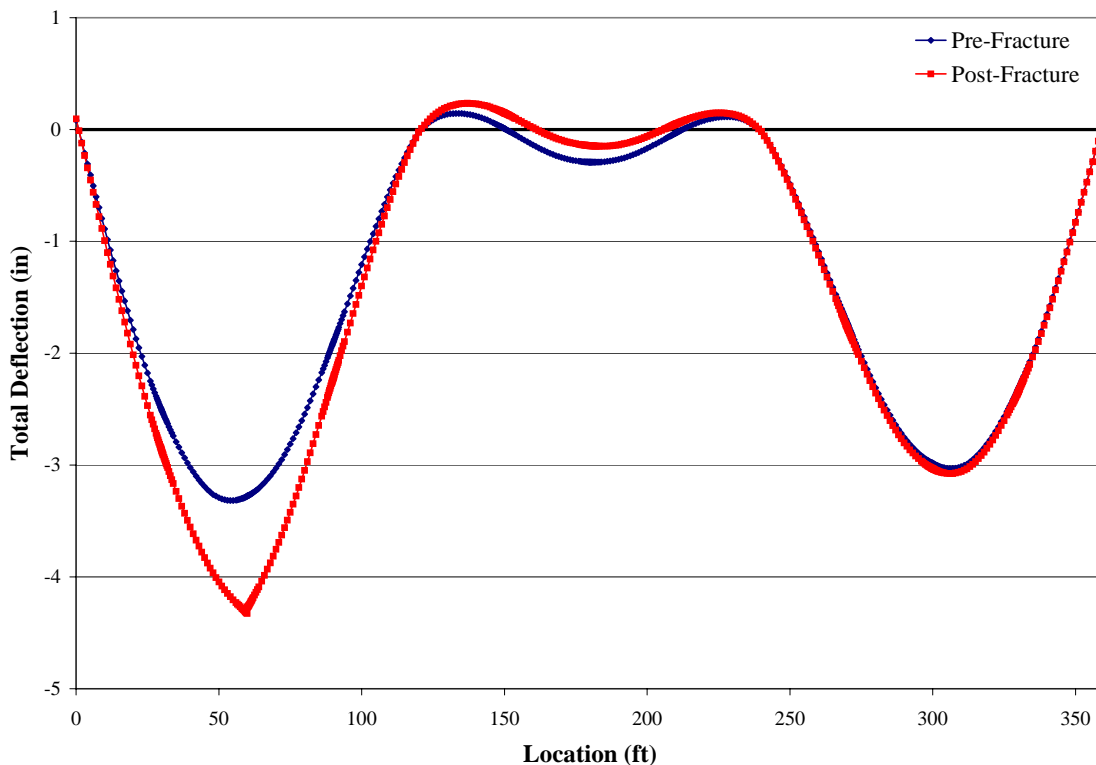


Figure 6-29: Total vertical deflections of the exterior girders before and after a full-depth web fracture at the centerline of the first span

Section 6.4 presented the expected response of a single span bridge during a full-depth web fracture event. Although a catastrophic failure was not indicated, the predictions made depended on the assumptions that went into the model. This study of multi-span bridges was designed to determine if, with similar assumptions, there was benefit from the additional spans, and if so, how much benefit there was. However, due

to the computation constraints discussed earlier, further assumptions had to go into the multi-span models. The single-span model was run again with these same variations (no rebar, rigid contact between the flange and haunch) and the change in deflection of the fractured spans was considered. This comparison is shown in Figure 6-30.

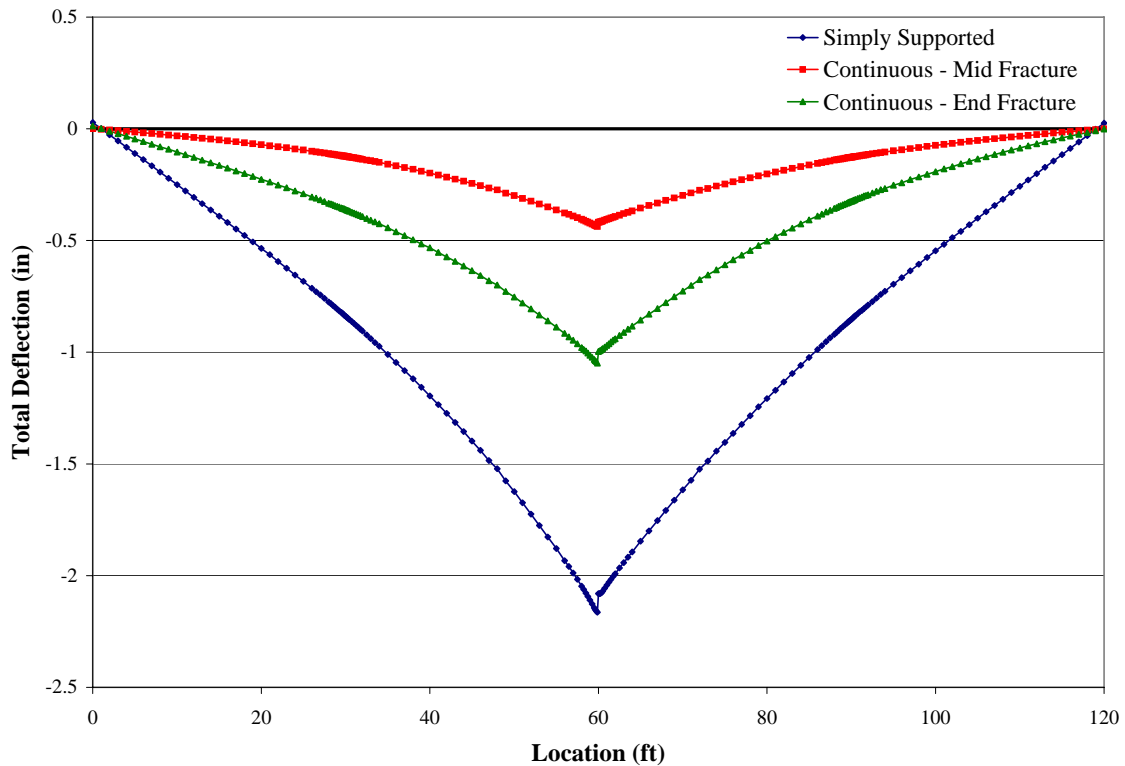


Figure 6-30: Change in displacement of the exterior girder during a full-web fracture for a single span design as compared to continuous bridges with end- and center-span fractures

The simply-supported bridge deflects more than twice as much as the continuous bridge with an end-span fracture, and over four times as much as the continuous bridge with a center-span fracture. None of the cases indicate full-scale failure will occur. Nonetheless, the serviceability limit state should be considered in the designation of a fracture-critical bridge because, even if a bridge does not collapse, it may not be possible for vehicles to drive safely off a fractured bridge if the deflections are excessively large. For the cases considered in this research, a 2-in. deflection over 120 ft would not cause any such problems. It is important to note, however, that the ratio of deflections for the

three different fracture scenarios is significant, and further studies considering alternate geometries should be considered.

6.6.3.2 Reaction Forces

The chief concern in considering reaction forces for a continuous beam is to ensure the end supports will not have uplift across the entire width of one girder. If uplift were to occur, a fracture would cause the girders to come off their supports, potentially causing catastrophic collapse. Uplift is more likely to occur in bridge geometries where the central span is significantly longer than the exterior spans. This study considers three equal-length spans, but it could be modified to test a bridge with short approach spans.

The reaction forces from one end support and one middle support from the first test (central span fracture) are shown in Figure 6-31 (an explanation for the locations of the supports was shown in Figure 6-22). As expected, the end support reactions decrease across the fracture event, while the middle support reactions increase. Although the end reactions are not large to begin with and then decrease across the event, there is still little indication that uplift would be a concern, with the reactions still totaling over 80 kip per bearing pad.

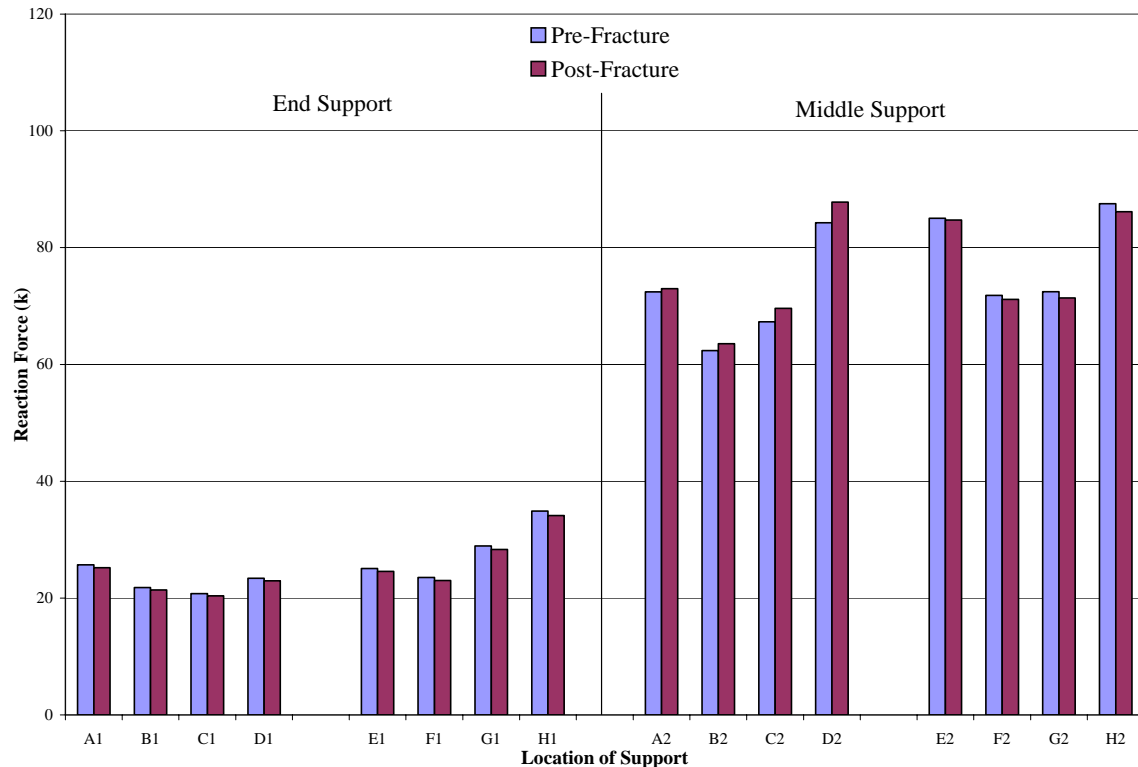


Figure 6-31: Reaction forces at an end support and a middle support (typical) before and after a full-depth web fracture at the centerline of the middle span

The reaction forces seen in the second study, where the fracture is initiated in an end span, have one main feature similar to the simply-supported case: on the far end support, the tendency to overturn can be seen. The far end of the fractured end span does not have the benefit of the weight of an additional girder adding overturning resistance the way the two supports of a fractured center span do. The middle support adjacent to the fractured span also shows some rotation towards the exterior of the curve. At the next support further down the length of the bridge, referred to as the “far middle” support, the change in reaction loads is constant and small, and the furthest support experiences almost no change. The support reaction changes can be seen in Figure 6-32, with the reaction locations numbered as before.

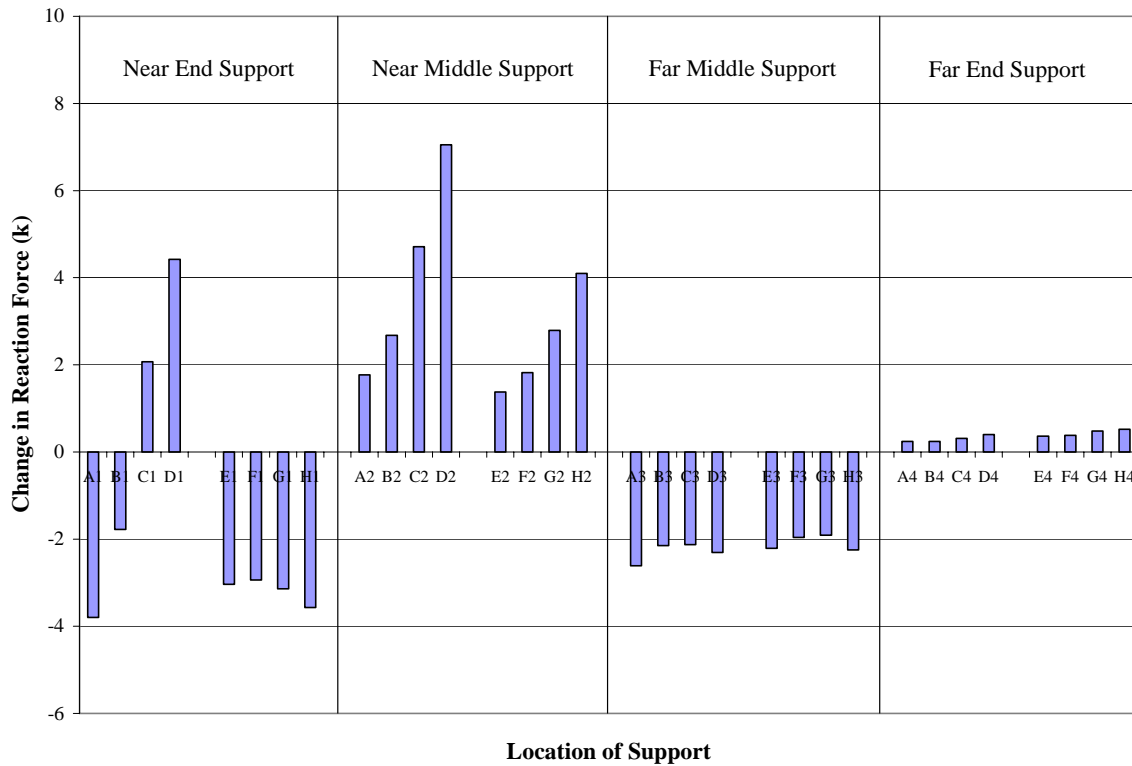


Figure 6-32: Change in support reactions during a full-depth web fracture event in an end span

As in the first study, the changes in the reaction forces are not large enough to induce total uplift of the bridge off the supports; the smallest vertical reaction is approximately 18 kip downward. Considering the data presented in Section 6.6.1 on the reaction forces of the small-radius bridges, uplift might become a problem during an end-span fracture of a small-radius bridge. As before, this problem could be neutralized by using support mechanisms that can resist uplift.

Considering the deflections and the reaction forces of the two fractured multi-span bridges investigated in this study, there is evidence that adding continuous spans to a fracture-critical-classified bridge could remove the necessity for that classification. The change in deflections seen during either a center- or end-span fracture event are small enough to allow for a safe closing of the bridge post-fracture even when the fracture is not readily apparent until drivers are on the bridge. As these twin-girder bridges are often

used for flyovers in large intersections, there are few single spans built that could not be made continuous with the spans surrounding it.

It is important, however, in calculating the redundancy in a multi-span bridge and considering the results presented here to include reflection on the overall properties of continuous and simply-supported spans. In their study on redundancy ratings for two-span bridges, Daniels et al. (1989) found that a two-span bridge had less post-fracture live load capacity than a simply-supported bridge because the benefit from the second span allowed for a decrease in section properties (e.g., height and thickness) for each of the two spans as compared to the section properties of a single span girder. The current study considered the exact same dimensions for the multi-span bridges as were used in the simply-supported case. If this deficiency is recognized during design and the continuous structure can be designed for the cantilevered service load scenario, the initial construction cost might be increased, but the lifecycle costs could be decreased by removing the fracture-critical designation.

6.7 SUMMARY AND CONCLUSIONS

This chapter presents preliminary verifications of the analytical model, comparisons between data that were measured and calculated, and predictions of response under full-depth web fracture (for bridges of varying geometries). The verifications considering different modeling assumptions for the analyses gave confidence that the parameters selected, including mesh densities, element types, and load applications, were appropriate. The analytical design that was chosen (and described in Chapter 5) reflected an appropriate and computationally-efficient method of predicting response.

The experimental and analytical data comparisons were performed for further validation, to indicate whether the analysis model was able to predict the behavior of a full-scale specimen. While the two sets of data did not correspond exactly, they were not expected to, considering the variability that came from the experimental measurement methods and the assumptions that went into the analytical model. Multiple full-scale

tests would help reduce that variability; however, multiple tests of that size were not an option. The accuracy of gauge placement and gauge readings was a function of the experimental test constructors and the gauges used.

The accuracy in the predictions of system-response is largely a factor of the assumptions that went into the analytical model. The importance of these assumptions, and suggestions for how to validate and improve on them, are given in the following chapter.

CHAPTER 7

Conclusions and Recommendations

7.1 SUMMARY OF RESEARCH

A major objective of the research project described in this thesis is the quantification of the inherent redundancy that may exist in trapezoidal box-girder bridges. Current AASHTO Specifications designate two-girder bridges of this type to be fracture-critical, and, as a result, they require frequent inspection cycles to guarantee their safety. In the past, there have been multiple instances of fractures in fracture-critical bridges without collapse, as described in Chapter 2. The main goals of this project were to determine whether an AASHTO-defined fracture-critical bridge could withstand a full-depth fracture under load without collapse and to develop a method for measuring redundancy in such a bridge.

It is important to note that the test set-up and corresponding models represented a worst-case scenario for loading on the structure at the time the simulated fracture was initiated. The likelihood of the truck being positioned in the precise location of the fracture and remaining in that location is expected to be extremely low. As an illustrative comparison, in the design of structures for progressive collapse, current guidelines recommend that only one-half of the service live loads be considered during the collapse event to reflect the low probability of a structure being under the full design load conditions at the time of collapse initiation by column failure (UFC 2005).

The analytical model described in this report was developed to mimic the behavior of the full-scale test specimen that was constructed and damaged. For the dynamic load amplification study, the truck load, which under normal conditions would be considered a live load, was amplified by the same ratio as the dead load to account for the stationary nature of the loading blocks on the test specimen during the experiment. Experimental data were compared with computed values to determine the accuracy of the

finite element model. The model was then used as a predictive tool for considering a full-depth fracture event, dynamic load effects, and variations in bridge details such as horizontal radius of curvature, continuity of spans, and external bracing. The following sections present the conclusions gathered from the models and suggest possible directions for future research in the analysis of redundancy in twin box girders.

7.2 CONCLUSIONS

Prior to making conclusions about the behavior of a fracture-critical trapezoidal box-girder bridge, it is necessary to recognize the assumptions made in the programming of the analytical model. Most important are those assumptions which involve the behavior of the concrete deck. Cracking of the concrete was not modeled in detail and thus a localized concrete tensile failure mode was not considered. To accommodate the influence of cracking in the model, nonlinear material response in the deck was approximated with a “smeared” material model. The analyses performed with this approximation are expected to capture the essential features of response when considering system-wide strength and stability.

The shear stud modeling method technique was based on a method previously shown to be satisfactory for shear considerations (Topkaya and Williamson 2003). The calculated strains in this study, however, which were primarily tensile, did not correlate well with measured test data. The differences in measured and calculated values could be insignificant considering the order of magnitude of the differential displacements (10^{-4}), but they might indicate that linear spring elements are not appropriate in regard to tensile pullout, as is expected during a full web fracture.

Within the framework of these assumptions and the modeling approach described in the previous chapters of this thesis, the following conclusions can be drawn regarding a full fracture event, dynamic load factors, and the influence of various bridge geometries.

7.2.1 Full Fracture Response

Results obtained from the finite element analyses indicate that the trapezoidal box-girder bridge studied in this project possesses a level of redundancy that will allow it to remain standing in a fractured, loaded state. Deflections caused by a full-depth web fracture were predicted to be less than 2.5 inches for the fractured (exterior) girder and less than 1.5 inches for the unfractured (interior) girder. The stresses induced in the bottom flange of the interior girder, the transverse and longitudinal rebar in the deck and rails, and the majority of the deck were sufficiently small so that they did not near the plastic range. Small sections of deck concrete showed minor plasticity, which could indicate local failures. The presence of reinforcing bars in the deck should minimize the system-wide impact of these localized failures.

7.2.2 Consideration of Dynamic Load Factors

The nature of a fracture event includes a rapid change in the geometry of a structural system. To capture the response of a structure through modeling requires consideration of this rapid change, which is most often done through dynamic calculations at the time of the fracture. However, dynamic calculations are significantly more time-consuming than static calculations, and thus finding an appropriate method of simulating the dynamic response while using static loads would be of benefit to designers wishing to study the redundancy of their structures.

This study compared the peak strains measured in the test specimen during the flange fracture event with strains induced at the same locations on two models where a percentage of the dead and live loads had been increased by 150% to 200%. The loads were amplified within two times the depth of the section, or 96 inches on either side of the fracture. The strains calculated were still less than those measured at the peak of the fracture event, indicating this method of approximating the dynamic loads was not appropriate. Further study is needed to determine how best to establish the impact of the rapid change at the time of the fracture and how loads should be modified to capture dynamic response using static loads.

7.2.3 Effect of Radius

Decreasing the horizontal radius of curvature of the bridge resulted in minimally higher deflections during a fracture event (on the order of 0.5 in.) than the original geometry. More significantly, a tighter radius reduced the induced stresses in the bottom flange of the unfractured girder, most likely due to a greater rotation of the structure towards the fractured side. This rotation was also reflected in the support reactions, where small uplift forces of approximately 10 kip were seen on the inside of the unfractured, interior girder supports at both ends for the geometry with $R = 400$ ft. If overturning is of concern during fracture of a tightly curved bridge, bearings that include vertical restraint could be used on the inside of the bearing points.

7.2.4 Effect of External Bracing

Because of the minimal response of the bridge to the full-depth fracture, the external braces were stressed to less than 8.0 ksi, which is far below yield. Pre-fracture stresses were less than 1.5 ksi, or possibly low enough to indicate an “infinite life” with regard to fracture criticality and could thus be left in place after construction without adding another potential initiation site for fracture. The braces, when modeled as remaining in place during the fracture event, also minimally reduced overall deflections of the fractured girder. Further study of braces that are designed to transfer significant loads in addition to restrain rotation during construction is warranted, with consideration of fatigue effects and fracture initiation at the connections.

7.2.5 Effect of Structural Redundancy

Adding continuity to fracture-critical bridges through additional spans helped reduce the deflections seen in the fractured span, both when the fracture is in the center span and when it is in an end span. This study included calculating the reaction forces at each of the four supports in a three-span bridge, with results that indicated uplift should not be a problem for a large radius of curvature ($R = 1365$ ft for this study). Considering

the previously discussed results that a small-radius bridge had minor uplift at the supports, supports with resistance against uplift might be needed.

A detail pointed out by Daniels et al. (1989) and reiterated by this author is that multi-span bridges often have a smaller cross-section than a simply-supported span, thus likely providing less redundancy than was seen in the structures considered in this study where the multi-span girders had the same cross-sectional dimensions as the simply-supported case. To remove fracture-critical designations and/or lessen inspection requirements, it is paramount that designers consider both the pre- and post-fracture behavior of a section. With proper consideration for the fractured state, a multi-span structure could be capable of resisting collapse following a fracture event.

7.3 RECOMMENDATIONS FOR FUTURE WORK

Removing the fracture-critical designation from trapezoidal box-girder bridges, or simply reducing the frequency of inspections of fracture-critical bridges, would save bridge owners like the Texas Department of Transportation millions of dollars every year (Connor et al. 2005). This study has shown that the designation may have been applied too liberally to bridges that do in fact have redundant load paths. Especially in the case of multi-span, continuous bridges, the loads originally carried by a fractured member can be held by the unfractured spans that are also a part of the system.

At the beginning of this study, three components were highlighted as being critical to the stability of a fractured bridge: the shear studs having the tensile capacity to bring load from the fractured girder into the deck, the deck having the moment capacity to transfer the load to the unfractured girder, and the unfractured girder having the capacity to hold the additional load. The model built in this study includes many assumptions about the behavior of the shear studs and deck, as were explained earlier. Future research using this model should begin by further validating and improving these assumptions. The following sections describe steps that can be taken to improve the fidelity of the finite element model.

7.3.1 Fracture

As was described in Section 5.3.3, the fracture in this model was created using ***model change**, a keyword in ABAQUS that removes elements at the beginning of a load step. The benefit of this method is that it is computationally simple and does not significantly increase job run times. The drawbacks include the need for the programmer to dictate the fracture path and timing of the event and an inability to capture dynamic response.

An alternate model could instead define coincident nodes at the fracture location. Through the preliminary steps, the nodes would be held together using applied surface or edge loads. At the time of the fracture, the loads would be released. To consider dynamic effects, an equal and opposite load could be applied on the same surfaces and edges, creating a multiplication factor of 2.0 in the change in the loads. This method was briefly tried as part of this study with some success; better results could come from using multiple jobs with imported data from previous analyses, rather than adding load steps individually to an input file.

The fracture model could also be run using an explicit solver such as ABAQUS/Explicit. Unlike ABAQUS/Standard, this computation method allows for the failure of elements without creating numerical problems in the formulation of the structural stiffness matrix. However, to define an explicit analysis could require specifying other parameters and material properties that are not known or easily assumed. The result is a prediction of behavior that is thought to be more accurate while actually depending more heavily on the assumptions defined by the programmer.

A goal in this study was to adequately approximate the response using a simple method with few assumptions and low computational needs. Future research should continue to consider the input information, computing ability, and time needed for complex analyses if the modeling techniques are to be used in a design office.

7.3.2 Shear Studs

The shear studs in the developed model are simulated using three one-dimensional spring elements between the top flange of the girder and the bottom of the concrete haunch. The linear spring element definition does not allow for separate stiffness values for compression and tension. The springs were thus defined with the stiffness measured by Sutton (2006), which is only accurate in the tensile direction. In compression, the stiffness should near infinity, as no shortening of the shear stud is expected. To prevent the haunch from passing through the top flange (which is impossible physically but possible numerically with a low compressive stiffness value), contact was established between the two surfaces. While successful at restricting this physical impossibility, the contact restriction at the boundary nearly doubled the total run time for the job.

In future studies, the shear studs could be modeled using truss elements. Unlike springs, trusses are assigned to a material which can have a different response in tension and compression. Additionally, because the truss elements must have some finite length, the model will not converge if the bottom of the haunch deflects further than the top of the flange. Alternatively, constraints other than contact could be used to limit the distance between two nodes, preventing compression of the springs and retaining the minimum initial spacing of the nodes.

The importance of the shear studs on the global behavior of the system is currently under investigation at the University of Texas at Austin. The first studies are showing that, if the loads get high enough, the orientation and height of the studs will change the strength and ductility of the stud-deck interaction (Sutton 2007). However, the finite element analyses calculated forces in the studs from static loading more than an order of magnitude smaller than the failure pullout loads measured by Sutton.

One possibility that needs more study is that dynamically-applied loads will significantly change the pullout behavior of the shear studs. The data gathered to date are for statically-applied loads, as are the analytically calculated expected loads. The dynamic failure load is unknown. Additionally, the calculated loads in the shear studs

could be higher under dynamic load scenarios (as opposed to the static studies performed in this study). A higher load in the shear studs could result in a viable failure mode that is not seen in the analytical model presented in this report.

Additional data from the stud-deck interaction studies will be able to help improve and validate the modeling method, especially if dynamic loads are considered. Full utilization of the tests being run in the laboratory would include modeling the test setup and comparing the shear stud strains and loads from the experimental program to calculated values from ABAQUS. The number of tests and the varying geometries being studied in the lab present a more controlled and repeatable situation than the full-scale test and would thus be beneficial for verifying the accuracy of the modeling method.

7.3.3 Concrete Material Model

The concrete deck used in this project, described in more detail in Section 5.2.4, was comprised of concrete solid elements with embedded rebar truss elements. The concrete material model attempted to capture the pre-cracking behavior of unreinforced concrete. Post-cracking, the concrete hardened slightly and then became “perfectly plastic”, so the deck elements would add zero stiffness to the model. This modified and approximate material model removed convergence problems previously experienced by the solver, but may not return behavior similar to true concrete response. The goal, however, was to allow individual elements to fail (as is likely in a severe fracture event, where crushing and cracking of the concrete is expected) while allowing the program to converge to an answer. This assumption may be appropriate considering this study is focusing on system response as opposed to individual small-scale failures, but verification would increase confidence in the answer.

7.3.4 Parameter Studies

The parameter studies run using the current finite element model and described more fully in Chapter 6 raised further questions regarding the importance of dynamic load effects, external bracing, and bridge geometry on the response of a fractured twin

box-girder bridge. The following studies are recommended to be performed, using either the current model or one that has been improved with the methods mentioned above:

- *Dynamic loading*
Consider alternate methods of loading to mimic the response of dynamic loads using static calculations. Current research and guidelines regarding progressive collapse could help determine appropriate load increase zones. Multiple geometries should be tested with the same formula for load application. Verification could come from smaller laboratory tests, as full-scale tests are not financially feasible.
- *External bracing*
Consider the effects of external braces that have been designed for load transfer and redundancy. Concerns include excessive twist of the unfractured girder and fatigue-critical connection details. Benefits could include reducing deflections in the fractured girder.
- *Continuous spans*
Consider continuous-span bridges that were designed to be continuous and thus likely have a smaller cross-section than the bridge modeled in this study. Longitudinal dimensions should also be varied to calculate response of bridges featuring a long central span in comparison to the end spans.

Each of these studies can also be expanded by introducing a second variable, such as radius of curvature in the continuous-span designs. As more data on response is gathered, it will become clearer which features of box-girder bridges are critical for maintaining stability post-fracture. The research to this point indicates that proper design of these critical details (e.g., uplift-resisting bearings on bridges with a small radius of curvature) will allow for post-fracture stability in twin box-girder bridges.

7.4 SUMMARY

The finite element analyses of twin steel trapezoidal box-girder bridges presented in this report indicate redundancy in this bridge design that surpasses current AASHTO estimations. With proper design that considers the benefit of structural indeterminacies (such as continuous spans) and includes restraint against uplift at the supports, a full-depth web fracture in one girder of a twin trapezoidal box-girder bridge does not guarantee the system-wide failure expected by AASHTO in their fracture-critical definition. By having the reserve capacity to maintain serviceability after a fracture, the criticality of a fracture in a girder is lessened, which should be reflected in inspection requirements.

APPENDIX A

Introduction to Finite Element Analysis

A.1 INTRODUCTION

The goal of structural analysis is to determine the variations in stresses and strains induced in a structure under load. With simple systems such as statically determinate trusses and beams, these values can be readily calculated. If a structure is statically indeterminate or there are multiple degrees of freedom, the complexity of the problem increases, and determining the response of such a system using hand-based procedures is not practical.

Finite element analysis (FEA) was developed as a method of solving for the response of a continuous system using discrete elements. The basis of the analysis methods can be compared to earlier techniques considering planar truss and beam elements, which, with two or six degrees of freedom, can be solved using hand calculations and simple computational tools (Bathe 1982). The growth of computer technology has allowed for more complex computations considering plane stress and strain formulations, three-dimensional problems, and shell behavior (Belytschko 2000). The influence of individual elements is combined to form a system of equations relating forces and displacements. Computer programs like ABAQUS (HKS 2006) and ANSYS (2005) were developed to compile this information and calculate the resulting displacements, and by association, strains and stresses.

This chapter introduces the basics of the methodology behind finite element analysis (considering only axial and beam members) so as to establish the rationale behind modeling decisions described in the main body of this report. Further explanation can be found in a finite element textbook such as Bathe (1996) or Cook et al. (2001).

A.2 OVERVIEW OF METHODOLOGY

The governing equation for deformation in continuous systems is known as the Boundary Value Problem (BVP). Considering the deflection in an axial element under load (shown in Figure A-1), the BVP, which considers kinematics, equilibrium, and constitution can be written as:

$$\frac{d}{dx} [E(x)A(x)u'(x)] = -p(x) \quad (1)$$

where

$E(x)$ = Young's modulus

$A(x)$ = cross-sectional area

$p(x)$ = loading per unit length

$u'(x)$ = derivative of the displacement at any point, x , along the length of the bar (strain).

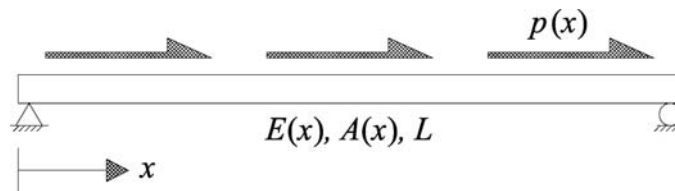


Figure A-1: Axial element with applied load $p(x)$

This equation states that the strain of the member (represented by $u'(x)$) is related to the stiffness of that member ($E(x) \cdot A(x)$) and the load that is applied. The equation is solved for the displacement along the length, $u(x)$.

For a prismatic bar with constant values of modulus and area, a simple loading scheme, and clear boundaries that restrict the value of $u(x)$ at a given x , the BVP can be solved directly, even by hand. However, if variations over the length are introduced (such as in the case of a tapered member), the equations to integrate can increase in order to the point of requiring numerical evaluation and approximation.

As an alternative, finite element analysis can be used. FEA considers a complex structure as a combination of smaller elements with known behavior. The behavior of the smaller elements is dictated by the user; for instance, a flexural member can be used rather than an axial member, if flexure is expected to occur and is of interest. Other common elements include shells, plates, and solids, which will not be discussed in detail here, but are considered in texts such as Bathe (1982).

Finite element analysis is based on four major steps: idealizing the configuration of a continuous system by using many smaller elements; establishing equilibrium at the nodes of each element; assembling the elements in a manner that considers compatibility at boundaries; and solving for the response of the elements as a system of equations. The two major methodologies, stiffness- (or displacement-) based and flexibility- (or force-) based, result in an approximation of the internal forces and displacements through a continuous structure. These methods are described in more detail in Sections A.2.1 and A.2.2, respectively.

In each case, the degrees of freedom are thought to behave similarly to a spring, with a direct relationship between the forces applied and the resulting displacements. The governing equation for the force in a spring is:

$$k \cdot u = F \quad (2)$$

where

k = spring stiffness

u = displacement induced under the applied force

F = applied force

Similarly, each approximation method formulates an equivalent stiffness of the structure in each degree of freedom at each node, as well as equivalent forces. The displacements are then found and used to calculate the response in the elements (e.g., stresses and strains).

A.2.1 Stiffness Method

The stiffness method of analysis is based in the Principle of Virtual Work (PVW). The Principle of Virtual Work is considered to be the “weak form” of the solution, as it is an approximate solution to the boundary value problem. The PVW is based on the idea that internal and external virtual work must be equal. “Virtual work” is a term referring to the work done in moving a point through a virtual (fictitious) displacement.

The stiffness method of analysis begins by assigning an assumed displaced shape, $u(x)$, for the member being analyzed. For instance, as it known that the response of a

prismatic axial member under load is to deform linearly, it is a reasonable first step to assume that the response of a tapered axial member will also be linear. Thus, the assumed displaced shape is defined by:

$$u(x) = a_0 + a_1x \quad (3)$$

where a_0 and a_1 are coefficients related to the boundaries on the element.

Using the PVW, this assumed shape can be used to find the internal and external virtual work experienced by the structure under a given load. For equilibrium to be met, the internal and external work values must be equal; or:

$$\int_0^L E(x) \cdot A(x) \cdot u'(x) \cdot \bar{u}'(x) \cdot dx = P \cdot \bar{u} \quad (4)$$

where

$\bar{u}'(x)$ = derivative of the virtual displacement over the length, x

P = applied load at the location \bar{u}

L = length of the member being analyzed

For low-order expressions for $E(x)$ and $A(x)$, this equation can be solved directly for $u(x)$.

A.2.1.1 Shape Functions

The PVW equation written above (Equation 4) is for the consideration of one degree of freedom, such as an axial member pinned at one end. The next step is to consider a more generic element. An element connects two or more nodes and is characterized by its behavior between those nodes. All considered degrees of freedom (displacement and rotation) exist only at those nodes. For assumed planar response, an axial member has two degrees of freedom (DOFs), as is shown in Figure A-2(a), while a beam has six DOFs (Figure A-2(b)).



Figure A-2: Axial degrees of freedom numbering and sign convention

Using variable boundary conditions (displacement and rotation limitations at $x = 0$ and $x = L$) that relate to the established degrees of freedom, a system of equations can be written from Equation 3, from which the coefficients a_0 and a_1 can be calculated:

$$\begin{aligned} u(0) &= a_0 = u_1 \\ u(L) &= a_0 + a_1 L = u_2 \\ a_1 &= \frac{u_2 - u_1}{L} \end{aligned} \quad (5)$$

Inserting the coefficients into Equation 3 and rearranging to group u_1 and u_2 , the equation for assumed displacement down the length of the member becomes:

$$u(x) = u_1 \left(1 - \frac{x}{L}\right) + u_2 \left(\frac{x}{L}\right) \quad (6)$$

Although it may be of little benefit while considering an axial member with only two DOFs (u_1 and u_2) it becomes much easier to consider $u(x)$ in matrix form for elements that have greater complexity and great numbers of DOFs:

$$u(x) = \begin{bmatrix} 1 - \frac{x}{L} & \frac{x}{L} \end{bmatrix} \begin{bmatrix} u_1 \\ u_2 \end{bmatrix} \quad (7)$$

The terms in the first matrix are referred to as the shape or interpolation functions for the element, and the matrix is given the designation of $\mathbf{L}(x)$. The order of x in the equations is equal to the order of the equation approximating the shape of the element between the nodes. The most common axial elements consist of two or three nodes (the third node generally being positioned at $x = L/2$).

A.2.1.2 Stiffness Matrix Calculation

The derivative of the new form of $u(x)$ can now be inserted into Equation 3. The derivative of the matrix of interpolation functions, $\mathbf{L}(x)$, is referred to as the strain-displacement matrix, $\mathbf{B}(x)$. The virtual displacement term can be removed from the equation by realizing that, if the virtual displacements are of the same form as the real displacements,

$$\bar{u}'(x) = \mathbf{B}(x) \cdot \bar{\mathbf{u}} \quad (8)$$

and

$$\int_0^L \mathbf{u}'(x) \cdot E(x) \cdot A(x) \cdot \bar{\mathbf{u}}'(x) \cdot dx = \bar{\mathbf{u}} \int_0^L \mathbf{B}^T(x) \cdot E(x) \cdot A(x) \cdot \mathbf{B}(x) \cdot dx \cdot \mathbf{u} \quad (9)$$

Combining this equation with Equation 3, and assuming that $\bar{\mathbf{u}}$ does not equal zero (a trivial case),

$$\int_0^L \mathbf{B}^T(x) \cdot E(x) \cdot A(x) \cdot \mathbf{B}(x) \cdot dx \cdot \mathbf{u} = P \quad (10)$$

where

$\mathbf{B}(x) = d\mathbf{L}(x)/dx =$ strain-displacement matrix

$\mathbf{u} =$ vector of displacement values (u_1, u_2 , etc)

$\mathbf{P} =$ vector of loads applied at nodes

This transformation is made using principles of linear algebra. For more information on matrix manipulation, reference Williams (2001).

Equation 10, which equates an integral multiplied by the nodal displacement values to the applied nodal loads, is of the same form as Equation 2, the load-displacement equation for a spring. The integral, which considers material properties, element geometry, and node layout, is referred to as the structural stiffness matrix, \mathbf{k} :

$$\mathbf{k} = \int_0^L \mathbf{B}^T(x) \cdot E(x) \cdot A(x) \cdot \mathbf{B}(x) \cdot dx \quad (11)$$

For an axial member, the stiffness matrix is 2×2 , symmetric across the diagonal. If the virtual displacement equation is not of the same form as the real displacement, the strain-displacement matrices will not be the same, and the stiffness matrix will not necessarily be symmetric.

A.2.1.3 Beam Elements

The stiffness matrix formulation for beam elements is very similar to axial elements. The differences include the number of degrees of freedom (shown in Figure A-3) and the order of the polynomial shape functions. The axial response in a beam (with small deflections) is uncoupled from the flexural. Cubic functions are needed to

capture the response in shear and flexure, while Equation 11 can still be used to calculate the axial stiffness contributions.

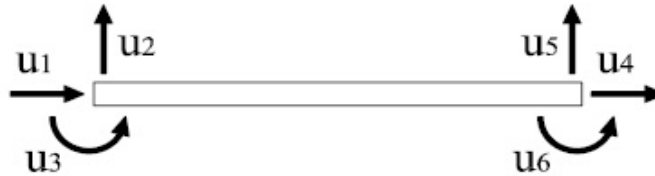


Figure A-3: Beam degrees of freedom numbering and sign convention

For beam elements, the shape functions are given the variable $\mathbf{H}(x)$. The strain-displacement matrix, which is the second derivative of the shape functions and is referenced as $\mathbf{H}''(x)$. Additionally, for flexure, the area of the member is of little importance while the moment of inertia governs the stiffness. The stiffness matrix equation can be written as

$$\mathbf{k} = \int_0^L (\mathbf{H}'')^T(x) \cdot E(x) \cdot I(x) \cdot \mathbf{H}''(x) \cdot dx \quad (12)$$

where

$$\mathbf{H}''(x) = d^2\mathbf{H}(x)/dx^2 = \text{strain-displacement matrix}$$

$$I(x) = \text{moment of inertia at location } x$$

When choosing an element to use in an analysis, it is important to consider the assumptions that have gone into forming the basic elemental properties. For instance, the response of a beam is based in beam theory, which focuses on flexure. In an analysis, beam elements should only be used when the assumptions of beam theory can be met; for instance, the length of a beam element should be significantly larger than any of the cross-sectional dimensions.

A.2.2 Flexibility Method

As an alternative to using the stiffness method, the \mathbf{k} matrix can be developed using the flexibility method. The flexibility method begins by recognizing redundant forces in an individual element and establishing equilibrium in the resulting statically determinant element. For instance, a beam element with no axial deformation (Figure

A-4(a)) would have two redundant forces. Those redundants could be the vertical reaction at both ends, or the vertical reaction and moment at one end. Using the independent (non-redundant) forces, the dependent reactions can be resolved using equilibrium. Further examples in this section will reference a beam with the moments as the independent forces, shown in Figure A-4(b).

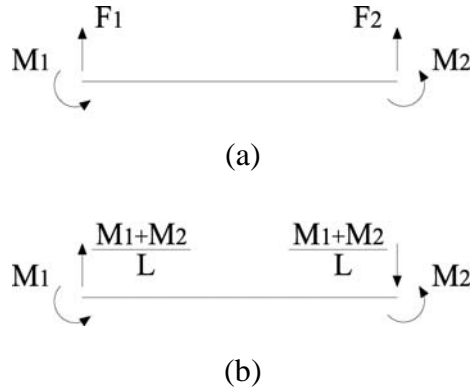


Figure A-4: (a) Forces on an axially rigid beam element; (b) dependent forces written in terms of independent forces

A.2.2.1 Force Distribution Functions

Equations for the shear, flexure, and axial forces at any point, x , in the beam can be written using just the independent forces. Considering the beam shown in Figure A-4(b), with $x = 0$ at the left end, the moment along the length can be written as:

$$M(x) = M_1 \left(\frac{1}{L} - 1 \right) + M_2 \left(\frac{1}{L} \right) \quad (13)$$

where

$M(x)$ = moment along the length of the beam

M_1 = moment at $x = 0$

M_2 = moment at $x = L$

This expression can also be written in matrix form, using a vector of force distribution functions, $\mathbf{D}(x)$, similar to the vector of shape functions used in the stiffness method:

$$M(x) = \mathbf{D}(x) \cdot \mathbf{Q}_0 \quad (14)$$

where

$\mathbf{D}(x)$ = vector of force distribution functions

\mathbf{Q}_0 = matrix of independent variables

The flexibility method uses the Principle of Complimentary Virtual Work, where, instead of using a virtual displacement, a virtual load is applied. Computing internal and external virtual work, as in Equation 4, results in an expression for the flexibility matrix, \mathbf{f} :

$$\mathbf{f} = \int_0^L \mathbf{D}^T(x) \cdot \frac{1}{E(x) \cdot \beta(x)} \cdot \mathbf{D}(x) \cdot dx \quad (15)$$

where

$\beta(x)$ = geometric parameter: $A(x)$ for axial members, $I(x)$ for flexural members

When considering shear or axial response in a beam, both the geometric parameter $\beta(x)$ and the expressions within $\mathbf{D}(x)$ change. An equation for $N(x)$, or axial force along the length of the element, is needed to calculate the axial response. Similarly, for shear, an equation for $V(x)$ is needed and, in Equation 15, the shear modulus, $G(x)$, should be used instead of the elastic modulus, $E(x)$. For shear, $\beta(x)$ would refer to the shear area of the element.

A.2.2.2 Stiffness Matrix Calculation

The flexibility matrix for an element cannot be used to directly compute the response of the element because of the assumptions on independent and dependent variables: the choice in variable definitions changes the resulting matrix. To capture the response of all degrees of freedom in the element, the matrix must be transformed to include both the independent and dependent variables.

The number of dependent variables is related to the degree of indeterminacy. The number of independent variables should be as small as possible to result in a statically determinate, stable structure. The dependent variables are then written in terms of the independent ones, such as is shown in Figure A-4(b). The relationship between the dependent and independent variables can be expressed using a matrix referred to as Φ :

$$\mathbf{Q}_1 = \Phi \cdot \mathbf{Q}_0 \quad (16)$$

where

\mathbf{Q}_1 = vector of dependent variables

\mathbf{Q}_0 = vector of independent variables

Φ = matrix relating independent and dependent variables

As an example, Equation 16 for the beam in Figure A-4(b) would be

$$\begin{bmatrix} F_1 \\ F_2 \end{bmatrix} = \begin{bmatrix} \frac{1}{L} & \frac{1}{L} \\ -\frac{1}{L} & -\frac{1}{L} \end{bmatrix} \cdot \begin{bmatrix} M_1 \\ M_2 \end{bmatrix} \quad (17)$$

The Φ matrix and the flexibility matrix, \mathbf{f} , are then used to calculate a stiffness matrix, where the stiffness matrix is partitioned into four sections, \mathbf{k}_{00} , \mathbf{k}_{01} , \mathbf{k}_{10} , and \mathbf{k}_{11} so that:

$$\mathbf{k} = \begin{bmatrix} \mathbf{k}_{00} & \mathbf{k}_{01} \\ \mathbf{k}_{10} & \mathbf{k}_{11} \end{bmatrix} \quad (18)$$

with:

$$\begin{aligned} \mathbf{k}_{00} &= \mathbf{f}^{-1} \\ \mathbf{k}_{01} &= \Phi \cdot \mathbf{f}^{-1} \\ \mathbf{k}_{10} &= \mathbf{f}^{-1} \cdot \Phi^T \\ \mathbf{k}_{11} &= \Phi \cdot \mathbf{f}^{-1} \cdot \Phi^T \end{aligned} \quad (19)$$

These expressions were derived using the concepts of partitioned matrices (McGuire et al. 2000). The resulting stiffness matrix can be used to solve for the nodal displacements, which can be used to calculate elemental stresses and strains.

It should be noted that the stiffness matrix derived for an element using the stiffness method is not the same as the one derived using the flexibility method. Similarly, the nodal force vectors (not described in this report) are not the same from each method. The calculated response of the structure (found using Equation 2) may be equivalent; variations come from inaccuracies in one or both methods (e.g., an

insufficient number of elements). The benefits and drawbacks of this method as compared to the stiffness method are presented in further detail in Section A.2.5.

A.2.3 Improving the Model

There are two simple ways to improve the quality of an approximation using finite element analysis. The first is referred to as p -type refinement and is achieved by increasing the order of the polynomial in the assumed shape. For example, Equation 3 would become:

$$u(x) = a_0 + a_1x + a_2x^2 \quad (20)$$

Using a higher-order polynomial means adding another node along the length of the member (generally equidistant from the boundary nodes). With another node, new interpolation functions must be developed considering the new boundary conditions.

The additional term in the $u(x)$ equation will increase the order of the interpolation functions. Especially in a case where the area of the beam is non-linear down the length, the integrals for the stiffness matrix terms quickly increase in order as well. The integrals are generally solved using Gaussian or Newton-Cotes quadrature, forms of numerical integration used to approximate the solution to complex integrals (further information on numerical integration can be found in Dahlquist and Bjork (1974)). Both methods require more terms to accurately estimate higher-order expressions. As a result, p -type refinement is generally only used to the third order.

Instead, n -type refinement can be used to improve the accuracy of an elemental model. In using n -type refinement, elements are subdivided. For instance, the response of a tapered axial beam could be calculated using two beams of length $L/2$ rather than one of length L . The two elements would feature unique cross-sectional properties (Figure A-5), thus capturing the effects of the taper without requiring a higher order polynomial.

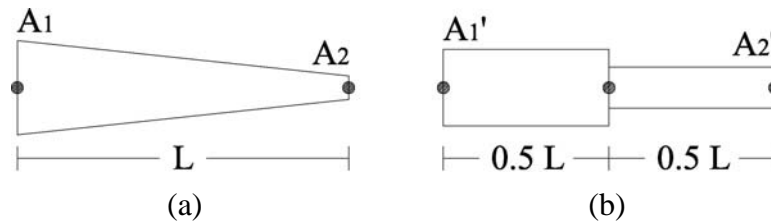


Figure A-5: (a) A tapered element, (b) represented by two constant-area members

If the two-element model is still not considered to be acceptable, the element can be subdivided further. Once further subdivisions converge to one value, or subsequent evaluations do not yield a different result, one can be satisfied with the number of elements, or mesh density, used for approximation. For example, when drawing a circle with straight lines, four or even eight might not be enough, but twenty could return results close to that which would be calculated using the true circle.

The main drawback of increasing the number of elements or the order of an approximation in a model is that the number of equations to be solved increases. One method of controlling the computation time is to use reduced integration. When using reduced integration, the number of sampling points used to approximate the integrals that define the stiffness matrix of each element is decreased. For example, a fourth-order polynomial can be calculated exactly using second-order Gaussian quadrature or approximately using first-order.

Reduced integration lessens the complexity of equations within each stiffness matrix term but returns a stiffness value smaller than the exact value. Considering the increased stiffness inherent in a finite element model, due to the use of small elements that do not necessarily deform as easily as a continuous system would, reduced integration can properly balance the stiffness of a system. This effect is discussed further in Chapters 5 and 6.

Reduced integration, however, has the potential to introduce response modes that are not captured by the integration points. This effect can be seen in Figure A-6, where the single integration point used for a four-noded element does not experience strain, even with the deformation of the element. The full-integration method, with four

integration points, would have shown strain change from the stresses applied. This shape can repeat through elements forming an hourglass appearance, and is thus referred to as hourglassing (Belytschko et al. 2006).

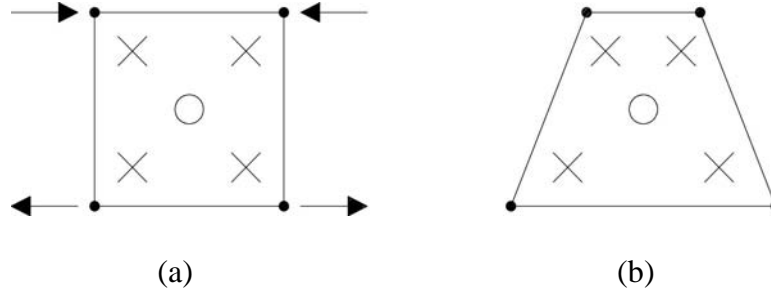


Figure A-6: Example mode shape not caught using reduced integration. Full integration points shown with X's, reduced integration point shown with single O.

A.2.4 Mapping Elements

In the case of a single-element model, the structural stiffness matrix is equal to the elemental stiffness matrix. Once more elements are introduced, each elemental stiffness matrix will contribute to the structural stiffness matrix. The contribution from each element is determined by orientation and correspondence with the directions of the global degrees of freedom. Calculating member response is a two-step process.

The first step is to consider the orientation of the element with regard to the global axes. The degrees of freedom shown in Figure A-2 are oriented with the local axes of each member (along the length and perpendicular to the length). In most analyses, the global degrees of freedom will not correspond with the local axes of each member. A transformation matrix, \mathbf{T} , is used to rotate the influence of a member:

$$\mathbf{k}_{global} = \mathbf{T}^T \cdot \mathbf{k}_{local} \cdot \mathbf{T} \quad (21)$$

where

\mathbf{k}_{global} = contribution of a single element to the global stiffness matrix

\mathbf{T} = transformation matrix

\mathbf{k}_{local} = stiffness matrix for an individual element

The transformation matrix consists of sine and cosine terms of the angle the element makes with the global axes and relates the local directions with global degrees of freedom. Using Equation 21, the local coordinates are mapped onto the global axes.

The second step determines how the local, rotated degrees of freedom correspond with the global DOFs. For instance, for a simply-supported (pin-roller) beam only the local DOFs 3, 4, and 6 (as defined in Figure A-2) would contribute to the global stiffness matrix. Assuming the global DOFs are assigned as shown in Figure A-7, the global stiffness matrix would be:

$$\mathbf{k}_{global} = \begin{bmatrix} \mathbf{k}_{33} & \mathbf{k}_{34} & \mathbf{k}_{36} \\ \mathbf{k}_{43} & \mathbf{k}_{44} & \mathbf{k}_{46} \\ \mathbf{k}_{63} & \mathbf{k}_{64} & \mathbf{k}_{66} \end{bmatrix} \quad (22)$$

where the k_{xx} values refer to the corresponding value in the elemental stiffness matrix. The same modifications must be made to nodal load vectors in order to capture the correct response at each degree of freedom. In multi-element structures, the stiffness associated with a global degree of freedom is simply the sum of the contributions from the surrounding elements. While somewhat tedious to do by hand, the mapping of elements is very systematic, and thus easily performed by a well-written computer program.



Figure A-7: Global degrees of freedom for a pin-roller simply supported beam

A.2.5 Choosing a Method

Both the stiffness and the flexibility method have strengths and weaknesses in calculation and accuracy of the solution. The accuracy of the stiffness method is based on the appropriateness of the assumed deflected shape and the size (or number) of the elements. A single-element member modeled with a low-order shape function is not likely to adequately approximate the true response of a geometrically complex beam.

However, the stiffness method develops the stiffness matrix directly, which, relative to the flexibility method, makes it more computationally efficient. Additionally, the shape functions are designed to calculate the displacement over the length of the element, meaning that with nodal values, the displacements at any point in the member can be calculated.

Because it is based in establishing equilibrium, the flexibility method can calculate nodal displacements exactly, guaranteeing accuracy of a model. Because there is no assumed deflected shape, the flexibility method is better than the stiffness method for non-linear material response. However, to form the stiffness matrix, the flexibility matrix must be modified by the Φ matrix, which adds a step to the analysis process. Also, because there are no shape functions in the flexibility method, the response is only calculated at the nodal locations. This latter limitation means that the response of a point that is of interest can only be captured if there is a node located there.

A.3 SUMMARY AND CONCLUSIONS

The theory of finite element analysis is based on using small elements with known behavior to estimate the response of a continuous system. This chapter presented two methods for formulating the stiffness matrix for an individual element, as would be used by a computer program such as ABAQUS or ANSYS. An understanding of the calculation methods of finite element programs was critical for choosing modeling techniques and assessing the validity and appropriateness of the model.

APPENDIX B
Full Input File

```

*heading
trapezoidal steel box girder model fsel AUGUST 2007
**
**
** -----
**
**
** NODE DEFINITION
**
**
** *system
0, 0, 0, 100, 0, 0
**
**
** Import text files of nodes to define horizontal planes at z=0, z=58
** (top of girder), z=58.01 (bottom of haunch), z=61 (top of
haunch),
** z=69 (top of deck), and z=97 (top of rails).
**
** *node, nset=line0, input=000s-final.txt
** *node, nset=line8, input=800s-final.txt
** *node, nset=line9, input=900s-final.txt
** *node, nset=line11, input=1100s-final.txt
** *node, nset=line19, input=1900s-final.txt
** *node, nset=line47, input=4700s-final.txt
**
**
** * Generate additional planes of elements between planes defined above
** to form 16 possible elements through the girders, 3 through the
** haunch, 8 through the deck, and 28 through the rails.
**
** *nfill, nset=face0
line0, line8, 16, 50
** *nfill, nset=face0
line9, line11, 2, 100
** *nfill, nset=face0
line11, line19, 8, 100
** *nfill, nset=face0
line19, line47, 28, 100
**
**
** * The following nsets are defined mainly for data acquisition
**
** *nset, nset=allnodes
face0
** *nset, generate, nset=bottomflange
8, 1800008, 10000
15, 1800015, 10000
23, 1800023, 10000
30, 1800030, 10000
**

```

```

**
** Define node sets for supports: four nodes across the middle of each
** girder, at each end. The near end is a roller and is constrained
** against horizontal movement using a spring element.
**
**
*nset, generate, nset=roller
10010, 10013, 1
10025, 10028, 1
*nset, generate, nset=pin support
1790010, 1790013, 1
1790025, 1790028, 1
*nset, nset=supports
roller, pin support
**
*boundary
roller, 2
pin support, 1, 3
**
*element, type=spring2, el set=supportspring
700001, 20007, 20008
*spring, el set=supportspring
1, 1
7.333
**
**
** END NODE/SUPPORT DEFINITION
**
** -----
**
** DEFINE SECTION PROPERTIES
**
** Listed thicknesses for steel plates are the average measured value
** found on the as-built bridge specimen
**
*shell section, el set=webs, material=steel
0.503
*shell section, el set=botflange, material=steel
0.757
*shell section, el set=topflange, material=steel, offset=spos
0.646
*shell section, el set=diaphragms, material=steel
0.5
*shell section, el set=diaphvert, material=steel
0.625
*shell section, el set=vert, material=steel
0.625
**
**
** The following beam sections are for the bracing members within and
** between the girders. The approximate L-shape member is
** defined using coordinates.
**
*beam section, el set=inttruss, section=arbitrary, material=steel
4, -4, 0.13, 0, 0.13, 0.530
0, -6.435, 0.305
0, 0.13, 0

```

```

4, 0. 13, 0. 530
*beam section, el set=toptruss, section=arbitrary, material=steel
4, -4, 0. 13, 0, 0. 13, 0. 530
0, -6. 435, 0. 305
0, 0. 13, 0
4, 0. 13, 0. 530
*beam section, el set=exttruss, section=arbitrary, material=steel
4, -4, 0. 13, 0, 0. 13, 0. 530
0, -6. 435, 0. 305
0, 0. 13, 0
4, 0. 13, 0. 530
**
**
** Because the fake elements have their own material, the sections
** must be defined individually
**
*solid section, el set=deck, material=conc
*solid section, el set=fakedeck, material=fakeconc
*solid section, el set=rails, material=railconc
*solid section, el set=fakerails, material=fakeconc
*solid section, el set=bigtrans, material=rebar
0. 62
*solid section, el set=smalltrans, material=rebar
0. 31
*solid section, el set=botlong, material=rebar
0. 31
*solid section, el set=topl ong, material=rebar
0. 20
*solid section, el set=railrebar, material=rebar
0. 20
*solid section, el set=fakedeckrebar, material=fakerebar
0. 01
*solid section, el set=fakerailrebar, material=fakerebar
0. 01
**
**
** END SECTION PROPERTY DEFINITIONS
**
** -----
**

```

```

**
** DEFINE MATERIALS
**
**
*orientation, name=standard, definition=coordinates
1, 0, 0, 0, 1, 0
1, 0
**
*material, name=steel
*elastic
29000, 0.3
*plastic
50.086, 0
51.0, 0.01804
62.4, 0.03707
70.2, 0.07454
71.5, 0.09284
65.0, 0.4
*density
7.33863e-7
**
*material, name=rebar
*elastic
29000, 0.3
*density
7.33863e-7
**
*material, name=fakerebar
*elastic
0.1, 0.3
*density
1e-15
**
*material, name=conc
*elastic
3875, 0.2
*plastic
3.09, 0
3.77, 0.0004
4.28, 0.0008
4.84, 0.0018
4.84, 0.01
*density
2.4576e-07
**
*material, name=railconc
*elastic
3000, 0.25
*plastic
3.09, 0
3.77, 0.0004
4.28, 0.0008
4.84, 0.0018
4.50, 0.0027
4.50, 0.01
*density
1.9225e-07
**
*material, name=fakeconc
*elastic

```

```

0. 1, 0. 25
*densi ty
1e-15
**
**
** END MATERIAL DEFINITIONs
**
**
** -----
**
** DEFINE GIRDER ELEMENTS
**
**
*el ement, type=s4r, el set=topfl ange
1001, 808, 10808, 10807, 807
21001, 815, 10815, 10814, 814
101001, 823, 10823, 10822, 822
121001, 830, 10830, 10829, 829
**
*el ement, type=s4r, el set=webs
3001, 808, 10808, 10708, 708
23001, 815, 10815, 10715, 715
3071, 700808, 710808, 710758, 700758
23071, 700815, 710815, 710765, 700765
3111, 1100808, 1110808, 1110708, 1100708
23111, 1100815, 1110815, 1110715, 1100715
**
*el ement, type=s4r, el set=botfl ange
40001, 9, 8, 10008, 10009
140001, 24, 23, 10023, 10024
**
**
*el gen, el set=topfl ange
1001, 180, 10000, 1, 2, 1, 1000
21001, 180, 10000, 1, 2, 1, 1000
101001, 180, 10000, 1, 2, 1, 1000
121001, 180, 10000, 1, 2, 1, 1000
**
*el gen, el set=webs
3001, 70, 10000, 1, 8, -100, 2000
23001, 70, 10000, 1, 8, -100, 2000
3071, 40, 10000, 1, 16, -50, 1000
23071, 40, 10000, 1, 16, -50, 1000
3111, 70, 10000, 1, 8, -100, 2000
23111, 70, 10000, 1, 8, -100, 2000
*el copy, el ement shi ft=100000, ol d set=webs, shi ft nodes=15, new
set=webs
**
**
*el gen, el set=botfl angei n
40001, 180, 10000, 1, 7, 1, 1000
*el gen, el set=botfl angeout
140001, 180, 10000, 1, 7, 1, 1000
**
**
*el set, el set=botfl ange
botfl angei n, botfl angeout
**
**
** defi ne end di afragms
**

```



```

**
*el ement, type=s4r
200001, 10009, 10109, 10108, 10008
*el gen, el set=di aph
200001, 22, 1, 1, 8, 100, 100
*el copy, el ement shi ft=10000, old set=di aph, shi ft nodes=1780000, new
set=di aph
**
**
** defi ne di aphragm sti ffeners
** NOTE: actual sti ffeners are six inches deep, 5/8" thick, both sides
** of di aphragm. These are twelve inches deep, one side.
**
**
*el ement, type=s4r, el set=di aphvert
50001, 11, 10011, 10111, 111
51001, 12, 10012, 10112, 112
52001, 13, 10013, 10113, 113
*el gen, el set=di aphvert
50001, 2, 16, 1, 8, 100, 100
51001, 2, 14, 1, 8, 100, 100
52001, 2, 12, 1, 8, 100, 100
*el copy, el ement shi ft=3000, old set=di aphvert, shi ft nodes=1790000,
new set=di aphvert
**
**
** defi ne top of di aphragms
**
**
*el ement, type=s4r
56000, 810, 10810, 10809, 809
*el gen, el set=di aphtop
56000, 5, 1, 1, 2, 10000, 10
*el copy, el ement shi ft=5, old set=di aphtop, shi ft nodes=15, new
set=di aphtop
*el copy, el ement shi ft=100, old set=di aphtop, shi ft nodes=1780000, new
set=di aphtop
**
*el ement, type=s4r
57001, 17, 10017, 10016, 16
57000, 16, 10016, 10015, 15
*el gen, el set=mi ddi aph
57001, 6, 1, 1, 2, 10000, 10
57000, 2, 7, 7, 2, 10000, 10
*el set, generate, el set=mi ddi aph1
57001, 57006, 1
57011, 57016, 1
*el copy, el ement shi ft=20, old set=mi ddi aph1, shi ft nodes=800, new
set=mi ddi aph
*el copy, el ement shi ft=100, old set=mi ddi aph, shi ft nodes=1780000, new
set=mi ddi aph
**
*el set, el set=di aphragms
di aph, di aphtop, mi ddi aph
**
*el set, generate, el set=di aphmi dtop
57021, 57026, 1
57031, 57036, 1
57121, 57126, 1
57131, 57136, 1

```

```

**
**
** DEFINE INTERNAL TRUSS ELEMENTS
**
**
*element, type=b31, el set=int1
58001, 120808, 120811
58002, 120811, 120815
58003, 120008, 120811
58004, 120015, 120811
*el copy, element shift=100, old set=int1, shift nodes=120000, new
set=int2
*el copy, element shift=100, old set=int2, shift nodes=320000, new
set=int3
*el copy, element shift=100, old set=int3, shift nodes=120000, new
set=int4
*el copy, element shift=100, old set=int4, shift nodes=220000, new
set=int5
*el copy, element shift=100, old set=int5, shift nodes=220000, new
set=int6
*el copy, element shift=100, old set=int6, shift nodes=120000, new
set=int7
*el copy, element shift=100, old set=int7, shift nodes=320000, new
set=int8
*el copy, element shift=100, old set=int8, shift nodes=120000, new
set=int9
*el set, generate, el set=inttruss
58001, 58900, 1
*el copy, element shift=100000, old set=inttruss, shift nodes=15, new
set=inttruss
**
**
** DEFINE INTERNAL TOP BRACING
**
**
*element, type=b31, el set=toptruss
59001, 10815, 120808
59002, 120808, 240815
59003, 240815, 560808
59004, 560808, 680815
59005, 680815, 900808
59006, 900808, 1120815
59007, 1120815, 1240808
59008, 1240808, 1560815
59009, 1560815, 1680808
59010, 1680808, 1790815
*el copy, element shift=100000, old set=top truss, shift nodes=15, new
set=toptruss
**
**
** DEFINE INTERNAL WEB STIFFENERS
**
**
*element, type=s4r
60001, 120008, 120108, 120109, 120009
60002, 240008, 240108, 240109, 240009
60003, 560008, 560108, 560109, 560009
60004, 680008, 680108, 680109, 680009
60005, 900008, 900058, 900059, 900009
60006, 1120008, 1120108, 1120109, 1120009

```

```

60007, 1240008, 1240108, 1240109, 1240009
60008, 1560008, 1560108, 1560109, 1560009
60009, 1680008, 1680108, 1680109, 1680009
*el gen, el set=vert
60001, 2, 6, 1000, 8, 100, 10
60002, 2, 6, 1000, 8, 100, 10
60003, 2, 6, 1000, 8, 100, 10
60004, 2, 6, 1000, 8, 100, 10
60005, 2, 6, 1000, 16, 50, 10
60006, 2, 6, 1000, 8, 100, 10
60007, 2, 6, 1000, 8, 100, 10
60008, 2, 6, 1000, 8, 100, 10
60009, 2, 6, 1000, 8, 100, 10
*el copy, el ement shi ft=100000, ol d set=vert, shi ft nodes=15, new
set=vert
**
**
** DEFINE EXTERNAL BRACING
**
**
*el ement, type=b31, el set=ext2
63200, 680815, 680823
63201, 680015, 680019
63202, 680019, 680023
63203, 680815, 680019
63204, 680823, 680019
*el ement, type=b31, el set=ext3
63300, 1120815, 1120823
63301, 1120015, 1120019
63302, 1120019, 1120023
63303, 1120815, 1120019
63304, 1120823, 1120019
*el set, generate, el set=exttruss
63200, 63204, 1
63300, 63304, 1
**
**
** END GIRDER DEFINITION
**
**
** -----
**

```

```

**
** DEFINE HAUNCH ELEMENTS
**
**
*element, type=c3d8r, elset=haunch
3002001, 20907, 20908, 30908, 30907, 21007, 21008, 31008, 31007
3002003, 20914, 20915, 30915, 30914, 21014, 21015, 31015, 31014
*elgen, elset=haunch
3002001, 2, 1, 1, 2, 100, 100, 176, 10000, 1000
3002003, 2, 1, 1, 2, 100, 100, 176, 10000, 1000
*elcopy, element shift=4, old set=haunch, shift nodes=15, new
set=haunch
**
**
** Above each end diaphragm, the haunch connects the top flanges as
** well as spans between the two girders. These extra elements are
** defined here.
**
*element, type=c3d8r, elset=haunchdiaph
3000013, 907, 908, 10908, 10907, 1007, 1008, 11008, 11007
*elgen, elset=haunchdiaph
3000013, 24, 1, 1, 2, 100, 100, 2, 10000, 1000
*elcopy, element shift=178000, old set=haunchdiaph, shift
nodes=1780000, newset=haunchdiaph
**
**
** DEFINE DECK ELEMENTS
**
**
*element, type=c3d8r, elset=maindeck
3000205, 1105, 1106, 11106, 11105, 1205, 1206, 11206, 11205
*elgen, elset=maindeck
3000205, 28, 1, 1, 180, 10000, 1000
**
**
** The deck elements below the rails are defined separately because the
** mesh density changes down the length with the rail element mesh
** density.
**
*element, type=c3d8r, elset=undrailslong
3000201, 1101, 1105, 11105, 11101, 1201, 1205, 11205, 11201
3050201, 501101, 501105, 511105, 511101, 501201, 501205, 511205, 511201
3100201,
1001101, 1001105, 1011105, 1011101, 1001201, 1001205, 1011205, 1011201
3150201,
1501101, 1501105, 1511105, 1511101, 1501201, 1501205, 1511205, 1511201
**
*elgen, elset=undrailslong
3000201, 30, 10000, 1000
3050201, 30, 10000, 1000
3100201, 30, 10000, 1000
3150201, 30, 10000, 1000
**
**
** In order to use the elcopy function, the area with increased mesh
** density was separated out, then copied twice down the length to
** capture the three expansion joint locations.
**
*element, type=c3d8r, elset=undrailsshort
3030201, 301101, 301103, 311103, 311101, 301201, 301203, 311203, 311201

```

```

3036201, 361101, 361102, 371102, 371101, 361201, 361202, 371202, 371201
3044201, 441101, 441103, 451103, 451101, 441201, 441203, 451203, 451201
*el gen, el set=undrailsshort
3030201, 2, 2, 1, 6, 10000, 1000
3036201, 4, 1, 1, 8, 10000, 1000
3044201, 2, 2, 1, 6, 10000, 1000
**
*el copy, element shift=50000, old set=undrailsshort, shift
nodes=500000, new set=undrails
*el copy, element shift=100000, old set=undrailsshort, shift
nodes=1000000, new set=undrails
**
*el set, el set=deckundrails
undrails, undrailsshort, undrailslong
**
*el copy, element shift=32, old set=deckundrails, shift nodes=32, new
set=deckundrails
**
**
** Throughout the deck definition, only one deck element has been
** defined vertically. At this point, the entire plane of elements
** is copied vertically. By separating it out like this, the deck
** elements can be viewed in the .odb file at 1 in. increments
** through the thickness.
**
*el set, el set=deck1
maindeck, deckundrails
**
*el copy, element shift=100, old set=deck1, shift nodes=100, new
set=deck2
*el copy, element shift=200, old set=deck1, shift nodes=200, new
set=deck3
*el copy, element shift=300, old set=deck1, shift nodes=300, new
set=deck4
*el copy, element shift=400, old set=deck1, shift nodes=400, new
set=deck5
*el copy, element shift=500, old set=deck1, shift nodes=500, new
set=deck6
*el copy, element shift=600, old set=deck1, shift nodes=600, new
set=deck7
*el copy, element shift=700, old set=deck1, shift nodes=700, new
set=deck8
**
*el set, el set=thdeck
deck1, deck2, deck3, deck4, deck5, deck6, deck7, deck8
**
*el set, el set=deck
haunch, thdeck, haunchdiaph
**
**
** DEFINE FAKE DECK AND FAKEHAUNCH ELEMENTS
** NOTE: Using shift nodes=0 will cause a warning to appear in the .dat
** file. There is no adverse effect on the analysis and the
** warning should not cause concern.
**
*el copy, element shift=1000000, old set=deck, shift nodes=0, new
set=fakedeck
**
**
** END DECK DEFINITION

```

```

**
**
** -----
**
**
** DEFINE REBAR WITHIN DECK ELEMENTS
**
**
**el ement, type=t3d2
700003, 1303, 11303
700005, 1305, 11305
**
**el gen, el set=botl ong
700003, 2, 32, 32, 180, 10000, 100
700005, 29, 1, 1, 180, 10000, 100
**
**el copy, el ement shi ft=100000, ol d set=botl ong, shi ft nodes=300, new
set=topl ong
**
**
** The longitudinal rebar connects each longitudinal node, and thus the
** definition and generation is very straightforward. The
** transverse rebar exists every 6 or 12 in. down the length, which
** means it must be defined at certain nodes but not at others.
**
**el ement, type=t3d2
500001, 11203, 11204
505301, 531203, 531204
510301, 1031203, 1031204
515301, 1531203, 1531204
**
**el gen, el set=bi gtrans
500001, 26, 10000, 100, 32, 1, 1
505301, 23, 10000, 100, 32, 1, 1
510301, 23, 10000, 100, 32, 1, 1
515301, 26, 10000, 100, 32, 1, 1
**
**
** NOTE: The midtrans elset name does not refer to the size of the
** rebar but to the nature of the definition; it was defined only as
** a middle step to allow for multiple copies to be made.
**
**el ement, type=t3d2, el set=mi dtrans
502601, 261203, 261204
503101, 311203, 311204
503901, 391203, 391204
504301, 431203, 431204
505001, 501203, 501204
**
**el gen, el set=mi dtrans
502601, 32, 1, 1, 4, 10000, 100
503101, 32, 1, 1, 3, 20000, 200
503901, 32, 1, 1
504301, 32, 1, 1, 4, 20000, 200
505001, 32, 1, 1, 3, 10000, 100
**
**el copy, el ement shi ft=5000, ol d set=mi dtrans, shi ft nodes=500000, new
set=small trans
**el copy, el ement shi ft=10000, ol d set=mi dtrans, shi ft nodes=1000000,
new set=small trans

```

```

**
*el set, el set=smalltrans
midtrans
**
**
** Copy the transverse rebar vertically to define the top layer of bars
**
**
*el copy, element shift=100000, old set=bigtrans, shift nodes=500, new
set=bigtrans
*el copy, element shift=100000, old set=smalltrans, shift nodes=500, new
set=smalltrans
**
**
*el set, el set=deckrebar
botlong, toplong, bigtrans, smalltrans
**
**
** DEFINE FAKEREBAR ELEMENTS
** NOTE: Using shift nodes=0 will cause a warning to appear in the .dat
** file. There is no adverse effect on the analysis and the
** warning should not cause concern.
**
*el copy, element shift=50000, old set=deckrebar, shift nodes=0, new
set=fakedeckrebar
**
**
** Constrain the fake and real rebar elements to move with the deck
** elements they are within.
**
*embedded element, host el set=deck
deckrebar, fakedeckrebar
**
**
** END DECK REBAR DEFINITION
**
** -----
**

```

```

**
** DEFINE RAIL ELEMENTS
**
**
** The rails are defined in a similar manner to the deckundrails
**   elements, as the mesh density increase requires varying element
**   definitions by longitudinal location.
**
*element, type=c3d8, elset=raillong
5000001, 1901, 1905, 11905, 11901, 2301, 2305, 12305, 12301
5050001, 501901, 501905, 511905, 511901, 502301, 502305, 512305, 512301
5100001,
1001901, 1001905, 1011905, 1011901, 1002301, 1002305, 1012305, 1012301
5150001,
1501901, 1501905, 1511905, 1511901, 1502301, 1502305, 1512305, 1512301
**
*elgen, elset=raillong
5000001, 7, 400, 40, 30, 10000, 1000
5050001, 7, 400, 40, 30, 10000, 1000
5100001, 7, 400, 40, 30, 10000, 1000
5150001, 7, 400, 40, 30, 10000, 1000
**
**
*element, type=c3d8, elset=railshort
5030001, 301901, 301903, 311903, 311901, 302101, 302103, 312103, 312101
5036001, 361901, 361902, 371902, 371901, 362001, 362002, 372002, 372001
5040001, 401901, 401902, 411902, 411901, 402001, 402002, 412002, 412001
5041001, 411901, 411902, 421902, 421901, 412001, 412002, 422002, 422001
5044001, 441901, 441903, 451903, 451901, 442101, 442103, 452103, 452101
**
*elgen, elset=railshort
5030001, 2, 2, 1, 14, 200, 20, 6, 10000, 1000
5036001, 4, 1, 1, 28, 100, 10, 4, 10000, 1000
5040001, 4, 1, 1, 6, 100, 10
5041001, 4, 1, 1, 28, 100, 10, 3, 10000, 1000
5044001, 2, 2, 1, 14, 200, 20, 6, 10000, 1000
**
*elcopy, element shift=50000, old set=railshort, shift nodes=500000,
new set=railgaps
*elcopy, element shift=100000, old set=railshort, shift nodes=1000000,
new set=railgaps
**
*elset, elset=inrail
raillong, railgaps, railshort
**
*elcopy, element shift=4, old set=inrail, shift nodes=32, new
set=outrail
**
*elset, elset=rails
inrail, outrail
**
**
** DEFINE FAKERAIL ELEMENTS
** NOTE: Using shift nodes=0 will cause a warning to appear in the .dat
** file. There is no adverse effect on the analysis and the
** warning should not cause concern.
**
*elcopy, element shift=1000000, old set=rails, shift nodes=0, new
set=fakerails
**

```



```

**
** END RAIL DEFINITION
**
**
** -----
**
**
** DEFINE REBAR WITHIN RAIL ELEMENTS
**
**
*element, type=t3d2
900102, 12102, 22102
900112, 13002, 23002
904112, 413002, 423002
909112, 913002, 923002
914112, 1413002, 1423002
900133, 14503, 24503
904133, 414503, 424503
909133, 914503, 924503
914133, 1414503, 1424503
**
**
** The rebar generation creates four rows of rebar. The bottom three
** have two bars in each row, the top one has just one (thus the
** absence of a 2,2,2 generation for the 33 elements. The 02
** elements are the only continuous ones (through the expansion
** joint location).
**
*elgen, elset=innrailrebar
900102, 178, 10000, 100, 2, 2, 2
900112, 37, 10000, 100, 2, 2, 2, 2, 900, 10
904112, 47, 10000, 100, 2, 2, 2, 2, 900, 10
909112, 47, 10000, 100, 2, 2, 2, 2, 900, 10
914112, 38, 10000, 100, 2, 2, 2, 2, 900, 10
900133, 37, 10000, 100
904133, 47, 10000, 100
909133, 47, 10000, 100
914133, 38, 10000, 100
**
*elcopy, element shift=1000000, old set=innrailrebar, shift nodes=32,
new set=outrailrebar
**
*elset, elset=railrebar
innrailrebar, outrailrebar
**
**
** DEFINE FAKERAILREBAR ELEMENTS
** NOTE: Using shift nodes=0 will cause a warning to appear in the .dat
** file. There is no adverse effect on the analysis and the
** warning should not cause concern.
**
*elcopy, element shift=50000, old set=railrebar, shift nodes=0, new
set=fakerailrebar
**
**
** Constrain the fake and real rebar elements to move with the deck
** elements they are within.
**
*embedded element, host elset=rails
railrebar, fakerailrebar

```

```

**
**
** Create one elset to contain all the rebar defined in the model
**
*el set, el set=rebar
deckrebar, railrebar
**
**
** END RAIL REBAR DEFINITION
**
**
** -----
**
** CONNECT HAUNCH TO TOP FLANGES USING SPRINGS
**
**
*spri ng, el set=shearstud1
1, 1
200
*spri ng, el set=shearstud2
2, 2
1000
*spri ng, el set=shearstud3
3, 3
200
**
** The spring stiffnesses given are explained in Chapter 5, and reflect
** on the expected strength of the shear stud in the given
** direction.
**
**
*el ement, type=spri ng2
7000001, 807, 907
7054001, 540807, 540907
7104001, 1040807, 1040907
7154001, 1540807, 1540907
**
*el gen, el set=SS1l ong
7000001, 3, 1, 1, 27, 10000, 1000
7054001, 3, 1, 1, 23, 10000, 1000
7104001, 3, 1, 1, 23, 10000, 1000
7154001, 3, 1, 1, 27, 10000, 1000
**
**
** Similar to with the transverse rebar, the shear studs are not
** defined at every longitudinal node. Thus, again, the definitions
** are split out to consider 12" spacing along the length.
**
*el ement, type=spri ng2, el set=SS1mi d
7028001, 280807, 280907
7030001, 300807, 300907
7034001, 340807, 340907
7040001, 400807, 400907
7046001, 460807, 460907
7050001, 500807, 500907
7052001, 520807, 520907
**
*el gen, el set=SS1mi d
7028001, 3, 1, 1

```

```

7030001, 3, 1, 1
7034001, 3, 1, 1
7040001, 3, 1, 1
7046001, 3, 1, 1
7050001, 3, 1, 1
7052001, 3, 1, 1
**
*el copy, element shift=50000, old set=SS1mid, shift nodes=500000, new
set=SS1-1
*el copy, element shift=100000, old set=SS1mid, shift nodes=1000000, new
set=SS1-1
**
*el set, el set=SS1-1
SS1mid, SS1long
**
**
** The studs have only been defined on the innermost flange. Those can
** now be copied to the other three flanges.
**
*el copy, element shift=3, old set=SS1-1, shift nodes=7, new set=SS1-2
*el copy, element shift=6, old set=SS1-1, shift nodes=15, new set=SS1-3
*el copy, element shift=9, old set=SS1-1, shift nodes=22, new set=SS1-4
*el set, el set=shearstud1
SS1-1, SS1-2, SS1-3, SS1-4
**
**
** DEFINE SHEAR STUDS IN 2, 3 DIRECTIONS
** NOTE: Using shift nodes=0 will cause a warning to appear in the .dat
** file. There is no adverse effect on the analysis and the
** warning should not cause concern.
**
*el copy, element shift=1000000, old set=shearstud1, shift nodes=0, new
set=shearstud2
*el copy, element shift=2000000, old set=shearstud1, shift nodes=0, new
set=shearstud3
**
**
** -----
**
** RESTRICT CONTACT BETWEEN FLANGE AND HAUNCH
**
** NOTE: The contact definition here returns many (~2500) warnings in
** the .dat file about restricting rotation between the DOFs. There
** has been no indication that this is a problem in running the job
** correctly.
**
**
*surface interaction, name=deckgirderint
**
**
*surface, name=flangesurface
topflange, sneg
diaphmidtopy, sneg
diaphmtopy, sneg
**
*nset, generate, nset=haunchnodes
907, 1800907, 10000
908, 1800908, 10000
909, 1800909, 10000

```

```

914, 1800914, 10000
915, 1800915, 10000
916, 1800916, 10000
922, 1800922, 10000
923, 1800923, 10000
924, 1800924, 10000
929, 1800929, 10000
930, 1800930, 10000
931, 1800931, 10000
*nset, nset=haunchnodes
910, 911, 912, 913, 917, 918, 919, 920, 921, 925, 926, 927, 928
10910, 10911, 10912, 10913, 10917, 10918, 10919
10920, 10921, 10925, 10926, 10927, 10928
20910, 20911, 20912, 20913, 20917, 20918, 20919
20920, 20921, 20925, 20926, 20927, 20928
1780910, 1780911, 1780912, 1780913, 1780917, 1780918, 1780919
1780920, 1780921, 1780925, 1780926, 1780927, 1780928
1790910, 1790911, 1790912, 1790913, 1790917, 1790918, 1790919
1790920, 1790921, 1790925, 1790926, 1790927, 1790928
1800910, 1800911, 1800912, 1800913, 1800917, 1800918, 1800919
1800920, 1800921, 1800925, 1800926, 1800927, 1800928
*surface, type=node, name=haunchsurface
haunchnodes, 20
**
*contact pair, interaction=deckgirderint
haunchsurface, flangesurface
**
**
** -----
**
**
** DEFINE CONTACT SURFACES FOR RAIL GAPS
**
** Each of the six gaps in the railing have contact defined with them,
** which involves defining the surfaces involved and then applying
** the constraint.
**
*surface interaction, name=raillgapint
**
**
** inner rail
**
**
*elset, generate, elset=innrail1e
5039091, 5039271, 10
5039092, 5039272, 10
5039093, 5039273, 10
5039094, 5039274, 10
*surface, name=innrail1s
innrail1e, S5
*elset, generate, elset=innrail2e
5041091, 5041271, 10
5041092, 5041272, 10
5041093, 5041273, 10
5041094, 5041274, 10
*surface, name=innrail2s
innrail2e, S3
**

```

```

*el set, generate, el set=i nrai l 3e
5089091, 5089271, 10
5089092, 5089272, 10
5089093, 5089273, 10
5089094, 5089274, 10
*surface, name=i nrai l 3s
i nrai l 3e, S5
*el set, generate, el set=i nrai l 4e
5091091, 5091271, 10
5091092, 5091272, 10
5091093, 5091273, 10
5091094, 5091274, 10
*surface, name=i nrai l 4s
i nrai l 4e, S3
**
*el set, generate, el set=i nrai l 5e
5139091, 5139271, 10
5139092, 5139272, 10
5139093, 5139273, 10
5139094, 5139274, 10
*surface, name=i nrai l 5s
i nrai l 5e, S5
*el set, generate, el set=i nrai l 6e
5141091, 5141271, 10
5141092, 5141272, 10
5141093, 5141273, 10
5141094, 5141274, 10
*surface, name=i nrai l 6s
i nrai l 6e, S3
**
*contact pair, interaction=ra i l gapi nt
i nrai l 2s, i nrai l 1s
i nrai l 1s, i nrai l 2s
i nrai l 4s, i nrai l 3s
i nrai l 3s, i nrai l 4s
i nrai l 6s, i nrai l 5s
i nrai l 5s, i nrai l 6s
**
**
** outer rail
**
**
*el set, generate, el set=outrai l 1e
5039095, 5039275, 10
5039096, 5039276, 10
5039097, 5039277, 10
5039098, 5039278, 10
*surface, name=outrai l 1s
outrai l 1e, S5
*el set, generate, el set=outrai l 2e
5041095, 5041275, 10
5041096, 5041276, 10
5041097, 5041277, 10
5041098, 5041278, 10
*surface, name=outrai l 2s
outrai l 2e, S3
**
*el set, generate, el set=outrai l 3e
5089095, 5089275, 10
5089096, 5089276, 10

```

```

5089097, 5089277, 10
5089098, 5089278, 10
*surface, name=outrai | 3s
outrai | 3e, S5
*el set, generate, el set=outrai | 4e
5091095, 5091275, 10
5091096, 5091276, 10
5091097, 5091277, 10
5091098, 5091278, 10
*surface, name=outrai | 4s
outrai | 4e, S3
**
*el set, generate, el set=outrai | 5e
5139095, 5139275, 10
5139096, 5139276, 10
5139097, 5139277, 10
5139098, 5139278, 10
*surface, name=outrai | 5s
outrai | 5e, S5
*el set, generate, el set=outrai | 6e
5141095, 5141275, 10
5141096, 5141276, 10
5141097, 5141277, 10
5141098, 5141278, 10
*surface, name=outrai | 6s
outrai | 6e, S3
**
*contact pair, interaction=raillgapi nt
outrai | 2s, outrai | 1s
outrai | 1s, outrai | 2s
outrai | 4s, outrai | 3s
outrai | 3s, outrai | 4s
outrai | 6s, outrai | 5s
outrai | 5s, outrai | 6s
**
**
** END RAIL CONTACT DEFINITION
**
** -----
**

```

```
**
** DEFINE MPCs AT MESH DENSITY INCREASE POINTS
**
**
** A sample of these files is included in Appendix E. Each one
** includes the restraints placed on nodes that are part of one
** element but not the neighboring elements.
**
** *mpc, i nput=WebMPCs. txt
** *mpc, i nput=DeckMPCs. txt
**
** *mpc, i nput=Rai l Edge1. txt
** *mpc, i nput=Rai l Edge2. txt
** *mpc, i nput=Rai l Edge3. txt
**
** *mpc, i nput=Gap1-7to14. txt
** *mpc, i nput=Gap1-14to28. txt
** *mpc, i nput=Gap1-28to14. txt
** *mpc, i nput=Gap1-14to7. txt
**
** *mpc, i nput=Gap2-7to14. txt
** *mpc, i nput=Gap2-14to28. txt
** *mpc, i nput=Gap2-28to14. txt
** *mpc, i nput=Gap2-14to7. txt
**
** *mpc, i nput=Gap3-7to14. txt
** *mpc, i nput=Gap3-14to28. txt
** *mpc, i nput=Gap3-28to14. txt
** *mpc, i nput=Gap3-14to7. txt
**
**
** -----
**
```

```

**
** DEFINE GENERAL ELEMENT SETS
**
**
*el set, el set=girders
topflange, webs, botflangein, botflangeout, diaph, diaphvert, diaphtop,
middiaph, vert
**
*el set, el set=bracing
intruss, extruss, toptruss
**
**
** The two types of flanges defined below are so defined to capture the
** difference between the internal and external sides and the
** different tributary areas from the deck.
**
*el set, generate, el set=flange1
2001, 2180, 1
21001, 21180, 1
22001, 22180, 1
101001, 101180, 1
102001, 102180, 1
121001, 121180, 1
*el set, generate, el set=flange2
1001, 1180, 1
122001, 122180, 1
**
*surface, type=element, name=flangetype1
flange1, sneg
*surface, type=element, name=flangetype2
flange2, sneg
**
**
** The in and outdeckedges are for applying the dead load of the rails
** before the elements are reactivated using *model change
**
*el set, generate, el set=indeckedge
3000901, 3179901, 1000
3030902, 3049902, 1000
3080902, 3099902, 1000
3130902, 3149902, 1000
3036903, 3043903, 1000
3036904, 3043904, 1000
3086903, 3093903, 1000
3086904, 3093904, 1000
3136903, 3143903, 1000
3136904, 3143904, 1000
*el set, generate, el set=outdeckedge
3000933, 3179933, 1000
3030934, 3049934, 1000
3080934, 3099934, 1000
3130934, 3149934, 1000
3036935, 3043935, 1000
3036936, 3043936, 1000
3086935, 3093935, 1000
3086936, 3093936, 1000
3136935, 3143935, 1000
3136936, 3143936, 1000
**
*surface, type=element, name=indeck

```



```

i ndeckedge, S2
*surface, type=el ement, name=outdeck
outdeckedge, S2
**
**
** -----
**
**
** DEFINE TRUCK LOADS
**
**
** The truck load locations correspond to the locations of the concrete
** blocks on the test specimen, which is not the exact same as an
** actual truck, but was necessary to correlate data.
**
**
**el set, el set=ax1-1
3110921, 3110922, 3110923
**el set, el set=ax1-2
3110927, 3110928
**el set, generate, el set=ax2
3077921, 3077928, 1
3078921, 3078928, 1
**el set, generate, el set=ax3
3063921, 3063928, 1
**
**surface, type=el ement, name=axl e1-1
ax1-1, s2
**surface, type=el ement, name=axl e1-2
ax1-2, s2
**surface, type=el ement, name=axl e2
ax2, s2
**surface, type=el ement, name=axl e3
ax3, s2
**
**
** -----
**
**
** DEFINE FRACTURE SETS
**
**
**el set, generate, el set=fractfl ange
140090, 146090, 1000
**
**
** The web fracture was originally defined in two vertical element
** pairs, so that one set could be removed in each subsequent step
** to look at the tip stresses.
**
**
**el set, el set=fractweb1
118090, 138090
117090, 137090
**el set, el set=fractweb2
116090, 136090
115090, 135090
**el set, el set=fractweb3
114090, 134090
113090, 133090
**el set, el set=fractweb4
112090, 132090

```

```

111090, 131090
*el set, el set=fractweb5
110090, 130090
109090, 129090
*el set, el set=fractweb6
108090, 128090
107090, 127090
*el set, el set=fractweb7
106090, 126090
105090, 125090
*el set, el set=fractweb8
104090, 124090
103090, 123090
**
*el set, el set=fractweb
fractweb1, fractweb2, fractweb3, fractweb4
fractweb5, fractweb6, fractweb7, fractweb8
**
**
*el set, el set=fracture
fractflange, fractweb
**
**
** -----
**
** DEFINE SETS FOR DATA ACQUISITION
**
**
** el set midspanInt refers to the central elements of the internal
** girder, where yielding was possible.
**
*el set, generate, el set=midspanInt
40089, 46089, 1000
40090, 46090, 1000
40091, 46091, 1000
**
**
** The following el sets define which elements correspond with gauge
** locations on the girders for the foil gauges, rosettes, and stud
** gauges. The stud nodes were also grouped so as to consider the
** spacing between the two nodes directly.
**
*el set, el set=foil gauges
6075, 7075, 14075, 15075, 41075, 45075,
141075, 145075, 34075, 35075, 26075, 27075,
106075, 107075, 114075, 115075, 134075, 135075, 126075, 127075
**
*el set, el set=rosettes
30075, 31075, 43075, 10075, 11075, 30106, 31106, 43106, 10106, 11106
**
**
*el set, el set=studgauges
8080003, 8150006, 8080006
8076006, 8122007, 8116007, 8090007, 8080007
8076007, 8056007, 8122012, 8107012, 8065012
**
*nset, nset=studnodes
560822, 560922, 650831, 650931, 760816, 760916
760822, 760922, 800809, 800909, 800816, 800916

```

800822, 800922, 900822, 900922, 1070831, 1070931
1160822, 1160922, 1220822, 1220922, 1220831, 1220931
1500816, 1500916
**
**
** END ELEMENT SET DEFINITIONS
**
**

```

** -----
** ++++++
** -----
**
** ADD LOADS IN STEPS
** -----1-----
**
** STEP ONE: REMOVE DECK AND RAIL ELEMENTS
*step, nlgeom=yes, name=s1removedeck
Remove deck and rail elements
*static
0.25, 0.25, 1e-05
**
*model change, type=element, remove
deck, inrail, outrail, rebar
**
*dl oad
gi rders, grav, 386.4, 0, -1, 0
braci ng, grav, 386.4, 0, -1, 0
**
*el print, el set=fracture
S
*node print, nset=bottomflange
U
**
*end step
**
** -----2-----
**
** STEP TWO: APPLY DEAD LOAD OF DECK TO GIRDER FLANGES
*step, nlgeom=yes, amplitude=ramp, name=s2appdeckload
Apply dead load of deck to girder flanges
*static
0.25, 0.25, 1e-05
**
*dsl oad
fl angetype1, p, -0.00485119
fl angetype2, p, -0.00431217
**
*el print, el set=fracture
S
*node print, nset=bottomflange
U
**
*end step
**
** -----3-----
**
** STEP THREE: REACTIVE DECK ELEMENTS, STRAIN FREE
*step, nlgeom=yes, name=s3adddeckelem
Reactivate deck elements, strain free
*static
0.25, 0.25, 1e-05
**
*model change, type=element, add=strain free
deck, deckrebar
**
*el print, el set=fracture

```

```

S
*node print, nset=bottomflange
U
**
*end step
**
** -----4-----
**
** STEP FOUR: REMOVE APPLIED FLANGE LOAD, TURN ON DECK GRAVITY LOAD,
** REMOVE FAKEDECK ELEMS
*step, nlgeom=yes, amplitude=ramp, name=s4loaddeck
Remove applied flange load, turn on deck gravity load
*static
0.25, 0.25, 1e-05
**
*dsl load
flangetype1, p, 0.0
flangetype2, p, 0.0
**
*dload
deck, grav, 386.4, 0, -1, 0
**
*model change, type=element, remove
fakedeck, fakedeckrebar
**
*el print, elset=fracture
S
*node print, nset=bottomflange
U
**
*end step
**
** -----5-----
**
** STEP FIVE: APPLY DEAD LOAD OF INSIDE RAIL TO EDGE OF DECK
*step, nlgeom=yes, amplitude=ramp, name=s5apprailload
Apply dead load of inside rail to edge of deck
*static
0.25, 0.25, 1e-05
**
*dsl load
ideck, p, 0.0018027
**
*el print, elset=fracture
S
*node print, nset=bottomflange
U
**
*end step
**
** -----6-----
**
** STEP SIX: REACTIVE INSIDE RAIL, STRAIN FREE
*step, nlgeom=yes, name=s6activesiderail
Reactivate inside rail, strain free
*static
0.25, 0.25, 1e-05
**
*model change, type=element, add=strain free
inrail, inrailrebar

```

```

**
*el print, el set=fracture
S
*node print, nset=bottomflange
U
**
*end step
**
** -----7-----
**
** STEP SEVEN: APPLY DEAD LOAD OF OUTSIDE RAIL TO EDGE OF DECK
*step, nlgeom=yes, amplitude=ramp, name=s7apprailoutload
Apply dead load of outside rail to edge of deck
*static
0.25, 0.25, 1e-05
**
*dsload
outdeck, p, 0.0018027
**
*el print, el set=fracture
S
*node print, nset=bottomflange
U
**
*end step
**
** -----8-----
**
** STEP EIGHT: REACTIVE OUTSIDE RAIL, STRAIN FREE
*step, nlgeom=yes, name=s8addrailelem
Reactivate outside rail, strain free
*static
0.25, 0.25, 1e-05
**
*model change, type=element, add=strain free
outrail, outrailrebar
**
*el print, el set=fracture
S
*node print, nset=bottomflange
U
**
*end step
**
** -----9-----
**
** STEP NINE: REMOVE APPLIED RAIL LOADS, TURN ON RAIL GRAVITY LOADS
*step, nlgeom=yes, name=s9loadrail, amplitude=ramp
Remove applied rail loads, turn on rail gravity loads
*static
0.25, 0.25, 1e-07
**
*dsload
indeck, p, 0.0
outdeck, p, 0.0
*dlload
rails, grav, 386.4, 0, -1, 0
**
*model change, type=element, remove
fakerrails, fakerrailrebar

```

```

**
*el print, el set=fracture
S
*node print, nset=bottomflange
U
**
*end step
**
** -----10-----
**
** STEP TEN: APPLY TRUCK LOADS
*step, nlgeom=yes, name=s10truckloads, amplitude=ramp
Apply truck loads above outside girder
*static
0.25, 0.25, 1e-05
**
*dsload
axle1-1, p, 0.033333
axle1-2, p, 0.025641
axle2, p, 0.03252033
axle3, p, 0.03252033
**
*el print, el set=fracture
S
*node print, nset=bottomflange
U
*el print, el set=foi gauges
LE
*el print, el set=rosettes
LEP
*el print, el set=exttruss
S
*node print, nset=supports
RF
*node print, nset=studnodes
U2
**
*end step
**
** -----11-----
**
** STEP ELEVEN: REMOVE EXTERNAL CROSS-BRACES
*step, nlgeom=yes, name=s11removebraces
Remove external cross-braces
*static
0.25, 0.25, 1e-05
**
*model change, type=element, remove
exttruss
**
*el print, el set=fracture
S
*el print, el set=midspanint
S
*node print, nset=bottomflange
U
*el print, el set=foi gauges
LE
*el print, el set=rosettes
LEP

```

```

*el print, el set=studgauges
E11
*node print, nset=supports
RF
*node print, nset=studnodes
U2
**
*end step
**
** -----12-----
**
** STEP TWELVE: REMOVE BOTTOM FLANGE ELEMENTS
*step, nlgeom=yes, name=12fractflange, amplitude=step, inc=1000
Remove the bottom flange elements
*static
0.0005, 0.1, 1e-05
**
*model change, type=element, remove
fractflange
**
*el print, el set=midspanInt
S
*node print, nset=bottomflange
U
*el print, el set=foilage
LE
*el print, el set=rosettes
LEP
*el print, el set=studgauges
E11
*node print, nset=supports
RF
*node print, nset=studnodes
U2
**
*end step
**
** -----13-----
**
** STEP THIRTEEN: REMOVE WEB ELEMENTS
*step, nlgeom=yes, name=s13fractweb, amplitude=step, inc=1000
Remove the web elements
*static
0.0005, 0.1, 1e-05
**
*model change, type=element, remove
fractweb
**
*el print, el set=midspanInt
S
*node print, nset=bottomflange
U
*el print, el set=foilage
LE
*el print, el set=rosettes
LEP
*el print, el set=studgauges
E11
*node print, nset=supports
RF

```



```

*node print, nset=studnodes
U2
**
*end step
**
** -----14-----
**
** STEP FOURTEEN: REMOVE TRUCK LOADS
*step, ngeom=yes, name=s14removetruck
Remove truck loads from outside girder
*static
0.25, 0.25, 1e-05
**
*dload
axle1-1, p, 0
axle1-2, p, 0
axle2, p, 0
axle3, p, 0
**
*el print, elset=midspanint
S
*node print, nset=bottomflange
U
*el print, elset=foilgauges
LE
*el print, elset=rosettes
LEP
*node print, nset=supports
RF
*node print, nset=studnodes
U2
**
*end step


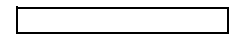
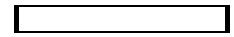

```

APPENDIX C

Table of Longitudinal Node Locations

Element No.	Location (ft)	Element No.	Location (ft)	Element No.	Location (ft)	Element No.	Location (ft)	Element No.	Location (ft)
0	0	16	16	66	46	116	76	166	106
1	1	17	17	67	47	117	77	167	107
2	2	18	18	68	48	118	78	168	108
3	3	19	19	69	49	119	79	169	109
4	4	20	20	70	50	120	80	170	110
5	5	21	21	71	51	121	81	171	111
6	6	22	22	72	52	122	82	172	112
7	7	23	23	73	53	123	83	173	113
8	8	24	24	74	54	124	84	174	114
9	9	25	25	75	55	125	85	175	115
10	10	26	26	76	56	126	86	176	116
11	11	27	26.5	77	56.5	127	86.5	177	117
12	12	28	27	78	57	128	87	178	118
13	13	29	27.5	79	57.5	129	87.5	179	119
14	14	30	28	80	58	130	88	180	120
15	15	31	28.25	81	58.25	131	88.25		
		32	28.5	82	58.5	132	88.5		
		33	28.75	83	58.75	133	88.75		
		34	29	84	59	134	89		
		35	29.25	85	59.25	135	89.25		
		36	29.5	86	59.5	136	89.5		
		37	29.625	87	59.625	137	89.625		
		38	29.75	88	59.75	138	89.75		
		39	29.875	89	59.875	139	89.875		
		40	30	90	60	140	90		
		41	30.125	91	60.125	141	90.125		
		42	30.25	92	60.25	142	90.25		
		43	30.375	93	60.375	143	90.375		
		44	30.5	94	60.5	144	90.5		
		45	30.75	95	60.75	145	90.75		
		46	31	96	61	146	91		
		47	31.25	97	61.25	147	91.25		
		48	31.5	98	61.5	148	91.5		
		49	31.75	99	61.75	149	91.75		
		50	32	100	62	150	92		
		51	32.5	101	62.5	151	92.5		
		52	33	102	63	152	93		
		53	33.5	103	63.5	153	93.5		
		54	34	104	64	154	94		
		55	35	105	65	155	95		
		56	36	106	66	156	96		
		57	37	107	67	157	97		
		58	38	108	68	158	98		
		59	39	109	69	159	99		
		60	40	110	70	160	100		
		61	41	111	71	161	101		
		62	42	112	72	162	102		
		63	43	113	73	163	103		
		64	44	114	74	164	104		
		65	45	115	75	165	105		

LEGEND:

	Expansion joints
	Internal bracing
	Internal & external bracing
	Truck axles

APPENDIX D

List of Commonly Used Keywords

Commonly used ABAQUS keywords:

- beam section
- boundary
- contact pair
- density
- dload
- dsload
- el print
- elastic
- elcopy
- element
- elgen
- elset
- embedded element
- heading
- material
- model change
- mpc
- nfill
- ngen
- node
- node print
- nset
- orientation
- plastic
- shell section
- solid section
- spring
- static
- step, end step
- surface
- surface interaction
- system

APPENDIX E
Example *.mpc File

The following code is an example of one of the additional text files that defines boundaries on the mesh density increase locations within the rail. The *bilinear* mpc type is written as the node being constrained followed by the four nodes constraining it, as is shown below in the ABAQUS User's Manual graphic and code explanation.

```
*mpc
bilinear, p, a,b,c,d
```

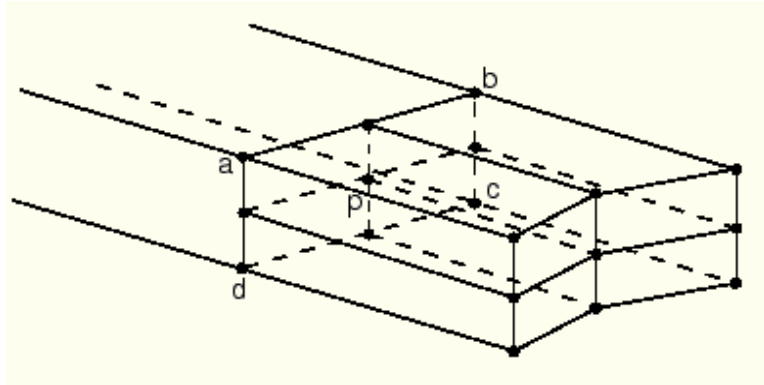


Figure E-1: Bilinear mpc explanation (HKS, Inc. 2006)

The mpc file Gap3-14to7.txt is given here:

```
bilinear, 1502103, 1502305,1502301,1501901,1501905
bilinear, 1502135, 1502337,1502333,1501933,1501937
**
bilinear, 1502503, 1502705,1502701,1502301,1502305
bilinear, 1502535, 1502737,1502733,1502333,1502337
**
bilinear, 1502903, 1503105,1503101,1502701,1502705
bilinear, 1502935, 1503137,1503133,1502733,1502737
**
bilinear, 1503303, 1503505,1503501,1503101,1503105
bilinear, 1503335, 1503537,1503533,1503133,1503137
**
bilinear, 1503703, 1503905,1503901,1503501,1503505
bilinear, 1503735, 1503937,1503933,1503533,1503537
**
bilinear, 1504103, 1504305,1504301,1503901,1503905
bilinear, 1504135, 1504337,1503933,1503533,1503537
**
bilinear, 1504503, 1504705,1504701,1504301,1504305
bilinear, 1504535, 1504737,1504333,1503933,1503937
```

References

- Abraham, F.F. and G. Huajian. (2000). "How Fast Can Cracks Propagate?" *Physical Review Letters*, Vol. 84, No. 14, pg 3113-3116.
- AC Engineering, Inc. (1996). "A Special Topic Seminar: ABAQUS Contact Problems Made Easy." West Lafayette, IN.
- Allaire, P.E. (1985). *Basics of the Finite Element Method: Solid Mechanics, Heat Transfer, and Fluid Mechanics*. Wm. C. Brown Publishers, Dubuque, Iowa.
- American Association of State Highway and Transportation Officials (AASHTO). (2004). *AASHTO LRFD Bridge Design Specifications*. Washington, D.C.
- Ibid (AASHTO). (2003). *AASHTO Guide Specifications for Horizontally Curved Steel Girder Highway Bridges*. Washington, D.C.
- American Concrete Institute. (2005). *Building Code Requirements for Structural Concrete (ACI 318-05)*. ACI Committee 318, Farmington Hills, MI.
- American Institute of Steel Construction (AISC). (2006). *Load and Resistance Factor Design Specification for Steel Buildings*. 13th Edition.
- ANSYS, Inc. (2005). *ANSYS*. Version 10.0. Canonsburg, PA.
- Barnard, T.J. (2006). "Constructing a Full-Scale Horizontally-Curved Twin Steel Trapezoidal Box Girder Bridge Segment to Determine Redundancies in Fracture Critical Bridges." Departmental Report presented to The University of Texas at Austin, in partial fulfillment of the requirements for the degree of Master of Science in Engineering.
- Bathe, K.-J. (1982). *Finite Element Procedures in Engineering Analysis*. Prentice-Hall, Inc., Englewood Cliffs, New Jersey.
- Bathe, K.-J. (1996). *Finite Element Procedures*. Prentice-Hall, Inc., Englewood Cliffs, New Jersey.
- Belytschko, T., Liu, W.K., and B. Moran. (2006). *Nonlinear Finite Elements for Continua and Structures*. Wiley, Hoboken, New Jersey.
- Branco, F.A. and Green, R. (1985). "Composite box girder behavior during construction." *Journal of Structural Engineering*, ASCE, Vol. 111, No. 3, pg 577-593.
- Bruhn, E.F. (1965). *Analysis and Design of Flight Vehicle Structures*. Tri-State Offset Company, Cincinnati, OH.

Chen, B.S. (1999). "Top flange lateral bracing of steel U-shaped girders." Thesis presented to The University of Texas at Austin, in partial fulfillment of the requirements for the degree of Master of Science in Engineering.

Chopra, A.K. (2000). *Dynamics of Structures: Theory and Applications to Earthquake Engineering*. 2nd Ed. Upper Saddle River, New Jersey.

CNN. (2002). "Bridge Disasters in the United States."
<<http://www.cnn.com/2002/US/05/26/bridge.accidents>> Published: 26 May 2002.
Accessed: 04 April 2007.

Computational Fracture Mechanics Research Group. (2007). *WARP3D*. Release 15.8. University of Illinois at Urbana-Champaign.

Computers and Structures, Inc. (2006). *Sap2000*. Advanced 10.0.9. Berkeley, CA.

Connor, R.J., Dexter, R., and H. Mahmoud. (2005). "Inspection and Management of Bridges with Fracture-Critical Details." *National Cooperative Highway Research Program Synthesis 354*. Transportation Research Board, National Academy Press, Washington, DC.

Cook, R.D., Malkus, D.S., Plesha, M.E., and R.J. Witt. (2001). *Concepts and Applications of Finite Element Analysis*. 4th Edition. John Wiley & Sons, Inc., New York.

Cowper, G.R. (1973). "Gaussian Quadrature Formulas for Triangles." *International Journal for Numerical Methods in Engineering*, Vol. 7, pg 405-408.

Crampton, D.D., McGormley, J.C., and H.J. Hill. (2007). "Improving Redundancy of Two-Girder Bridges." *Proceedings, Transportation Research Board Annual Meeting*. Washington, D.C.

Crisfield, M.A. (1991). *Non-Linear Finite Element Analysis of Solids and Structures, Vol. 1*. John Wiley & Sons, Inc., New York.

Dahlquist, G., and A. Bjork. (1974). *Numerical Methods*. Prentice Hall, Inc., Englewood Cliffs, New Jersey.

Daniels, J.H., Kim, W., and J.L. Wilson. (1989). "Recommended Guidelines for Redundancy Design and Rating of Two-Girder Steel Bridges." *National Cooperative Highway Research Program Report 319*. Transportation Research Board, National Academy Press, Washington, D.C.

Davidson, J.S., Abdalla, R.S., and M. Madhavan. (2004). "Stability of Curved Bridges During Construction." University Transportation Center for Alabama, Birmingham, AB.

- Dexter, R.J., Wright, W.J., and J.W. Fisher. (2004). "Fatigue and Fracture of Steel Girders." *Journal of Bridge Engineering*, ASCE, Vol. 9, No. 3, pg 278-286.
- Dowling, P.J. (1975). "Strength of Steel Box-Girder Bridges." *Journal of the Structural Division*, ASCE, Vol. 101, No. 9, pg 1929-1947.
- Failla, K.S. (1985). "New Mianus Bridge Report Disputes Earlier Study." *Civil Engineering*, Vol. 55, No. 4, pg. 10.
- Fisher, J.W. Photos from within Connor et al. (2005).
- Fisher, J.W., Pense, A.W., and R. Roberts. (1977). "Evaluation of Fracture of Lafayette Street Bridge." *Journal of the Structural Division*, ASCE, Vol. 103, No. 7, pg 1339-1357.
- Frank, K.H. (2007). CE 386P class notes and personal correspondence.
- Gilchrist, Christopher (1997). "Buckling Behavior of U-Shaped Girders," thesis presented to The University of Texas at Austin, in partial fulfillment of the requirements for the degree of Master of Science in Engineering.
- Ghosn, M., and F. Moses. (1998). "Redundancy in Highway Bridge Superstructures." *National Cooperative Highway Research Program Report 406*. Transportation Research Board, National Academy Press, Washington, D.C.
- Hellen, T.K. (1972). "Short Communications: Effective Quadrature Rules for Quadratic Solid Isoparametric Finite Elements." *International Journal for Numerical Methods in Engineering*, Vol. 4, pg 597-600.
- Hibbitt, Karlsson, and Sorensen, Inc. (HKS, Inc.). (2006). *ABAQUS/CAE*. Version 6.6-1. Providence, RI.
- Ibid. *ABAQUS/Explicit*. Version 6.6-1. Providence, RI.
- Ibid. *ABAQUS/Standard*. Version 6.6-1. Providence, RI.
- Ibid. *ABAQUS/Viewer*. Version 6.6-1. Providence, RI.
- Ibid. *Keywords Manual*. Version 6.6-1. Providence, RI.
- Ibid. *Standard User's Manual*. Version 6.6-1. Providence, RI.
- Ibid. *Theory Manual*. Version 6.6-1. Providence, RI.

- Hughes, J.R. (2000). *The Finite Element Method: Linear Static and Dynamic Finite Element Analysis*. Dover Publications, Mineola, New York.
- Idriss, R.L, White, K.R., Woodward, C.B., and D.V. Jauregui. (1995). "Evaluation and testing of a fracture critical bridge." *NDT&E International*, Vol. 28, No. 6, pg 339-347.
- Irons, B.M. (1971). "Quadrature Rules for Brick Based Finite Elements." *International Journal for Numerical Methods in Engineering*, Vol. 3, pg 293-294.
- Kassimali, A. (1999). *Matrix Analysis of Structures*. Brooks/Cole Publishing Company, Pacific Grove, CA.
- Kollbrunner, C.F. and K. Basler. (1969). *Torsion in Structures: An Engineering Approach*. Springer-Verlag, Berlin, Germany.
- Liu, W.D., Ghosn, M., and F. Moses. (2001). "Redundancy in Highway Bridge Substructures." *National Cooperative Highway Research Program Report 458*. Transportation Research Board, National Academy Press, Washington, D.C.
- Lovejoy, S.C. (2003). "Determining Appropriate Fatigue Inspection Intervals for Steel Bridge Members." *Journal of Bridge Engineering*, ASCE, Vol. 8, No. 2, pg 66.
- McGuire, W., Gallagher, R.H., and R.D. Ziemian. (2000). *Matrix Structural Analysis: Second Edition*. John Wiley & Sons, Inc., New York.
- Microsoft Corporation. (2001). *Microsoft Notepad*. Version 5.1. Redmond, WA.
- Ibid. (2003). *Microsoft Office Excel 2003*. 11.8134.8132. Redmond, WA.
- Ibid. (2001). *Microsoft Windows XP Professional*. Version 5.1.2600. Redmond, WA.
- McGuire, W., Gallagher, R.H., and R.D. Ziemian. (2000). *Matrix Structural Analysis: Second Edition*, John Wiley & Sons, Inc., New York.
- National Bridge Inspection Standards (1988). Code of Federal Regulations. Title 23, Part 650.
- Popp, D. (2004). "UTrAp 2.0: Linearized Buckling Analysis of Steel Trapezoidal Girders." Thesis presented to The University of Texas at Austin, in partial fulfillment of the requirements for the degree of Master of Science in Engineering.
- Popp, D., Topkaya, C., and E.B. Williamson. (2004). *UTrAp 2.0: Analysis of Curved Steel Box Girders During Construction*. Version 2.0. The University of Texas at Austin.

Quiel, S. (2003). "Forensic Analysis of the Steel Girder Fracture in the I-95 Brandywine River Bridge." University of Notre Dame Research Experience for Undergraduates. Newark, DE.

Ruth, P., Marchand, K.A., and E.B. Williamson. (2006). "Static Equivalency in Progressive Collapse Alternative Path Analysis; Reducing Conservatism While Retaining Structural Integrity." *Journal of Performance of Constructed Facilities*, ASCE, Vol. 20, No. 4, pg. 349-364.

Salmon, C.G., and J.E. Johnson. (1980). *Steel Structures: Design and Behavior*. 2nd Edition. Harper & Row, Publishers, Inc., New York, NY.

Ibid. (1996). *Steel Structures: Design and Behavior*. 4th Edition. Harper & Row, Publishers, Inc., New York, NY.

Scheffey, C.F. (1971). "Pt. Pleasant Bridge Collapse: Conclusions of the Federal Study." *Civil Engineering*, Vol. 41, No. 7.

Schwendeman, L.P. and Hedgren, A.W. (1978). "Bolted repair of fractured I-79 girder." *Journal of the Structural Division*, ASCE, Vol. 104, No. 10, pg 1567-1669.

Sennah, K.M. and Kennedy, J.B. (2002). "Literature Review in analysis of box girder bridges." *Journal of Bridge Engineering*, ASCE, Vol. 7, No. 2, pg 134-143.

Sennah, K.M. and Kennedy, J.B. (2001). "State-of-the-art in design of curved box-girder bridges." *Journal of Bridge Engineering*, ASCE, Vol. 6, No. 3, pg 159-167.

Stith, J.C. (2007). Personal correspondence.

Sutton, J.P. (2007). "Evaluating the Redundancy of Steel Bridges: Effect of a Bridge Haunch on the Strength and Behavior of Shear Studs under Tensile Loading." Thesis presented to The University of Texas at Austin, in partial fulfillment of the requirements for the degree of Master of Science in Engineering.

Texas Department of Transportation (TxDOT). (2003) *Traffic Rail: Type T501*. <<ftp://ftp.dot.state.tx.us/pub/txdot-info/cmd/cserve/standard/bridge/rlstde16.pdf>> Published: February 2003. Accessed: 02 July 2007.

Timoshenko, S.P., and J.M. Gere. (1961). *Theory of Elastic Stability*. 2nd Edition. McGraw-Hill Book Company, Inc., New York, NY.

Tolnai, M.A. (2005). "Analytical simulation of vehicular impact on retrofit bridge barriers." Thesis presented to The University of Texas at Austin, in partial fulfillment of the requirements for the degree of Master of Science in Engineering.

Topkaya, C. (2002). "Behavior of curved steel trapezoidal box girders during construction." Dissertation presented to The University of Texas at Austin, in partial fulfillment of the requirements for the degree of Doctor of Philosophy in Engineering.

Topkaya, C. and Williamson, E.B. (2003). "Development of computational software for analysis of curved girders under construction loads." *Computers and Structure*, Vol. 81, pg 2087-2098.

Topkaya, C., Williamson, E.B., and K.H. Frank. (2004). "Behavior of curved steel trapezoidal box girders during construction." *Engineering Structures*. Vol. 26, No. 6, pg 721-733.

United Facilities Criteria (UFC). (2005). *Design of Buildings to Resist Progressive Collapse*. UFC 4-023-03. Washington, DC.

Washabaugh, P.D. and W.G. Knauss. (1994). "A Reconciliation of Dynamic Crack Velocity and Rayleigh Wave Speed in Isotropic Brittle Solids." *International Journal of Fracture*, Vol. 65, No. 2, pg 97-114.

Widianto. (2003). "General behavior of a steel trapezoidal box-girder during construction." Thesis presented to The University of Texas at Austin, in partial fulfillment of the requirements for the degree of Master of Science in Engineering.

Williams, G. (2001). *Linear Algebra with Applications*. 4th Edition. Jones and Bartlett Publishers, Sudbury, MA.

Williamson, E.B. (2007). CE 381P class notes and personal correspondence.

VITA

Catherine Grace Hovell was born in Stamford, Connecticut on May 23, 1983, the daughter of Peter F. and Margaret M. Hovell. She is the sister of John Hovell. She attended Darien High School in Darien, Connecticut, from which she graduated in 2001. She obtained her Bachelor of Science in Civil Engineering from the University of Virginia in May 2005, having written an undergraduate thesis on low-clearance bridge design using Ultra-High Performance Concrete. She entered the Graduate School at the University of Texas in August 2005. While at the University of Texas, she worked as a Graduate Research Assistant at the Phil M. Ferguson Structural Engineering Laboratory. She received her Masters of Science in Engineering degree in August 2007.

Permanent address: 22 Brushy Hill Road
Darien, CT 06820

This thesis was typed by the author.